View metadata, citation and similar papers at core.ac.uk
brought to you by CORE
provided by CERN Document Server

CERN, January 2008

RD50 Status Report 2007

Radiation hard semiconductor devices for very high luminosity colliders

Centro Nacional de Microelectrónica (IMB-CNM, CSIC), Barcelona, Spain
Juan Pablo Balbuena, Daniela Bassignana, Francesca Campabadal, Sergio Díez, Manuel Lozano, Giulio Pellegrini, Joan Marc Rafí, Miguel Ullán

Dipartimento Interateneo di Fisica & INFN - Bari, Italy
Marianna Ambrico, Donato Creanza, Mauro De Palma, Teresa Ligonzo, Norman Manna, Valeria Radicci, Luigi Schiavulli

Brookhaven National Laboratory, Upton, NY, USA
Jim Kierstead, Zheng Li

Department of Physics, University of Bologna, Bologna, Italy
Anna Cavallini

National Institute for Materials Physics, Bucharest - Magurele, Romania
Manuela Buda, Sorina Lazanu, Lucian Pintilie, Ioana Pintilie, Andreia-Ioana Popa

University of Bucharest, Faculty of Physics, Romania
Ionel Lazanu

CERN, Geneva, Switzerland
Paula Collins,Manuel Fahrer, Maurice Glaser, Herbert Hödlmoser, Christian Joram, Katharina Kaska, Alessandro La Rosa, Julien Mekki, Michael Moll[*]

Universitaet Dortmund, Lehrstuhl Experimentelle Physik IV, Dortmund, Germany
Claus Goessling, Reiner Klingenberg, Jens Weber, Renate Wunstorf

CiS Institut für Mikrosensorik gGmbH, Erfurt, Germany
Ralf Roeder, Dieter Stolze, Hartmut Uebersee

University of Exeter, Department of Physics, Exeter, EX4 4QL, United Kingdom
James Adey, A. Blumenau, J. Coutinho, T. Eberlein, C. Fall, J. Goss, B. Hourahine, Robert Jones, N. Pinho

Fermilab, USA
Selcuk Cihangir, Simon Kwan, Leonard Spiegel, Ping Tan

---

[*] Co-spokesperson

INFN Florence – Department of Energetics, University of Florence, Italy
Emilio Borchi, Mara Bruzzi†, Ettore Focardi, David Menichelli, Stefania Miglio, Monica Scaringella, Carlo Tosi

University of Freiburg
Simon Eckert, Susanne Kuehn, Gregor Pahn, Ulrich Parzefall

Dept. of Physics & Astronomy, Glasgow University, Glasgow, UK
Richard Bates, Andrew Blue, Peter Bussey, Craig Buttar, Freddie Doherty, Lars Eklund, Celeste Fleta, Alison G Bates, Lina Haddad, Grant James, Keith Mathieson, J. Melone, Val OShea, Chris Parkes, David Pennicard

Institute for Experimental Physics, University of Hamburg, Germany
Peter Buhmann, Doris Eckstein, Eckhart Fretwurst, Frank Hönniger, Robert Klanner, Gunnar Lindström, Uwe Pein

Helsinki Institute of Physics, Helsinki, Finland
Jaakko Härkönen, Katri Lassila-Perini, Panja Luukka, Jukka Nysten, Eija Tuominen, Esa Tuovinen

Ioffe Phisico-Technical Institute of Russian Academy of Sciences, St. Petersburg, Russia
Vladimir Eremin, Igor Ilyashenko, Alexandr Ivanov, Evgenia Kalinina, Alexander Lebedev, Nikita Strokan, Elena Verbitskaya

Institute of Physics PAS and Institute of Electronics Technology, Warszawa, Poland
Adam Barcz

Institute of Electronic Materials Technology, Warszawa, Poland
Andrzej Brzozowski, Pawel Kaminski, Roman Kozlowski, Michal Kozubal, Zygmunt Luczynski, Marius Pawlowski, Barbara Surma, Jaroslaw Zelazko

University of Karlsruhe, Institut fuer Experimentelle Kernphysik, Karlsruhe, Germany
Wim de Boer, Alex Furgeri, Frank Hartmann, Valery Zhukov

Institute for Nuclear Research of the Academy of Sciences of Ukraine, Radiation PhysicDepartments
L. Barabash, A. Dolgolenko, A. Groza, A. Karpenko, V. Khivrich, V. Lastovetsky, P. Litovchenko, L. Polivtsev

Department of Physics, Lancaster University, Lancaster, United Kingdom
Timothy John Brodbeck, Duncan Campbell, Alexandre Chilingarov, Gareth Hughes, Brian Keith Jones, Terence Sloan

Department of Physics, University of Liverpool, United Kingdom
Anthony Affolder, Phillip Allport, Themis Bowcock, Gianluigi Casse, Joost Vossebeld

Jožef Stefan Institute and Department of Physics, University of Ljubljana, Ljubljana, Slovenia
Vladimir Cindro, Irena Dolenc, Gregor Kramberger, Igor Mandic, Marko Mikuž, Marko Zavrtanik, Dejan Zontar

† Co-spokesperson

Université catholique de Louvain, Institut de Physique Nucléaire, Louvain-la-Neuve, Belgium
Eduardo Cortina Gil, Ghislain Grégoire, Vincent Lemaitre, Otilia Militaru, Krzysztof Piotrzkowski

Belarusian State University, Minsk
Nikolai Kazuchits, Leonid Makarenko

Groupe de la Physique des Particules, Université de Montreal, Canada
Sébastien Charron, Marie-Helene Genest, Alain Houdayer, Celine Lebel, Claude Leroy

State Scientific Center of Russian Federation, Institute for Theoretical and Experimental Physics, Moscow, Russia
Andrey Aleev, Alexander Golubev,, Eugene Grigoriev, Aleksey Karpov, Alxander Martemianov, Sergey Rogozhkin, Alexandre Zaluzhny

MPI Munich, Halbleiterlabor, Germany
Ladislav Andricek, Anna Macchiolo, Hans-Günther Moser, Richard Nisius, Rainer Richter, Qingyu Wei

Department of Physics and Astronomy, University of New Mexico, Albuquerque, NM, USA
Igor Gorelov, Martin Hoeferkamp, Jessica Metcalfe, Sally Seidel, Konstantin Toms

The National Institute for Nuclear Physics and High Energy Physics (NIKHEF)
Fred Hartjes, Els Koffeman, Harry van der Graaf, Jan Visschers

University of Oslo, Physics Department/Physical Electronics, Oslo, Norway
Andrej Kuznetsov, Lars Sundnes Løvlie, Edouard Monakhov, Bengt G. Svensson

Dipartimento di Fisica and INFN Sezione di Padova, Padova, Italy
Dario Bisello, Andrea Candelori, Vladimir Khomenkov, Alexei Litovchenko, Devis Pantano, Riccardo Rando

I.N.F.N. and Università di Perugia - Italy
Gian Mario Bilei, Daniele Passeri, Marco Petasecca, Giorgio Umberto Pignatel

Universita` di Pisa and INFN sez. di Pisa, Italy
Jacopo Bernardini, Laura Borrello, Suchandra Dutta, Francesco Fiori, Alberto Messineo

Institute of Physics, Academy of Sciences of the Czech Republic, Praha, Czech Republic
Jiri Popule, Petr Sicho, Michal Tomasek, Vaclav Vrba

Charles University Prague, Czech Republic
Jan Broz, Zdenek Dolezal, Peter Kodys, Alexej Tsvetkov, Ivan Wilhelm

Czech Technical University in Prague, Czech Republic
Dominik Chren, Tomas Horazdovsky, Zdenek Kohout, Vladimir Linhart, Stanislav Pospisil, Michael Solar, Vít Sopko, Bruno Sopko, Josef Uher

Paul Scherrer Institut, Laboratory for Particle Physics, Villigen, Switzerland
Ulrike Grossner, Roland Horisberger, Tilman Rohe

Purdue University, USA
Gino Bolla, Daniela Bortoletto, Kim Giolo, Jun Miyamoto, Carsten Rott, Amitava Roy, Ian Shipsey, SeungHee Son

University of Rochester, USA
Veronique Boisvert, Regina Demina, Sergey Korjenevski, Paul Tipton

Santa Cruz Institute for Particle Physics, USA
Alexander Grillo, Hartmut Sadrozinski, Bruce Schumm, Abraham Seiden, Ned Spencer

SINTEF ICT, Blindern, Oslo, Norway
Thor-Erik Hansen

Experimental Particle Physics Group, Syracuse University, Syracuse, USA
Marina Artuso, Gwenaelle Lefeuvre

Tel Aviv University, Israel
J. Guskov, Sergey Marunko, Arie Ruzin, Tamir Tylchin

Experimental Physics Department, University of Torino, Italy
Elisabetta Colombo, Alessandro Lo Giudice, Claudio Manfredotti, Paolo Olivero

Fondazione Bruno Kessler - FBK, Povo, Trento, Italy
Maurizio Boscardin, Gian - Franco Dalla Betta, Paolo Gregori, Claudio Piemonte, Alberto Pozza, Sabina Ronchin, Mario Zen, Nicola Zorzi

IFIC, joint research institute of CSIC and Universitat de Valencia-Estudi General, Valencia, Spain
Carmen Garcia, Sergio González Sevilla, Carlos Lacasta, Ricardo Marco, Salvador Marti i Garcia, Mercedes Minano

Institute of Materials Science and Applied Research, Vilnius University, Vilnius, Lithuania
Eugenijus Gaubas, Arunas Kadys, Vaidotas Kazukauskas, Stanislavas Sakalauskas, Jurgis Storasta, Juozas Vidmantis Vaitkus

Contents

1. Introduction
2. Executive Summary
3. Defect and Material Characterization
4. Defect Engineering
5. Pad Detector Characterization
6. New Structures
7. Full Detector Systems
8. Resources

1 Introduction

The objective of the CERN RD50 Collaboration is the development of radiation hard semiconductor detectors for very high luminosity colliders, particularly to face the requirements of a possible upgrade scenario of the LHC to a luminosity of $10^{35}cm^{-2}s^{-1}$, corresponding to expected total fluences of fast hadrons above $10^{16}cm^{-2}$ at a bunch-crossing interval of ~25 ns [1, 2]. This document reports the status of research and main results obtained after the fith year of activity of the collaboration.

Presently, RD50 counts a total of 259 members with 49 participating institutes. This comprises 40 institutes from 17 different countries in West and East Europe, 8 from North America (USA, Canada) and one from middle east (Israel). During the fifth year of activity two workshops and collaboration board meetings have been held to discuss the recent results and co-ordinate the research activities of RD50: 4-6 June 2007, Vilnius, Lithuania and November 12-14, 2007 at CERN. Each workshop has registered a quite high rate of participation, counting an average of 60 participants with about 30 talks. Additionally a dedicated “RD50 workshop on defect analysis in radiation damaged silicon detectors” was held at the University of Vilnius focussing on the progress of the RD50 WODEAN project on the investigation of microscopic defects in silicon. More details including all electronic versions of the presentations can be found on the collaboration web-site [3].

Review papers describing the common research activities of the RD50 collaboration have been published in 2003 to 2006 [4-12] and in 2007 [13]. As in the previous years, the research activity of RD50 has been presented in form of oral contributions at several international conferences and workshops [14]:

- 11th Vienna Conference on Instrumentation, February, 19-24, 2007, Vienna, Austria [15]
- ACES - Common ATLAS CMS Electronics Workshop, March 19-21, 2007, CERN [16]
- 8th International Conference on Large Scale Applications and Radiation Hardness of Semiconductor Detectors, June 27-29, 2007, Florence, Italy [17]
- CMS Upgrade - Sensor Working Group Meeting, August 2, 2007, CERN [18]
- ATLAS Pixel: B-layer Replacement Workshop, September 28-29, CERN [19]
- 2007 IEEE Nuclear Science Symposium (NSS), October 28 to November 3, Honolulu, Hawaii [20, 21]
- LHCb Velo Workshop, September 13-14, CERN [22]

The scientific organization of RD50 is structured in five research lines as shown in Table 1-1. The management of the research lines is assigned to members of RD50 of proven relevant experience (conveners). Compared to 2006 the number of research lines was reduced by one. The former research line “New Materials” was suppressed and the remaining activity in the working field included as a working group into the research line “Pad Detector Characterization”. This step was taken as the work on GaN and SiC did not show promising results in terms of bringing forward feasible detector solutions in the given timeframe for SLHC detector developments. In the framework of the research activity of each research line, working groups are active with specific tasks. Each working group is composed of few institutes, which are directly involved in the research program and co-ordinated by an RD50 member. Table 1-1 lists working groups and common activities within each project, with the corresponding co-ordinator.

Besides working groups, common activities were continued or have been started on subjects of common interest. Some of these activities are partially supported with the RD50 common fund. Examples are the common purchase of FZ and MCZ silicon wafers that could only be purchased in big quantities or the expensive processing of a batch of detectors in a 6” processing line with a RD50 common mask.

	Project Convener	Main Research Activity	Working groups and common acitivities
Spokespersons Mara Bruzzi (INFN and Uni. of Florence) and Michael Moll (CERN)	**Defect/Material Characterisation** Bengt G. Svensson Univ. Oslo, Norway	Characterisation of the microscopic properties of standard-, defect engineered and new materials, pre- and post-irradiation.	(1) WODEAN – Workshop on Defect Analysis in Silicon (G.Lindstroem)
	Defect Engineering Eckhart Fretwurst Univ. of Hamburg, Germany	Development and testing of defect engineered silicon: Oxygen enriched FZ (DOFZ), High res. Cz, MCZ, Epitaxial, Si enriched with Oxygen dimers	(1) RD50 wafer procurement (M.Moll)
	Pad Detector Characterisation Gregor Kramberger, Ljubljana Univ., Slovenia	Characterisation of macroscopic properties of heavily irradiated single pad detectors in different operational conditions.	(1) Standardisation of macroscopic measurements (A.Chilingarov) (2) New materials (E.Verbitskaya)
	New Structures Richard Bates Univ. of Glasgow, UK	Development of 3D, semi-3D and thin detectors and study of their pre- and post-irradiation performance.	(1) 3D (M.Boscardin) (2) Semi-3D (Z.Li)
	Full Detector Systems Gianluigi Casse Univ. of Liverpool, UK	- Systematic characterisation of segmented (microstrips, pixels) LHC-like detectors. - Links with LHC experiments	(1) Pixel detectors (D.Bortoletto and T.Rohe) (2) Micron 6" production (H.Sadrozinski, SCIPP)

Table 1-1.: Organisation structure of the research activity in RD50.

In the next section our scientific work is reviewed in an executive summary. This section is followed by five sections describing the status of the research activities of each individual research line. Finally a work plan, milestones and an overview about the needed resources for 2008 are given.

References for Chapter 1

[1] R&D Proposal - DEVELOPMENT OF RADIATION HARD SEMICONDUCTORDEVICES FOR VERY HIGH LUMINOSITY COLLIDERS, LHCC 2002-003 / P6, 15.2.2002.

[2] RD50 Status Report 2004 – Radiation hard semiconductor devices for very high luminosity colliders, CERN-LHCC-2004-031 and LHCC-RD-005, January 2005

[3] RD50 collaboration web site: http://www.cern.ch/rd50/.

[4] **Michael Moll** on behalf of the CERN RD50 collaboration, "Development of radiation hard sensors for very high luminosity colliders - CERN - RD50 project – "Nucl. Instr. & Meth. in Phys. Res. A 511 (2003) 97-105.

[5] **Mara Bruzzi** on behalf of the CERN RD50 Collaboration, "Material Engineering for the Development of Ultra-Radiation Hard Semiconductor Detectors", Nucl. Instrum. & Meth. A 518, 1-2, 2004, 336-337.

[6] **Panja Luukka** on behalf of the CERN RD50 Collaboratin "Status of Defect Engineering Activity of the RD50 Collaboration" Nucl. Instrum. & Meth. A 530, 1-2, 2004, 152-157.

[7] **Michael Moll et al. (RD50 Collaboration)**, "Development of radiation tolerant semiconductor detectors for the Super-LHC", NIMA 546 , 99-107 (2005).

[8] **M. Bruzzi et al. (RD50 Collaboration)**; "Radiation-hard semiconductor detectors for SuperLHC"; NIMA, 541, 189-201 (2005).

[9] **F.Fretwurst et al. (RD50 Collaboration)**, "Recent advancements in the development of radiation hard semiconductor detectors for S-LHC"; NIMA 552, 7-19 (2005).

[10] **Andrea Candelori** on behalf of the CERN RD50 collaboration, "Radiation-hard detectors for very high luminosity colliders"; NIMA, 560, 103-107, (2006).
[11] **Michael Moll** on behalf of the CERN RD50 collaboration, "Radiation tolerant semiconductor sensors for tracking detectors"; Michael Moll; NIMA, 565, 202-211, (2006).
[12] **Panja Luukka,** "Recent progress of CERN RD50 Collaboration";; Trans. Nonferrous Met. Soc. China, 16, s133-s136, (2006).
[13] **Gregor Kramberger,** "Recent results from CERN RD50 collaboration"; NIMA, 583, 49-57, (2007).
[14] Electronic versions of the talks are available on the RD50 www-page under http://www.cern.ch/rd50/doc/
[15] "RD50 Status: Developing radiation tolerant materials for ultra rad-hard tracking detectors", Richard Bates, Glasgow University, UK.
[16] "Very radiation hard sensors", Michael Moll, CERN, Switzerland.
[17] "Status of the CERN RD50 collaboration", David Menichelli, Florence University, Italy.
[18] "Report on recent RD50 activities and future plans", Michael Moll, CERN, Switzerland.
[19] "Radiation Tolerant Silicon Sensors", Michael Moll, CERN, Switzerland.
[20] "RD50: Development of Radiation Hard Tracking Detectors", Hartmut F.-W. Sadrozinski, SCIPP UC Santa Cruz, USA.
[21] "Development of 3D Detectors for Very High Luminosity Colliders"", Celeste Fleta, Glasgow University, UK.
[22] "RD50 technology advances", Michael Moll, CERN, Switzerland.

2 Executive Summary

2.1 Defect and Material Characterization (DMC)

- *Defect clusters* have been studied applying the DLTS (Deep Level Transient Spectroscopy) technique. The used samples were made from Magnetic Czochralski silicon (MCz), Floating Zone (FZ) and epitaxial silicon (EPI). Measurements performed after 6 MeV electron irradiation were compared to measurements performed after neutron irradiation in order to identify defects related to clusters ('disordered regions'). The isothermal annealing of the cluster related levels E4 and E5, located ~0.37 and ~0.45 eV below the conduction band, was studied in detail and a correlation with the annealing of the radiation induced leakage current could be established.

- *Acceptor levels* created after neutron irradiation in EPI and MCz silicon were identified using the TSC (Thermally Stimulated Current) method. Three levels, labeled H(116K), H(140K) and H(152K), were identified and their energy levels as well as their hole capture cross sections were measured. The observation of a Poole-Frenkel effect on all three levels clearly characterized them as acceptor levels contributing to the negative radiation induced space charge. An isothermal annealing study clearly demonstrated that these levels are responsible for the 'reverse annealing' of hadron irradiated silicon detectors.

- *FTIR (Fourier Transform Infrared Absorption)* measurements gave a further hint that the 936 cm^{-1} band can be assigned to the I_2O defect. Moreover, it is speculated that the E4/E5 levels are arising from the same defect center as the 936 cm^{-1} band as the defects anneal in a correlated way.

- *Hall effect, magnetoresistance and lifetime measurements* were performed on neutron irradiated silicon. The recombination lifetime was found to decrease linearly with increasing neutron fluence over 4.5 orders of magnitude ranging from 10^{12} to some 10^{16} n/cm^2.

2.2 Defect Engineering (DE)

- *Standard and Oxygen enriched FZ silicon (DOFZ)*: Both material types have been studied mainly for comparison with the other type of materials under investigation by the RD50 collaboration as for example high resistivity Magnetic Czochralski silicon (MCz), epitaxial silicon (EPI) or pre-irradiated FZ and MCz silicon. In 2007 also intense work on p-type material has been performed, motivated by promising results of improved charge collection properties in structured detectors (strip and 3D detectors).

- *Donor and acceptor generation in epitaxial and MCZ silicon*: Diffusion oxygenated epitaxial silicon EPI-DO was introduced as a new defect engineered material. This material exhibits a much larger oxygen dimer concentration in comparison to non oxygenated epi silicon (EPI-ST) of the same layer thickness. The present assumption was that the introduction rate of shallow donors is related to the content of dimers in the material. Detailed investigations into the formation of donors in EPI-DO, EPI-ST and MCz after irradiation with neutrons have been performed. The ratios of the donor concentrations in EPI-DO, EPI-ST and MCz are 1.0 to 0.69 to 0.38. These ratios neither reflect the corresponding ratios of the oxygen

concentrations as measured by SIMS nor the O_{2i} concentrations as deduced from the concentration of the IO_{2i} complex in these materials. Especially the low concentration found in MCz silicon contradicts the expectation that the donor concentration should be the same as found in EPI-DO since the oxygen contents are nearly identical. This means that the mechanism of the donor formation is so far not understood. Possibly other impurities like hydrogen may be involved in the reaction mechanism. On the other hand three hole traps could be identified by recent TSC studies to be deep acceptors in the lower half of the band gap being negatively charged at room temperature, contributing therefore with their full concentration to the space charge in the depleted region, and they are responsible for the reverse annealing of the effective space charge concentration.

- *Hydrogen in silicon*: A further defect engineering approach is the enrichment of silicon with hydrogen. It is expected that hydrogen may passivate radiation induced defects. A major problem of hydrogenation is the quantitative evaluation of the hydrogen content. The sensitivity for the detection of hydrogen by the SIMS method is ten times lower compared to deuterium. Therefore, in a first test experiment FZ samples were implanted with 710 keV deuterons. From the measured depth profiles of the deuterium concentration for as implanted samples and after annealing at 400 °C for one hour it could be concluded that also an implantation of hydrogen and a subsequent diffusion at elevated temperatures can be monitored by SIMS measurements. In a second experiment 50 µm thick EPI-diodes grown on 300 µm Cz substrates will be implanted through the substrate with 5.5 MeV protons. This will result in a layer with the maximal hydrogen concentration located near to the interface between the substrate and the epi layer. This way the EPI-diodes will not be damaged by the proton beam. Several annealing procedures are assigned for a proper diffusion of the implanted hydrogen into the epitaxial layer which will be controlled by SIMS measurements.

- *Pre-irradiated detectors* are detectors produced from a silicon material that prior to processing has been exposed to an irradiation usually performed in a nuclear reactor. It is assumed that this pre-irradiation is forming gettering sites inside the material that are reducing the detector radiation damage. Neutron radiation responses of pre-irradiated n- and p-type FZ detectors have been compared to the response of standard and NTD (Neutron Transmutation Doped) detectors. Some indications have been found for a reduced negative space charge built up in the pre-irradiated detectors.

2.3 Pad Detector Characterization (PDC)

- A new method for the *reconstruction of the electric field profile* in irradiated silicon diodes was presented. It allows for a more precise reconstruction of the electric field than a previously used method and was successfully applied to determine the electric field in proton and neutron irradiated epitaxial silicon sensors.

- A *comprehensive review of damage parameters* was performed collecting results obtained over the recent years on various detector materials. Special emphasis was put on the analyses of data obtained on n- and p-type MCZ silicon. The fact that both materials (n- and p-type!) do not type invert during high energy proton irradiation remains a riddle to be solved.

- *Bias-dependent damage*: It was verified that the damage in all silicon materials (FZ, EPI, MCZ) is bias dependent. Regardless of the space charge sign the effective space charge density increases in irradiated detectors when a voltage is applied. Contrary, the leakage current is not affected by the applied voltage.

- The *inverse trapping time* for electrons and its annealing was measured on thinned detectors up to a fluence of $3x10^{15}$ n/cm^2. It was found that the inverse trapping time increases linearly up to this fluence.

- The *Charge collection efficiency* was measured on pad and strip detectors made from MCZ, FZ and EPI silicon after proton, pion and neutron irradiation using beta-sources.

- *Silicon Carbide* – Proton irradiation: The goal of the study was the improvement of the characteristics of SiC p+–n–n+ structures irradiated by 8 MeV protons. Samples irradiated by the equivalent fluence of $3\cdot10^{15}$ cm^{-2} were annealed in vacuum in two steps at 600ºC and 700ºC. The CCE measurements were carried out at forward and reverse bias voltage. The CCE improvement occurred at each step, and its twofold total improvement was observed regardless to the bias polarity. The negative effect of detector polarization was observed that may be caused by the carrier trapping to the residual non-annealed defects.

2.4 New Structures (NS)

- A further set of *thin detectors* is under production in the framework of RD50. Several wafers of epitaxial and SOI silicon strip and pad detectors of 75 to 150 µm thickness are expected to be processed until Summer 2008.

- Characterization of *Single Column Type 3D sensors:* 3D-stc sensors produced by FBK-irst have been investigated by means of position sensitive multichannel Transient Current Technique (TCT) and by means of Charge Collection Efficiency tests performed with Infrared lasers and β-sources. The performance obtained before and after irradiation is matching the results expected from simulations.

- *Double sided 3D detectors* have been produced at CNM Barcelona. The devices have both p- and n- columns, as in a 'full 3D detector'. However, contrary to 'full 3D detectors' the holes of one doping type are etched from the front side of the wafer, and the holes of the other type are etched from the back side. Furthermore, the columns do not pass through the full thickness of the substrate. First electrical tests of these devices show promising results.

- *3D Double-side Double Type Column (3D-DDTC) sensors* have been produced at FBK-irst in a very similar design compared to the above mentioned sensors from CNM. The first electrical tests of the sensors show very good results.

- *Full 3D sensors* have been produced at IceMOS, Northern Ireland. These devices have the contacts for both type of columns on the same side. The sensors have been produced, but are not tested yet.

2.5 Full detector Systems (FDS)

- *CCE measurements on p-type strip detectors after severe neutron irradiations* have been performed using fast LHC readout electronics. The results are in line with the previously obtained results obtained after 24 GeV/c proton irradiations and demonstrate that after a fluence of $3x10^{15}$ neutrons about 12000 electrons can be collected with very high voltages applied (1000V). A long term annealing experiment showed no degradation in the obtained CCE over time.

- Results on the *RD50 Micron 6" wafer program*: The measurements performed on Pad detectors and on Single Sided Strip detectors (SSD's) made with different crystals and performed with different methods and read-out electronics showed a very good agreement. The CCE measurements show that the total collected charge, therefore the trapping, does not depend on the different crystal type. The same CCE is expected provided that sufficient bias can be applied to the detector. The measurements have shown that with neutron irradiation the low resistivity, inverting MCz n-type substrate can offer significant advantages of CCE at low voltages due to the lower depletion voltage after irradiation. The studies of the annealing effects on the CCE of SSD's has confirmed that a limited variation of the CCE is observed over a period equivalent to 3 years at room temperature.

- In the framework of the Italian *SMART project* strip detectors produced from n- and p-type MCZ, EPI and FZ silicon and irradiated with 24 GeV/c protons, 26 MeV protons and reactor neutrons have been investigated using the readout electronics designed for the CMS Tracker. The measurements confirm the good performance of single sided p-type silicon detectors against single sided n-type strip detectors.

3 Defect and Material Characterization

3.1 General introduction and remarks

During 2007 (and in accordance with our long-term strategy), the activity in the DMC research line has to a large extent been focused on cluster related defects, which are considered to be responsible for the reverse leakage current and charge carrier trapping in silicon particle detectors. In particular, charge carrier trapping is considered to be the ultimate limitation for detector applications using semiconductor materials but the identity of the main responsible trap(s) remains unknown.

Moreover, the DMC core activities are since the fall of 2006 performed in a closely coordinated manner through the network WODEAN (named after the workshop "WOrkshop on DEfect Analysis" held in Hamburg, Aug-2006), initiated and skillfully managed by the Hamburg group. Hallmarks for WODEAN are; (i) ***use all available methods*** (DLTS, TSC, PITS, PL, trecomb, FTIR, PC, EPR, diode C/V, I/V and TCT), (ii) ***concentrate on a single material only*** (MCz is chosen with extension to std. FZ for checking of unexpected results. FZ supposed to be cleaner, MCz has larger O concentration) (iii) ***use only one type of irradiation*** (most readily available is the TRIGA reactor at Ljubljana) and ***do limited number of fluence steps between $3x10^{11}$ and $3x10^{16}$ n/cm²*** (same for all analysis methods!) and (iv) ***use the same isothermal annealing steps for all methods***. This is a rather unique approach and it is our firm believe/ambition that more efficient progress will be made through WODEAN than by pursuing the more traditional approach based on loosely coordinated and single efforts. In fact, the results obtained during 2007 are encouraging and evidence for a microscopic identification of one crucial cluster defect is presented.

3.2 Defect clusters after neutron and electron irradiation studied by DLTS, TSC and FTIR

It is generally accepted, that the evolution in time of both the leakage current and N_{eff} after hadronic irradiation is due to cluster related defects. Five defect levels associated with extended lattice defects were detected by means of DLTS and TSC measurements. They are labelled in the following as E4, E5, H(116K), H(140K) and H(152K). All are acceptor like defects but the first two ones have energy levels in the upper part of the Silicon gap while the energy levels of the latter three ones are located in the lower part of the gap.

3.2.1 The E4 and E5 levels

These defects were investigated by means of DLTS in different type of silicon diodes (MCz, FZ, EPI-ST and EPI-DO diodes) after low irradiation fluences of 6 MeV electrons and 1 MeV neutrons. Special attention was paid to the annealing behaviour of the cluster related defects E4 and E5, via isothermal annealing studies at different temperatures. Storage temperature of samples between measurements was -20 °C.

3.2.1.1 6 MeV electron irradiation

Figure 3-1 shows the evolution of the E4 and E5 levels, located ~0.37 and ~0.45 eV below the conduction band edge, E_c, respectively, as a function of time at room temperature. The spectra in Fig.3-1 are differential ones with respect to the spectrum obtained after 2036 h at RT in order to remove the contributions from more stable and overlapping levels, like the single negative charge of the divacancy center, and clearly resolve the E4 and E5 levels. The close one-to-one proportionality between the intensities of the two peaks provide strong evidence that that they originate from the same defect center and they are presumably due to different charge state transitions of this defect[1]. In addition, the generation rate of E4/E5 increases relative to that of the vacancy oxygen center (VO)

with electron energy (as well as projectile mass using neutrons and ions) suggesting that the E4/E5 defect is cluster like (higher order).

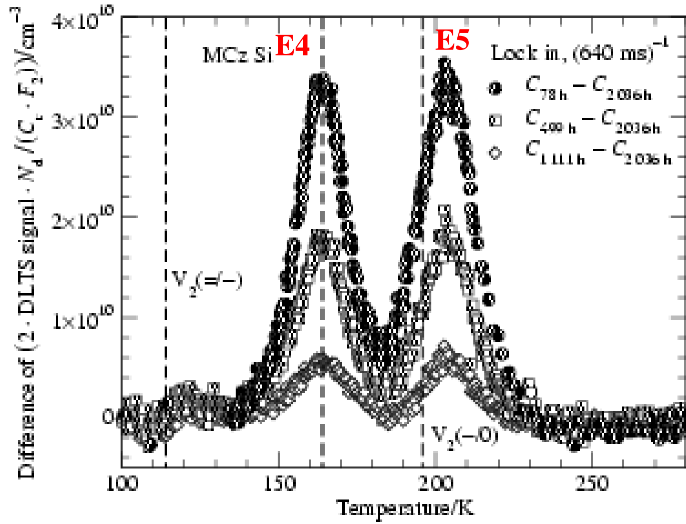

Fig.3-1 Difference-DLTS spectra of a MCz Si diode irradiated with 6 MeV electrons to a fluence of 5x10^{12} cm^{-2} for different annealing times at RT.

The possible correlation of E4/E5with the annealing of the radiation induced current was investigated in FZ and EPI diodes via annealing studies at 60°C. The irradiation fluences were 3x10^{13} e/cm^2 for FZ and EPI DO diodes and 2x10^{13} e/cm^2 for EPI ST. The time evolution of concentration of E4 and E5 defects as well as of radiation induced leakage current, all normalised to the irradiation fluence are shown in Fig.3-2.

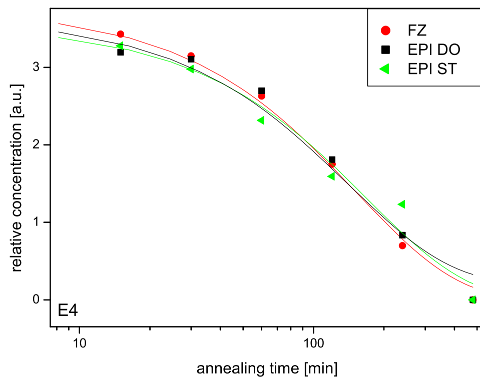

a)

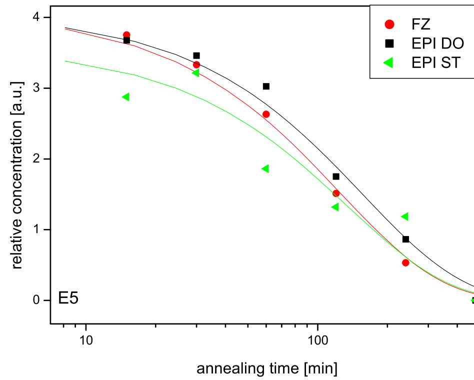

b)

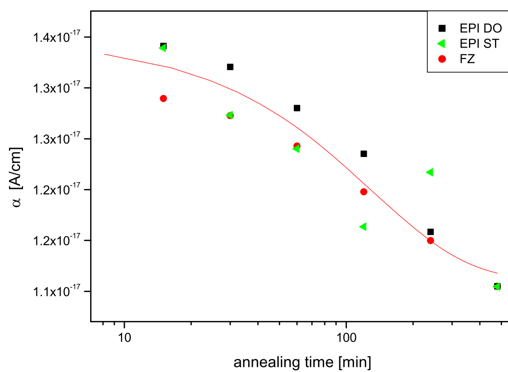

c)

Fig.3-2 The time evolution of E4 (a) and E5 (b) defects concentration and of radiation induced leakage current (c), all normalised to the irradiation fluence.

The different defect concentrations of E4 and E5 obtained in different materials is not necessarily due to some differences between the investigated materials but may be also due to the real accumulated fluences which may be not the same with the nominal ones The time constants for the annealing of E4 and E5 were obtained by first order exponential decay fits as it is shown in the figure and the obtained values are given in Tab. 3-I. The current related damage rate α is decreasing with a time constant of $\tau_{(\alpha)=}$ 131±33 min.

Tab. 3-I: Time constants for the annealing of E4 and E5 after 6MeV electron irradiation.

Defect		FZ	EPI DO	EPI ST
$\tau_{(E4)}$	[min]	153±9	166±16	169±22
$\tau_{(E5)}$	[min]	126±9	157±14	136±33

3.2.1.2 Neutron irradiation

The irradiation fluences were $6x10^{11}$ n/cm^2 for FZ, EPI-ST and EPI-DO and $3x10^{11}$ n/cm^2 for MCz. The time evolution of concentration of E4 and E5 defects as well as of radiation induced leakage current, all normalised to the irradiation fluence are shown in Fig.3-3.

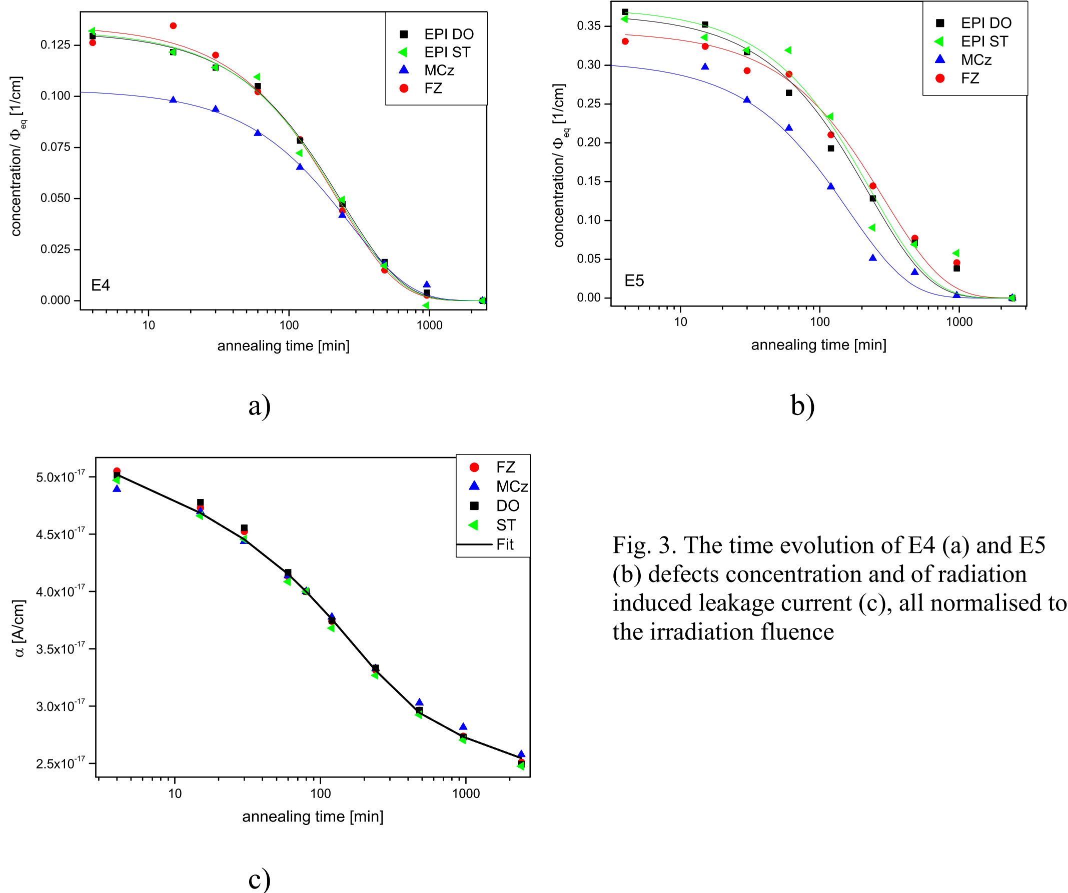

Fig. 3. The time evolution of E4 (a) and E5 (b) defects concentration and of radiation induced leakage current (c), all normalised to the irradiation fluence

The time constants for the annealing of E4 and E5 were obtained by first order exponential decay fits as it is shown in the figure and the obtained values are given in Tab. 3-II. The current related damage rate α is decreasing with a time constant of $\tau_{(\alpha)=}$ 173±9 min.

Tab. 3-II: Time constants for the annealing of E4 and E5 and current related damage rate α after 1MeV neutron irradiation.

Defect		FZ	MCz	EPI DO	EPI ST
$\tau_{(E4)}$	[min]	222±13	270±10	238±7	230±14
$\tau_{(E5)}$	[min]	291±31	161±16	224±23	233±35

These correlation studies between the DLTS investigations and I-V measurements performed at room temperature revealed that after electron irradiation the time constants for the annealing of E4, E5 and α are very similar suggesting a possible direct correlation between these defects and α . After neutron irradiation however, this correlation is not clearly seen. While α as measured by I-V at room temperature is independent on the material type having the value $\tau_{(\alpha)}$=173±9 min the time constants for annealing out of E4 and E5 defects are up to 60% larger than that of the leakage current $\tau_{(\alpha)}$=173±9 min.

3.2.2 H(116K), H(140K) and H(152K) cluster related defects

In order to investigate the effect of cluster related defects on the annealing of N_{eff} , TSC studies were performed on diodes exposed to fluences of $5x10^{13}$ cm^{-2} neutrons. The annealing was performed at 80°C. The recorded TSC spectra are shown in Fig. 3-4a and b for neutron irradiated EPI-DO and MCz, respectively. Fig. 4a contains also a comparison of the spectrum recorded for forward injection with the one obtained for only electron injection both after the same annealing time. The signals denoted with H(116K), H(140K) and H(152K) are corresponding to hole traps and they are caused by hadron irradiation only. While the H(116K) and H(140K) signals were never detected after gamma- or low energy electron irradiation the peak denoted here as H(152K) was so far attributed entirely to the donor state of the C_iO_i complex regardless of the irradiation type or filling temperature (T_0).

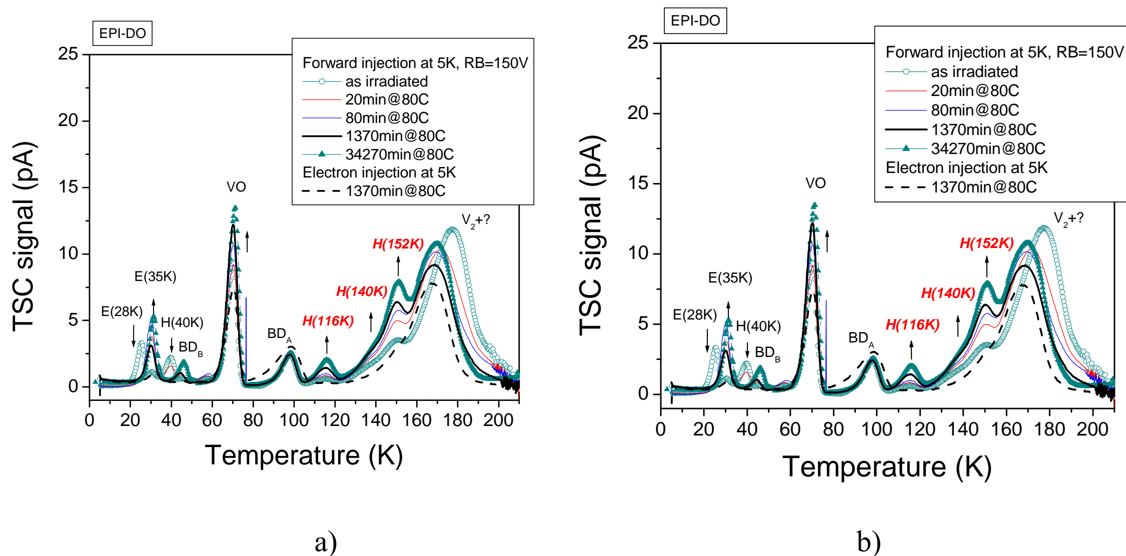

Fig.3-4. TSC spectra after forward injection on: a) neutron irradiated EPI-DO diode after different annealing times at 80 ^{0}C, T_0 = 5K; b) neutron irradiated MCz diode after different annealing times at 80 ^{0}C, T_0 = 5K

We have demonstrated that for T_0 < 30K the C_iO_i traps cannot be filled by forward biasing [2]. This means that the H(152K) signal shown in Fig.2a and b recorded after forward injection at 5K is not affected by the emission from the C_iO_i center. In addition, all the H(116K), H(140K) and H(152K) defects show a significant field-enhanced emission as revealed by the TSC measurements under different reverse biases depicted in Fig.3-5.

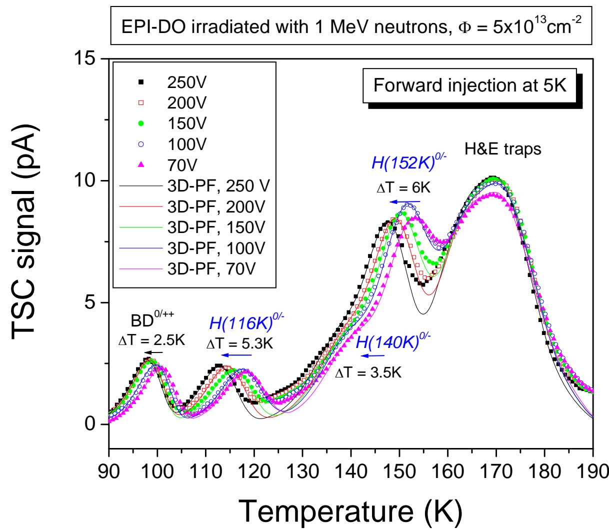

Fig.3-5. TSC spectra for different applied biases on neutron irradiated EPI-DO after 34270 min at 80 ^{0}C - experimental (scatters) and calculated (3D-PF lines).

While the defect concentration can be calculated from the peak area delimited by the TSC spectrum the evaluation of trapping parameters for Coulombic centers needs more considerations. The linear dependence of the electric field throughout the diode thickness will cause different emission rates for centers located in different depth regions of the diode. This is the reason for broadening and asymmetry of the TSC peaks, causing a very inaccurate evaluation of the emission rates using the common methods based on Arrhenius plots. For investigating this type of centers we have applied the three-dimensional Poole-Frenkel effect (3D-PF) model where we accounted for the spatial distribution of the electric field inside the diodes. The parameters for the zero field emission rates describing the experimental results are: $\sigma_p^{116K} = 4\cdot10^{-14}$ cm^2 and $\Delta H_a^{116K} = 0.33$eV, $\sigma_p^{140K} = 2.5\cdot10^{-15}$ cm^2 and $\Delta H_a^{140K} = 0.36$eV as well as $\sigma_p^{152K} = 2.3\cdot10^{-14}$ cm^2 and $\Delta H_a^{152K} = 0.42$eV. Examples of the calculated TSC curves are given in Fig. 4 as 3D-PF lines together with the measured spectra. It can be seen that the 3D-Poole Frenkel formalism considered for a linear distribution of the electric field reproduces the measured spectra. This is finally pointing out that the hole traps H(116K), H(140K) and H(152K) are acceptors in the lower part of the silicon gap and thus they contribute with their full concentration as negative space charge to N_{eff}^0 in n-type silicon diodes. In Fig. 3-6 the change in N_{eff} after irradiation, determined by C-V measurements at RT, are represented and compared with the change of N_{eff}^0 due only to the H(116K), H(140K) and H(152K) centers. Is resulting thus that these acceptors are responsible for the

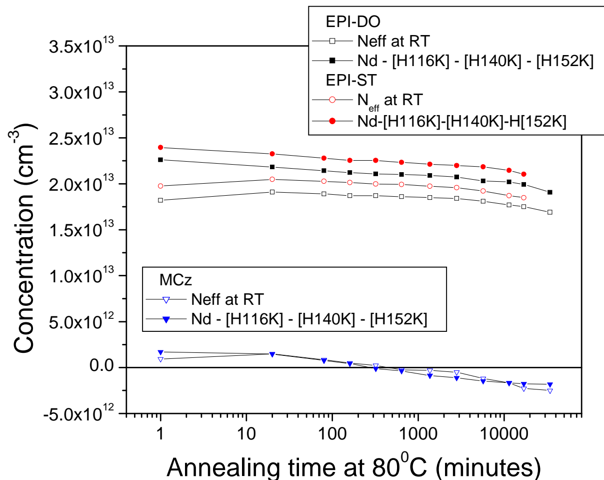

Fig.3-6. Change of N_{eff} determined at 293K from C-V measurements (open symbols) and calculated change of N_{eff} due to the negative space charge introduced by H(116K), H(140K) and H(152K) traps (filled symbols).

long term annealing of N_{eff} in hadron irradiated silicon diodes. The difference seen for EPI diodes may very well be due to the vacancy-phosphorus centers (donor removal), which should have an enhanced generation in this sample (due to the higher P content).

2.3. 936 cm^{-1} infrared absorption band

FTIR measurements of neutron-irradiated MCz samples using fluences between 1x10^{15} and 3x10^{16} cm^{-2} reveal, in addition to the characteristic absorption at 836 cm^{-1} caused by the neutral VO center, a pronounced absorption at 936 cm^{-1} (measurement temperature 25 K), Fig,3-7. The identity of the 936 cm^{-1} band, which is due to a local vibrational mode of oxygen, is reasonably well-established and it is ascribed to a disilicon-interstitial-oxygen pair $(I_2O)^2$. The generation of the 936 cm^{-1} band is enhanced by neutron irradiation relative to that for low MeV electron irradiation, consistent with the assignment to I_2O. Further, the 936 cm^{-1} has a limited temperature stability and disappears after a few hours at 80 °C, as illustrated by the difference-spectra in Fig.3-8. In fact, a detailed study of the annealing kinetics yields a first-order process (exponential decay) with very similar values as those obtained for the annealing of the E4/E5 center. Hence, it may be speculated that 936 cm^{-1} band and the E4/E5 levels are due to the same defect center, that is, the I_2O pair. Moreover, since E4/E5 is a crucial defect for the leakage current in irradiated Si particle detectors these results can have large implications for defect engineering of future radiation hard Si detectors; an obvious conclusion would be to use silicon wafers that are both oxygen lean and carbon lean. Further work is in progress to substantiate these indications.

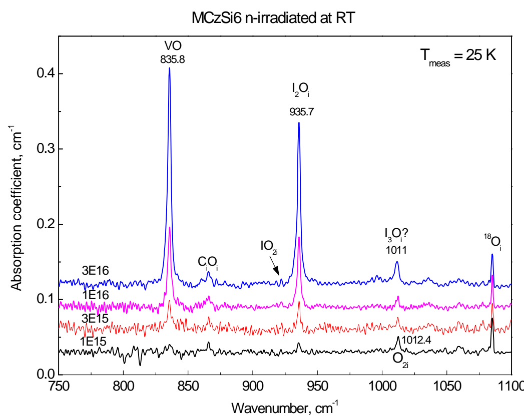

*Fig.3-7*Absorption spectra at 25 K for different absorption neutron fluences

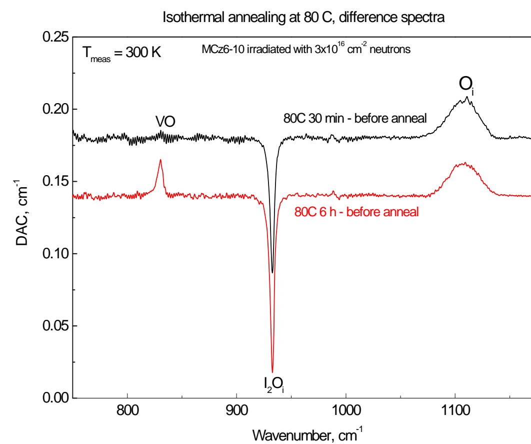

Fig.3-8 Difference between FTIR spectra before and annealing at 80 °C.

3.3 Defect clusters after neutron irradiation; analysis by Hall effect, magnetoresistance and lifetime measurements

In low fluence samples (≤10^{12} cm^{-2}), the mobility of free carriers measured by Hall effect and magnetoresistance are very similar for temperatures around 300 K. However, if the fluence increases or/and the temperature is lowered a significant difference between the mobility values appears. This implies that the samples become inhomogeneous, rather than displaying different scattering mechanisms, and the carriers move predominantly through 'percolation channels'. These results are illustrated in Figs.3-9 and 3-10 and the conclusions are also supported by the transient Hall effect measurements performed after illumination, Fig.3-11, providing evidence for local electric fields (Fermi level pinning) caused by regions having a high defect density.

The Hall mobility is more sensitive to localization of the current flow than that of the magnetoresistance and the decrease observed in both Figs.3-9 and 3-10 is mostly related to narrowing of the conducting channels. The increase in magnetoresistance mobility with decreasing temperature shows a more expected behaviour and the close to linear dependence corresponds to the prevailing of scattering by defect clusters or/and dislocations.

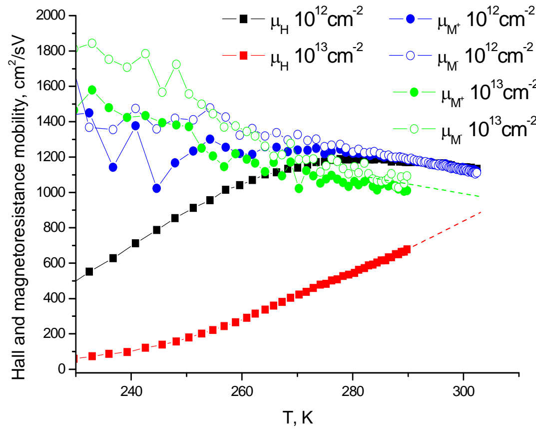

Fig.3-9 Hall and magnetoresistance versus sample temperature

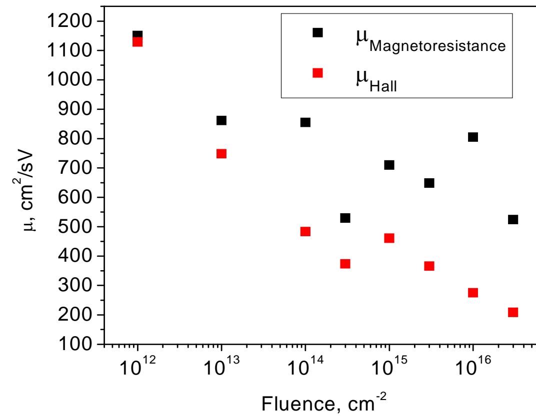

Fig.3-10 Hall and magnetoresistance versus versus neutron fluence

Fig.3-11 Hall mobility transients after excitation by a short light pulse at room temperature.

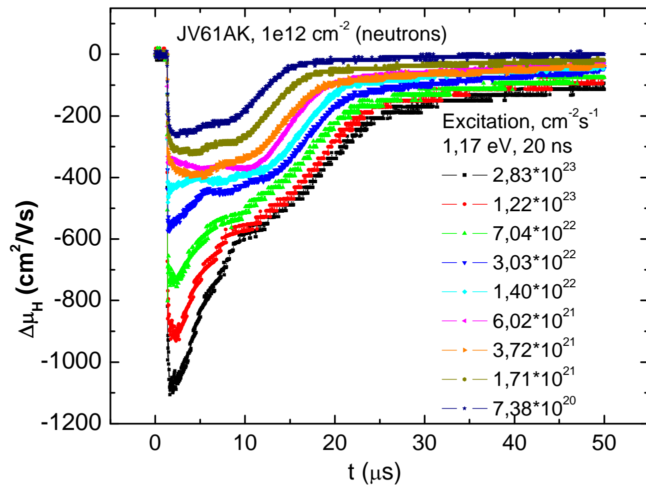

Fig.3-12 shows the recombination lifetime versus neutron fluence ranging from 10^{12} to $3x10^{16}$ cm^{-2}. The lifetime, measured by microwave absorption in combination with transient grating technique using short laser pulse excitation, exhibits a nearly linear decrease with the fluence in the non-annealed samples. Some deviations occur for the highest fluences and especially in the annealed samples; this indicates changes in the recombination process and/or changes in the structure of the recombination/trapping centers. However, the overall conclusion is that the lifetime is controlled by linear fluence effects and only minor deviations occur despite the fact that localized regions with high density of cluster defects prevail after the neutron irradiation.

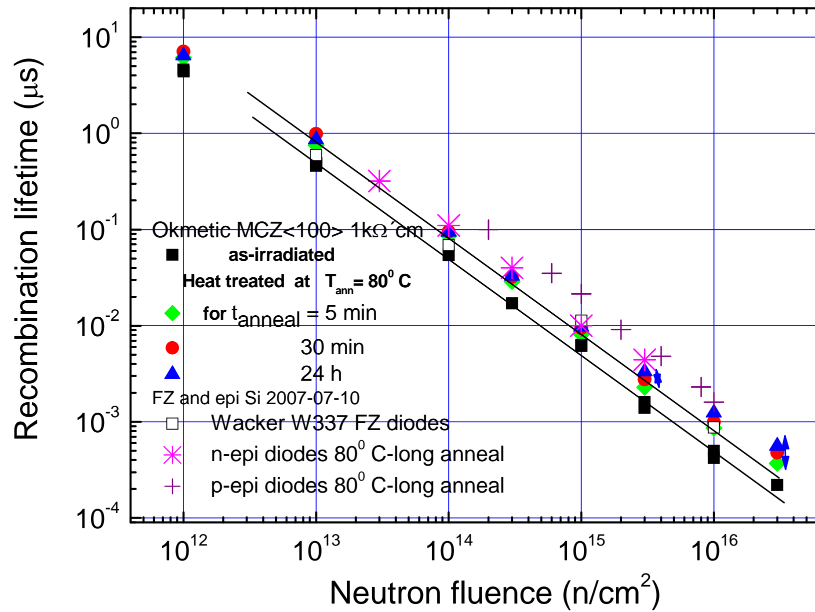

Fig.3-12 Recombination lifetime versus neutron fluence in three different types of silicon materials after irradiation and irradiation plus isothermal annealing at 80 °C.

3.4 On the validity of NIEL scaling

It is frequently assumed that changes of electrical properties of semiconductor devices are proportional to the non-ionizing energy loss (NIEL)[3] (or elastic energy deposition) during particle irradiation and different ways of scaling experimental data are used [4] for various irradiation conditions, radiation fields and materials. The radiation fields in the interaction cavity at the new high energy facilities in HEP as LHC, SLHC and VLHC for example, or in space, where new missions and experiments will be operated, are indeed extremely complex; tests for concrete studies of the behaviour of different materials and devices are difficult, time consuming and expensive. Thus, accurate scaling of degradation effects is highly desirable. However, until now there is no real theoretical – microscopic understanding/validation of why radiation damage should scale with NIEL. In particular, this holds for the formation of cluster defects.

In the present activity, we try to bring some clarification on this critical issue and a main challenge is the comparison between NIEL and experimental data for defect generation. This is due to the fact that an intermediate stage exists in the ‘chronological order’ of the production of permanent degradation/damage. NIEL refers to the energy transferred into atomic displacements, i.e. to a number of vacancies and interstitials. In the semiconductors of interest (e.g. Si, Ge, GaAs and others) these defects have a high mobility and could interact mutually or with other defects and residual impurities in the lattice, producing the “stable” degradation/damage, which is observed experimentally. Hence, conditions such as impurity concentrations and mobility, irradiation temperature, flux, defect concentrations and mobility, and fluence are of crucial importance. The resulting defect evolution becomes complex [5] and an accurate description of the dominant processes, in terms of a quantitative simulation model of the defect evolution, is a main goal of this activity.

3.5 References for Chapter 3

[1] J.H. Bleka, E.V. Monakhov, B.G. Svensson and B.S. Avset, Phys. Rev. B **76**, 233204 (2007)

[2] J. Hermansson, L.I. Murin, T. Hallberg, V.P. Markevich, M. Kleverman, J.L. Lindström and B.G. Svensson, Physica B **302-303**, 188 (2001)

[3] G. Lindström, Nucl. Instr. Meth. Phys. Res. A **512**, 30–43 (2003)

[4] H-H Fischer, K. Thiel, SPENVIS&GEANT4 Workshop, ESA GSP 2005, Faculty Club Leuven, October 2005

[5] I. Lazanu, S. Lazanu , Physica Scripta **66**, 125 (2002).

4 Defect Engineering

4.1 Standard and DOFZ silicon

Both standard and oxygenated FZ (DOFZ) silicon is mainly investigated for comparison with high resistivity Magnetic Czochralski silicon (MCz), epitaxial silicon (EPI) or pre-irradiated FZ and MCz silicon. In 2007 intense work had been performed on p-type material, motivated by promising results of improved charge collection properties in structured detectors (strip detectors). In heavily damaged detectors the degradation of the charge collection efficiency by charge carrier trapping is one of the limiting factors for the innermost layers of the tracking detectors in SLHC experiments. In case of strong trapping segmented n^+-p-p^+ structures present the advantage that the signal is dominated by electron collection and, therefore, less trapping is expected due to the higher mobility of electrons (shorter collection time) compared to holes.

Thin segmented detectors with short strips or pixels manufactured in n^+-n or n^+-p technology as well as 3-D detectors are options for optimizing the charge collection efficiency.

4.2 Epitaxial and MCz silicon

In continuation of the research plan new n- and p-type epitaxial layers with a thickness of 100 and 150 µm were grown by ITME. The pad-diodes were manufactured by CiS using different process technologies, either the standard process technology (denoted as EPI-ST) or performing an oxygen enrichment of the epi layer by a heat treatment for 24 hours at 1100 °C (denoted as EPI-DO), preceding the standard process steps. This way not only the oxygen concentration should be manipulated in the epi-layer but also the concentration of oxygen dimers. Since for all processed p-type devices break down voltages below full depletion were measured, they were not included in the irradiation campaign with 24 GeV/c protons in 2007.

4. 2.1 Material properties

In table 4-2-1 the main properties of the different n-type epitaxial layers and process variants are summarized.

Table 4-2-1 Material properties of EPI-layers

EPI-material	Type	Thickness [µm]	Resistivity ρ [Ω·cm]	Oxygen* [10^{16} cm^{-3}]
EPI-ST	n	72	150	9.2
EPI-DO	n	72	150	65
EPI-ST	n	100	300	5.4
EPI-DO	n	100	300	28
EPI-ST	n	150	480	4.5
EPI-DO	n	150	480	14

* the given concentrations represent mean values derived from the measured SIMS depth profiles.

The depth profiles of the resistivity for the 100 and 150 µm epi-layers are displayed in Fig. 4-2-1. The mean values are (300 ± 10) and (480 ± 14) Ω·cm for the 100 and 150 µm epi-layers respectively. For the Sb doped Cz substrate a value of $\rho = (1.2 \pm 0.3)\cdot 10^{-2}$ Ω·cm is observed.

The oxygen and carbon concentrations had been measured by Secondary Ion Mass Spectroscopy (SIMS) for the epi-layers [1]. In Fig. 4-2-2 the depth profiles are displayed for an EPI-ST sample after being fully processed and for an EPI-DO sample after oxygen enrichment, as mentioned above, followed by the standard process steps.

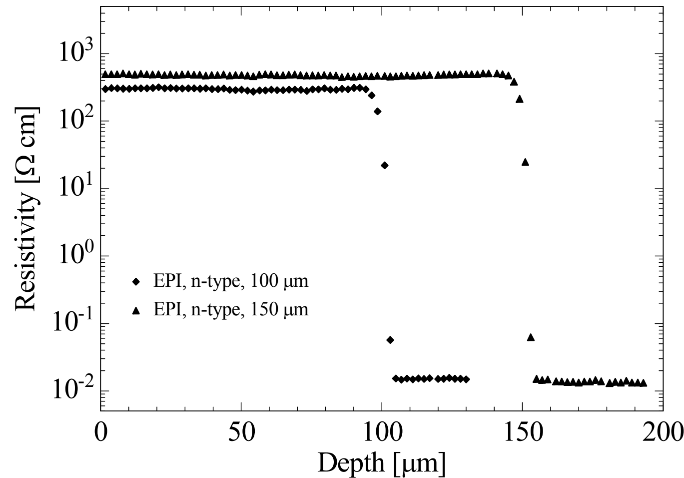

Fig. 4-2-1 Resistivity depth profiles as measured by spreading resistance for 100 and 150 μm n-type epi layer.

As can be seen for the as processed standard epi-layers (EPI-ST) oxygen is out-diffusing from the Cz substrate into the epi-layer up to a depth from the epi-layer substrate interface of about ½ of the total epi-layer thickness. The depth profile of the oxygen concentration near to the front side is due to an in-diffusion from the SiO_2-Si interface leading to an error function like distribution of the oxygen concentration in this surface region. In total a O-depth profile is achieved, which starts at the front side of the epi-layer with a concentration of about $8 \cdot 10^{16}$ cm^{-3}, decreases to values of about $2 \cdot 10^{16}$ cm^{-3} in a depth of 40 μm for the 100 μm epi-layer and about $9 \cdot 10^{15}$ cm^{-3} at 60 μm for the 150 μm layer. After these minimal values the concentrations increase up to $3.5 \cdot 10^{17}$ cm^{-3} at the epi-layer substrate interface for the 100 μm layer and $2.9 \cdot 10^{17}$ cm^{-3} for the 150 μm layer. Similar strong non-homogeneous profiles are typically observed for samples of fully processed epi-layers without the oxygenation treatment [2].

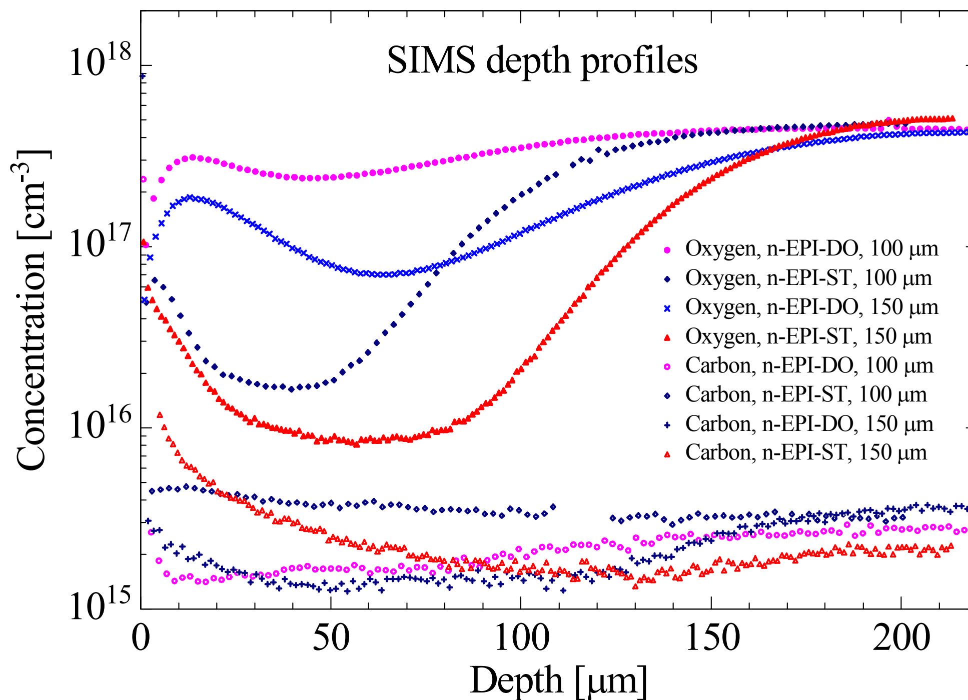

Fig. 4-2-2 Oxygen and carbon concentration profiles measured with SIMS in 100 and 150 μm n-type epi-silicon: after oxygen enrichment and full processing (EPI-DO), after standard processing (EPI-ST).

The oxygen enrichment at 1100 °C promotes further the out-diffusion from the substrate resulting in more homogeneous distributions throughout the main part of the epi bulk excluding the surface region of 10 µm, where a decrease of the oxygen concentration is observed, most likely caused by an out-diffusion of oxygen.

The carbon concentrations in the epi-layers vary between $1.2\cdot10^{15}$ cm^{-3} and $5\cdot10^{15}$ cm^{-3} for the different processing procedures but these values are supposed to be already below the detection limit of the SIMS-method.

For the MCz sample the SIMS depth profile of the oxygen concentration is shown in Fig. 4-2-3. Also in this case an out-diffusion of oxygen at the surface can be seen. As the carbon concentration is concerned, a value of $[C] = 2.5\cdot10^{15}$ cm^{-3} is observed. As mentioned before such a small concentrations is expected to be below the detection limit.

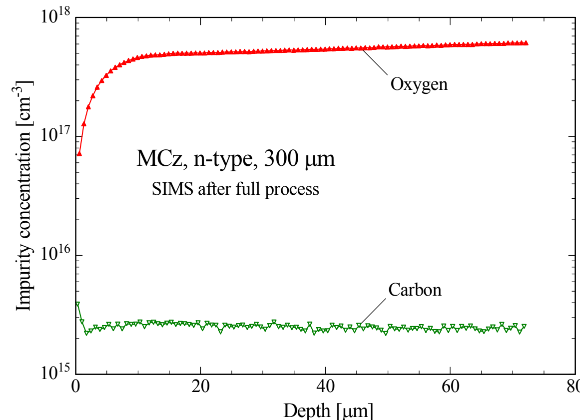

Fig. 4-2-3 Oxygen and carbon concentration profiles measured with SIMS in 300 µm thick n-type MCz silicon after full processing.

4.2.2 Donor and acceptor generation in EPI- and MCz-silicon

It had been shown that the space charge sign of n-type epi-layers with a thickness of 25, 50 and 75 µm and a resistivity of 50 Ω·cm stays positive after 24 GeV/c proton damage up to fluences of 10^{16} cm^{-2} [2]. For large fluences in epi-diodes the creation of acceptors is obviously always overcompensated by an introduction of shallow donors. The formation of these shallow donors was investigated by the Thermally Stimulated Current (TSC) method and it was demonstrated that the TSC signal due to the shallow donor had a very similar dependence on the material as the average oxygen concentration and the stable damage generation [2, 3]. It is believed that this radiation induced donor is related to oxygen dimers O_{2i}.

Previous DLTS studies [4] had shown that the introduction rate of the O_{2i} related defect IO_{2i} exhibits a quadratic dependence on the oxygen concentration in the material as suggested by the result of L. I. Murin et al. [5]. As the IO_{2i} defect complex can be regarded as an indicator for the presence of O_{2i} in silicon it is suggested that under some prerequisites its concentration may be taken as a relative measure for the O_{2i} concentration in the material. The importance of O_{2i} for the formation of shallow donors in silicon after 24 GeV/c proton irradiation had been outlined in several papers [2, 3, 6].

It is expected that for neutron damage the introduction of shallow donors differs considerably to that induced by charged hadrons because neutron damage is dominated by cluster generation while charged hadrons produce more point defects. Therefore, investigations of macroscopic device properties in correlation with microscopic studies (TSC measurements) in 72 µm standard (EPI-ST) and diffusion oxygenated epitaxial layers (EPI-DO) as well as 300 µm MCz material were performed after exposure to reactor neutrons [7]. For example the development of the effective doping concentration as function of fluence (see Fig. 4-2-4) indicates that all materials undergo space charge sign inversion, depending on the initial doping concentration (donor removal) and the effective introduction of acceptors and donors. The space charge sign inversion had been proven by TCT-measurements with 670 nm laser light.

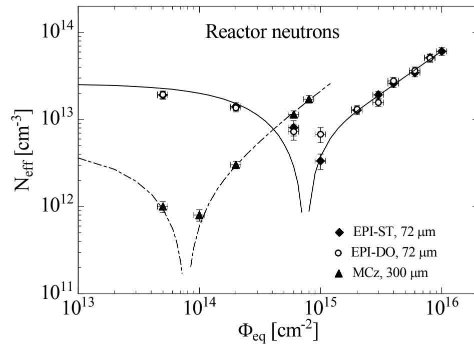

Fig. 4-2-4 Effective doping concentration as function of fluence, as measured after annealing for 8 minutes at 80 °C.

In earlier studies on 50 µm n-type epi-devices with an initial doping of about $7\cdot10^{13}$ cm^{-3} it was demonstrated that this material does not undergo type inversion during exposures to reactor neutrons [2]. Thus, the question is why the 72 µm epi-material undergoes type inversion no matter of the epi-type (EPI-ST or EPI-DO). A natural explanation would be that in this case the introduction rate of shallow donors is suppressed or strongly reduced to a level sufficiently below that of acceptors.

TSC measurements on all materials after irradiation with $5\cdot10^{13}$ n/cm^2 demonstrate that shallow donors (denoted as bistable donor $BD^{0/++}$ in Fig. 4-2-5) are generated in both epi-materials but in a much lower concentration in MCz material. All spectra shown in Fig. 4-2-5 are taken for a reverse bias voltage which guaranties that the diodes stay fully depleted in the overall TSC temperature range. For the first time the bistability of the BD center could be directly observed in the EPI-DO diode as shown in Fig. 4-2-6. In the TSC spectrum measured directly after irradiation a peak at 49 K (attributed to $BD^{+/++}$) is recorded which vanishes after a short storage time of 3 hours at room temperature, but during a second measurement a strong increase of the (0/++) transition of the BD center is observed.

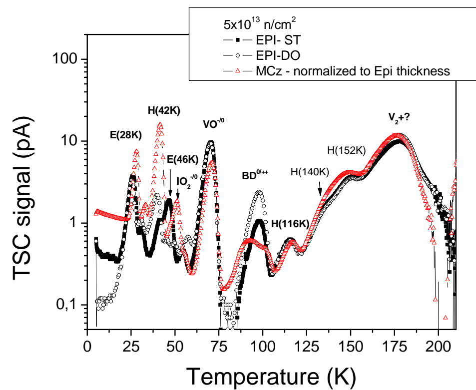

Fig. 4-2-5 TSC spectra after irradiation with $5\cdot10^{13}$ n/cm^2 recorded on a EPI-ST, EPI-DO and MCz diode. The TSC current of the 300 µm thick MCz diode is normalized to the thickness of the EPI diodes (72 µm).

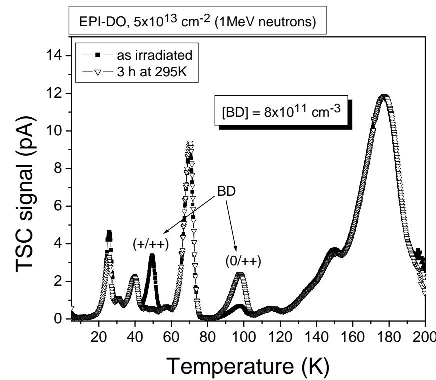

Fig. 4-2-6 TSC spectra recorded on a EPI-DO diode as irradiated to $5\cdot10^{13}$ n/cm^2 and after storage for 3 hours at 295 K.

The donor activity of both BD transitions had been proven by the temperature shift of their peak position as function of the applied bias voltage (Poole-Frenkel effect) which is shown in Fig. 4-2-7. In addition to the bistable donor BD a TSC signal at 45 K (labeled E(45K) shows also a strong temperature shift of the peak position to lower temperatures with increasing bias voltage pointing to a donor characteristic of this defect (see Fig. 4-2-8).

Annealing at 80 °C showed that the concentration of donors slightly increases (about 20 %) during the first period of about 80 minutes in all materials (Fig. 4-2-9). The concentrations refer to the sum of the $BD^{0/++}$ signal and the TSC-peak E(45K). The introduction of these donors depends strongly on the material type. The BD concentration in the EPI-DO material is about a factor 1.5 larger compared to EPI-ST. This trend is understandable considering the higher oxygen concentration in EPI-DO but the

corresponding ratio of the oxygen concentration is about 7. On the other hand the much lower BD concentration in the MCz material was not expected since the oxygen concentration is

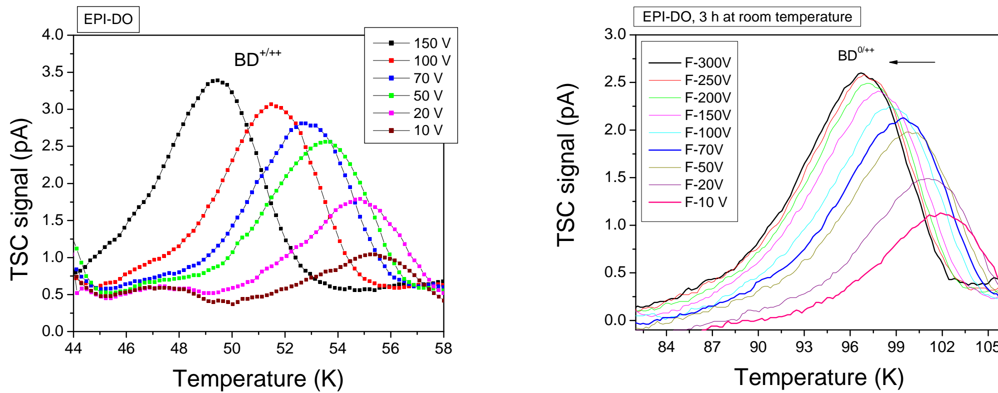

Fig. 4-2-7 Donor activity of the BD(+/++) (left hand side) and the BD(0/++) transition (right hand side). The TSC peaks are shifted to lower temperatures when increasing the reverse bias applied during TSC measurement.

nearly the same as measured in EPI-DO. Thus, a direct correlation of the BD concentration with the oxygen content in the material as measured by the SIMS-method cannot be stated. It is suggested that oxygen dimers O_{2i} are involved in the creation of these donors but so far this hypothesis could not be substantiated by experimental results. Especially the nearly identical oxygen content in MCz and EPI-DO would point to a similar concentration of O_{2i} [4] and, therefore, to a similar generation rate for the donors which is in contradiction to the observation.

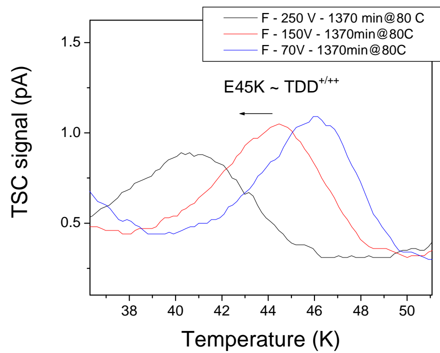

Fig. 4-2-8 Dependence of the E(45K) peak position on the applied reverse bias voltage (Pool-Frenkel effect).

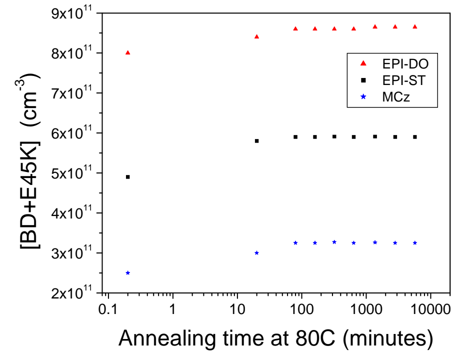

Fig. 4-2-9 Annealing behavior of the donor concentration (BD + E45K) at 80 °C in 72 μm EPI-DO, EPI-ST and 300 μm MCz diodes.

According to the TSC spectra in Fig. 4-2-5 three signals are observed in the temperature range between 110 K and 160 K which are hole traps and indicated by H(116K), H(140K) and H(152K). Recent TSC studies on these defects are described in the section 3 "Material and Defect Characterization" of this status report. So far the hole trap H(152K) was attributed to the donor state of the C_iO_i complex but it was proven by TSC measurements on γ-irradiated devices that at filling temperatures below 30 K the C_iO_i defect cannot be charged. In addition all three traps have an electric field enhanced emission characteristic, they are only detected after hadron irradiation and their long term annealing behavior can be fully correlated with the reverse annealing of the effective doping concentration.

In summary, all three hole traps are cluster related defects, they are acceptors with levels in the lower half of the band gap being negatively charged at room temperature and contribute therefore

with their full concentration to the space charge in the depleted region. These very recent results can be regarded as a major step forward in the understanding of the hadron damage in silicon on the basis of defect generation and defect kinetics.

Very first studies on all EPI devices (72, 100, 150 µm) after 24 GeV/c proton irradiation were performed. The development of the effective doping concentration N_{eff} as function fluence (1MeV neutron equivalent values) is shown in Fig. 4-2-10. Taking into account charge collection measurements for 670 nm laser light pulses as well as short term annealing experiments it could be concluded that the space charge of all devices stays positive in the overall fluence range under investigation.

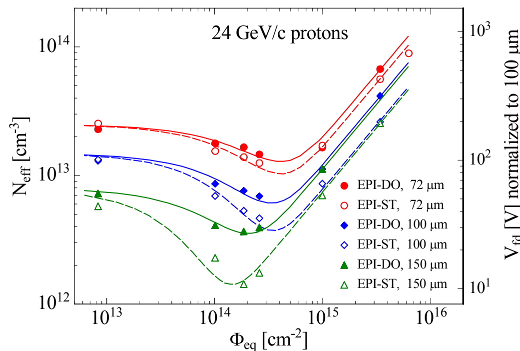

Fig. 4-2-10 Effective doping concentration as function of fluence for 72, 100 and 150 µm thick EPI-DO and EPI-ST devices after exposure to 24 GeV/c protons.

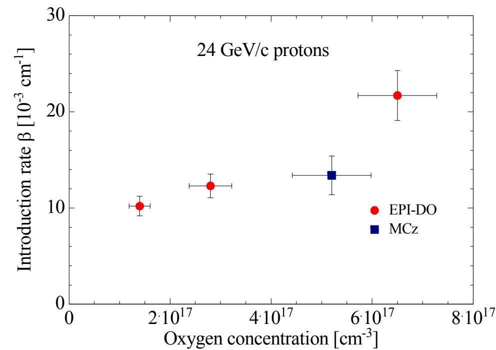

Fig. 4-2-11 Effective introduction rate of positive space charge versus average oxygen concentration in EPI DO and MCz diodes.

The fluence dependence of N_{eff} can be described by donor removal in the low fluence range and it is suggested that in the high fluence range the creation of shallow donors overcompensates the generation of acceptors. A further hint to this suggestion is the increase of the introduction rate β ($N_{eff}(\Phi_{eq}) = \beta\cdot\Phi_{eq}$ for $\Phi_{eq} > 10^{15}$ cm^{-2}) with the increasing oxygen content in EPI-DO and MCz diodes as shown in Fig. 4-2-11. The β values derived for EPI-ST devices were not included in Fig. 4-2-11 because of their very inhomogeneous oxygen concentrations. For a quantitative evaluation of the introduction of donors and acceptors detailed DLTS and TSC measurements will be performed.

4.3 Hydrogenation of silicon

A further defect engineering approach is the enrichment of silicon with hydrogen. It is well-known that hydrogen can easily penetrate into silicon crystals at various stages of detector processing [8]. It is expected that an enrichment with hydrogen will lead to more radiation tolerant devices due to hydrogen passivation of radiation induced defects [8, 9] and an acceleration of oxygen diffusion by promoting the formation of oxygen dimers O_{2i} [10-12].

A major problem of the hydrogen enrichment is the quantitative evaluation of the hydrogen content. The lower limit for the detection of hydrogen by the SIMS method is about 10^{17} cm^{-3}. A ten times higher sensitivity can be achieved for deuterium. Therefore, in a very first test experiment FZ samples were implanted with 710 keV deuterons. The dose value was chosen to be 10^{16} cm^{-2}. In order to prevent a fast out-diffusion of deuterium through the surface a 50 nm silicon nitride was deposited on top of the samples. Fig. 4-3-1 presents depth profiles of the implanted deuterium concentration as recorded by the SIMS technique. The as implanted profile has a peak concentration of about $2\cdot10^{20}$ cm^{-3} at a depth of 7.5 µm which corresponds to the range of 710 keV deuterons in silicon. A heat treatment at 400 °C for one hour leads to a considerable broadening of the primary profile by diffusion. For one sample the nitride layer was removed before heating resulting in a larger diffusion length in the direction towards the surface and a less pronounced tail in the direction of the bulk compared to the sample with the nitride layer on top of the surface. This experiment shows that also hydrogen can be detected by SIMS if the concentration exceeds values above 10^{17}cm^{-3}.

In a second experiment an array of nine 50 µm thick EPI-diodes grown on 300 µm Cz substrates will be implanted through the substrate with 5.5 MeV protons. This energy was chosen in order to get a layer with the maximal concentration at a position in the substrate which is about 15 µm away from the interface. This way the EPI-diodes will not be damaged by the proton beam. Several annealing procedures are assigned for a proper diffusion of the implanted hydrogen into the epitaxial layer which will be controlled by SIMS measurements. In case a sufficient large and homogeneously distributed hydrogen concentration can be achieved dedicated irradiation experiments are planed for the search of hydrogen related defects and possible improvements of the detector properties.

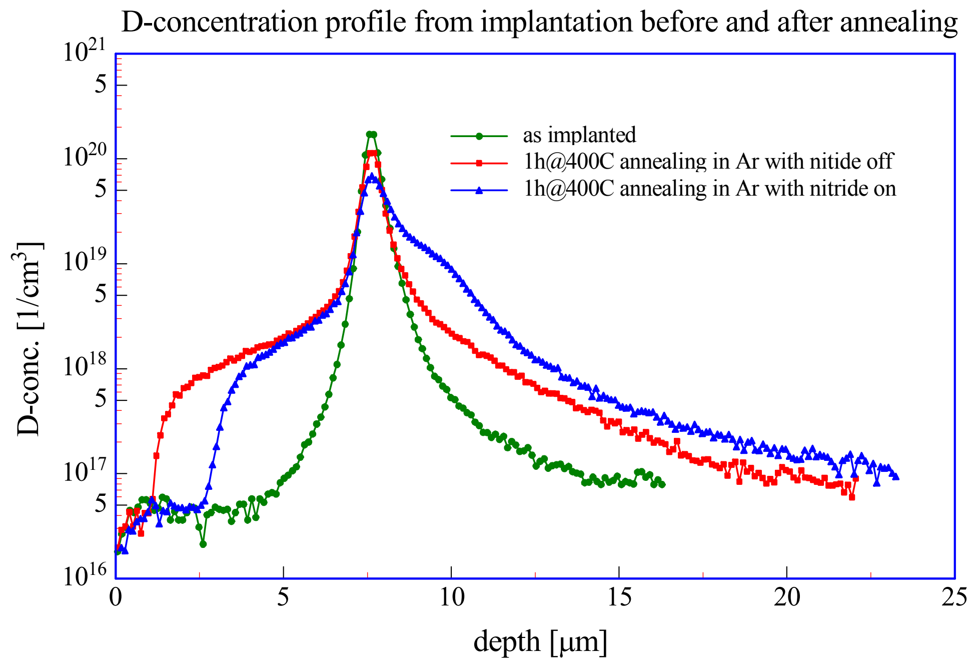

Fig. 4-3-1 Deuterium concentration depth profiles recorded by SIMS for as implanted and annealed samples at 400 °C for 1 h in Ar with and without a nitride surface layer.

4.4 Defect engineering by pre-irradiation treatments

In the frame of the RD50 research project, the INFN in Padova, the Institute of Nuclear Research (KINR) in Kiev, ITC IRST in Trento and CNM in Barcelona have investigated radiation hardening by preliminary neutron irradiation of silicon, which is expected to create gettering sites in the silicon bulk. Preliminary irradiation of silicon by fast neutrons and the subsequent annealing lead to the formation of sinks for primary radiation defects. These sinks are complexes of radiation-induced defects with neutral impurities, such as C and O, always present in the silicon wafers. The effect of pre-irradiation on the development of the effective doping concentration and the generation current as function of fluence for n- and p-type material was already described in the RD50 status report 2006 [13].

4.5 References for Chapter 4

[1] A. Barcz, SIMS laboratory, Physics Institute of the Polish Academy of Science, Warsaw, Poland

[2] G. Lindström, I. Dolenc, E. Fretwurst, F. Hönniger, G. Kramberger et al., Nucl. Instr. and Meth. A 568 (2006) 66-71

[3] I. Pintilie, M. Buda, E. Fretwurst, G. Lindström, J. Stahl, Nucl. Instr. and Meth. A 556 (2006) 197-208

[4] F. Hönniger, E. Fretwurst, G. Lindström, G. Kramberger, I. Pintilie, R. Röder, Nucl. Instr. and Meth. A 583 (2007) 104-108
[5] L.I. Murin, T. Hallberg, V.P. Markevich and J.L. Lindström, Phys.Rev.Letters Vol. 80 Number 1 (1998) 93-96
[6] G. Lindström, E. Fretwurst, F. Hönniger, G. Kramberger, M. Möller-Ivens, I. Pintilie, A. Schramm, Nucl. Instr. and Meth. A 556 (2006) 451
[7] E. Fretwurst, F. Hönniger, G. Kramberger, G. Lindström, I. Pintilie, R. Röder, Nucl. Instr. and Meth. A 583 (2007) 58-63
[8] S.J. Pearton, J.W. Corbett, M. Stavola, Hydrogen in Crystalline Semiconductors, Springer Verlag, Berlin 1992
[9] O.V. Feklisova, N. Yarykin, Semicond. Sci. Techn. 12 (1997) 111
[10] R.C. Newman, J.H. Tucker, A.R. Brown, S.A. McQuaid, J. Appl. Phys. 70, No.6 (1991) 3061
[11] V.P. Markevich, L.I. Murin, J.L. Lindström, M. Suezawa, Semiconductors 34, No. 9 (2000) 998
[12] R.C. Newman, J. Phys.: Condens. Matter 12 (2000) R335
[13] RD50 Status Report 2006, CERN-LHCC-2007-05 and LHCC-RD-013, CERN, January 2007

5 Pad Detector Characterization

5.1 Electric field profile

5.1.1 New method of electric field profile reconstruction from current pulse response data

A new method for the reconstruction of the electric field profile E(x) in irradiated Si detectors was developed by the Ioffe team. The method is based on the approach for double peak (DP) electric field distribution with three regions – two space charge regions (SCR) adjacent to the detector contacts and a base region *in between* [1-3]. The electric field in the base arises from a potential drop over high resistivity bulk of irradiated silicon and is non-zero. Therefore the current pulse response arises from the drift of non-equilibrium carriers through the entire detector thickness. This approach was successfully applied for the E(x) reconstruction using the DP current pulse response of silicon detectors irradiated with 1 MeV neutrons and 24 GeV/c protons. The procedure involves reconstruction of the electric field by fitting the simulated pulse response to the experimental one through the adjustment of the electric field and width of each of the three regions while fulfilling the condition:

$$\int_0^d E(x)dx = V \qquad (1)$$

where d is the detector thickness and V is the applied bias voltage. The restrictions of the method are a significant amount of free parameters that make the procedure time consuming while still considering linear electric fields in each SCR.

The new method of E(x) reconstruction eliminates the restrictions mentioned above. The method includes direct analysis of the current pulse which results from collection of non-equilibrium carriers that traverse the detector bulk and change the drift velocity in accordance with the electric field profile. Calculation of the E(x) profile is made from the collected charge, which is evaluated by integration of the pulse response over the drift time. The correction of the collected charge for carrier trapping, which is described by the trapping time constant τ_{tr} as an adjusted parameter, is incorporated in the procedure as a correction of the current pulse response:

$$i(t)_{corr} = i(t) \cdot \exp\left(t / \tau_{tr}\right) \qquad (2)$$

The criteria for verification of the resulting E(x) profile are fulfillment of Eq. (1), and similarity of the trapping time constant value to referred data [4-6]. Calculations were carried out numerically using specially developed software based on MS EXCEL.

Confirmation of the developed method is illustrated by reconstruction of the electric field profile in detectors from bulk n-type MCZ Si processed in Russia and irradiated by 24 GeV/c protons with the fluence of $\Phi_p = 1 \cdot 10^{15}$ cm^{-2} at CERN. The measurements of the current pulse response described here and in Section 1.2 were carried out in the Ioffe institute using a Transient Current Technique (TCT) setup. An laser with a wavelength of 870 nm was used for non-equilibrium carrier generation. All measurements were done at 20°C with a laser illuminating the p^+ side of the detector i.e. the response resulted from electron collection. The current pulse responses were recorded by a LeCroy oscilloscope with a bandwidth of 500 MHz.

Figure 5-1 shows the current pulse response at four bias voltages (a) and reconstructed E(x) distributions (b). The coordinate x = 0 corresponds to the p^+ contact. Evolution of the DP electric field distribution is clearly observed in the E(x) profiles. A sequential increase of the electric field strength adjacent to the n^+ contact occurs while the electric field at the p^+ contact decreases. The drop of the reconstructed electric field at the p^+ contact (E tends to zero at x = 0) is related to the interference of the electron drift itself with the non-zero rise time of the pulse due to system response of the experimental setup. The decay of the electric field near the n^+ contact is the consequence of gradual

pulse decay. This electric field decay is a "virtual" effect presumably related to two effects: uncertainty in the time when the drift process of the "electron cloud" with finite length of several μm is completed and interference of the electron drift with diffusion inside this "cloud" that may also increase the dimensions of the drifting "cloud" and the relevant collection time. Therefore the E(x) profile near the detector contacts should be considered as a fair approximation.

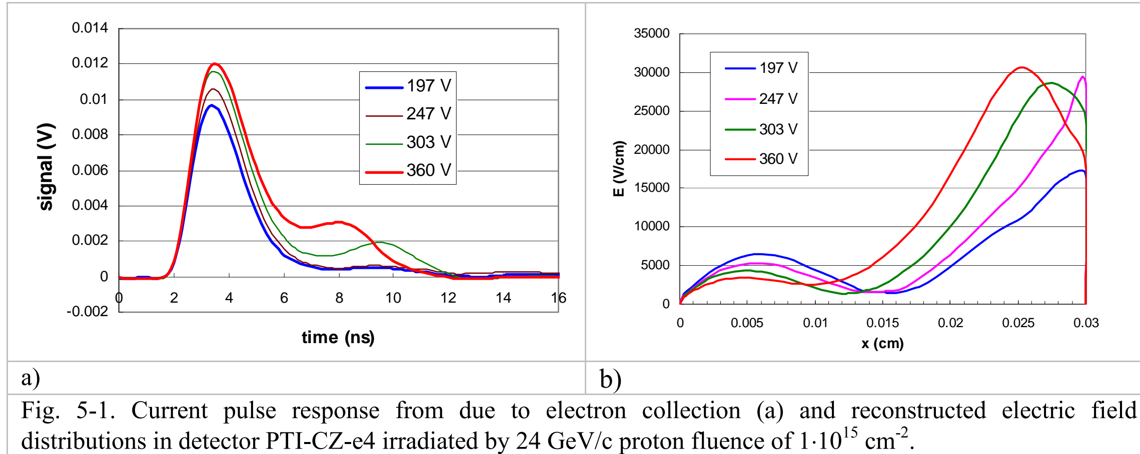

Fig. 5-1. Current pulse response from due to electron collection (a) and reconstructed electric field distributions in detector PTI-CZ-e4 irradiated by 24 GeV/c proton fluence of $1\cdot10^{15}$ cm^{-2}.

The trapping time constant evaluated from the E(x) calculations was equal to 1.9 ns which is similar to the referred value of 1.8 ns [4].

5.1.2 Electric field distribution in epi-Si based detectors

The method described in 5.1.1 was applied to the reconstruction of the electric field distribution in detectors from epitaxial n-type Si that were elaborated and studied in the scope of the SMART project. The detectors were processed by IRST, Trento, and had a "p^+ - n epi-Si - n^+ wafer" structure. The thickness of the epi-layer was 150 μm. After irradiation the detectors were annealed at 80°C for 60 min. The measurements of the current pulse response were carried out in the Ioffe institute jointly with the SMART team. Earlier results on the study of these epi-detectors were presented in [7, 8].

The problem of the current pulse response measurements for detectors based on epitaxial layers arises from the small thickness of these detectors in which the carrier drift time is comparable with the time resolution of the experimental TCT setup. Detectors with increased thickness of 150 μm used in this study are favorable for TCT application with time resolution of ~1 ns. For a better time resolution the measurements started at reduced bias voltages that led to the decrease of drift velocity and increased the collection time.

In Figs. 5.2 and 5.3 the current pulse responses for two detectors, W12 SMG22 and W12 SMG15, irradiated by 26 MeV protons and 1 MeV neutrons with the equivalent fluences Φ_{eq} of $7\cdot10^{14}$ cm^{-2} and $8.5\cdot10^{14}$ cm^{-2}, respectively, are presented. The measurements of detector W12 SMG22 are carried out at RT and -10°C. It can be seen from the comparison of Figs. 5-2, a and c, that the detector becomes fully depleted at RT at lower V (~54 V) as compared to -10°C(~92 V). The DP shape of the response is clearly observed at lower bias voltages which transformed into a single peak with the ascending slope. This behavior is typical for irradiated detectors in which space charge sign inversion (SCSI) occurs. Along with this, specific features of the pulse shape were observed that appeared as the pulse rise with two slopes - fast rise and slower rise, and an increased rise time of the response, respectively [8]. These features were presumably attributed to the influence of high resistivity base region with a lower electric field which extends from the p^+ contact inside the epi-layer and leads to the increase of the response rise time. For detector irradiated by neutrons the prolonged pulse rise with two slopes is especially pronounced and observed at V≤150 V.

For correct data treatment the choice of time interval for the current pulse integration is quite important. To minimize the uncertainty of the starting and final points of the drift process and the interference of drift and diffusion at the pulse decay, the starting point for integration was fixed at the

level of 0.5 of the first peak (or a single peak) amplitude. The final point was chosen at the level of 0.5 of the amplitude of the second peak (or single peak).

It can be seen from the reconstructed electric field profiles that in both detectors a low field region extends from the p^+ contact into the epi-layer. In detector W12 SMG15 irradiated by 26 MeV protons a region with higher field immerses a low field region in which E is about 1 kV/cm only, and the electric field distribution becomes close to linear above the bias of 45 V at RT and 100 V at -10°C. In detector W12 SMG15 irradiated with higher equivalent fluence the electric field gradient stays various over the epi-layer width even at the bias of 190 V. The base region width is larger than in detector W12 SMG22 that correlates to the pronounced value of the pulse rise with two slopes. Similar to the E(x) profiles in detectors from bulk silicon, the decay of the electric field near the n^+ contact is the consequence of the gradual pulse decay.

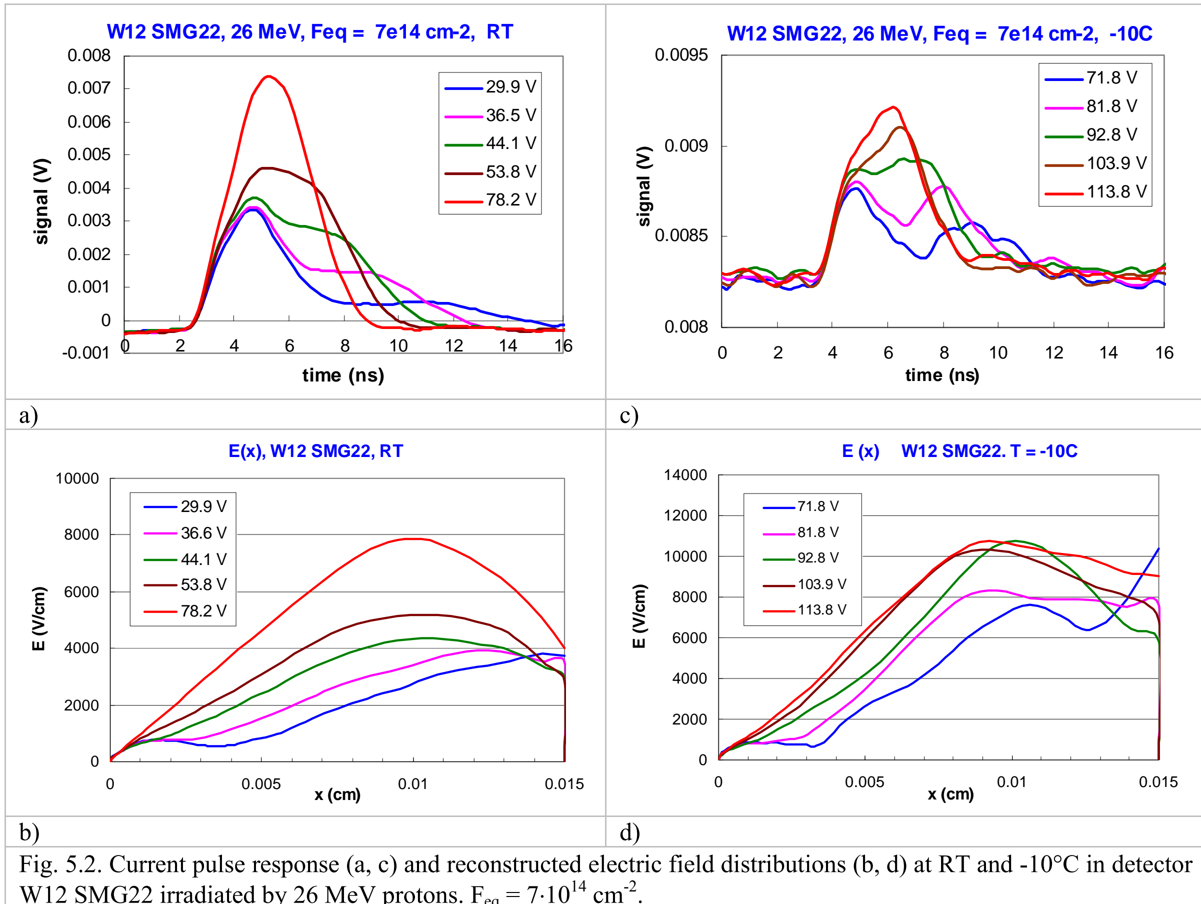

Fig. 5.2. Current pulse response (a, c) and reconstructed electric field distributions (b, d) at RT and -10°C in detector W12 SMG22 irradiated by 26 MeV protons. $F_{eq} = 7\cdot10^{14}$ cm^{-2}.

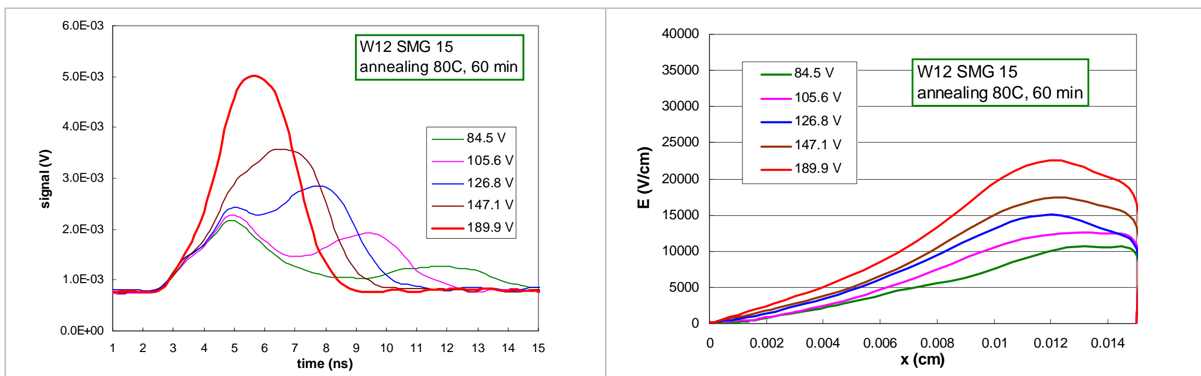

Fig. 5.3. Current pulse response (a) and reconstructed electric field distributions (b) at RT in detector W12 SMG25 irradiated by 1 MeV protons. $F_{eq} = 8.5\cdot10^{14}$ cm^{-2}.

The first results on the electric field reconstruction enabled us to evaluate the trapping time constants for proton and neutron irradiated detectors that are 2.1 ns and 1.5 ns, respectively. These values are lower that those predicted for bulk Si. This reduction may be partially related to the non-uniformity of the oxygen profile inside epitaxial layers that probably affects introduction of radiation defects. This subject needs further study with larger statistics of investigated epi-detectors. The other topic for further consideration is correction of the results on the electric field profile near the detector contacts. This may be realized by improvement of the setup time resolution, or special treatment of the pulse that can minimize the influence of the system response.

Conclusions

1. SCSI occurs in epi-Si detectors irradiated by 26 MeV protons and 1 MeV neutrons with the equivalent fluence of $(7\text{-}8)\cdot 10^{14}$ cm^{-2}.
2. DP response in epi-Si irradiated detectors is related to the base region with a reduced electric field rather than with DP electric field distribution.
3. The base region extends near the surface of the epi-layer that increases the rise time of the pulse response arisen from electron collection.
4. New method of E(x) reconstruction in irradiated Si detectors is universal and dependent only on a minimal number of parameters.

5.2 Effective doping concentration in different materials

The evolution of effective doping concentration after irradiation can be described by three terms ("Hamburg model" [9]): the decay of effective acceptors immediately after irradiation ("beneficial annealing" - *Na*), stable part (*Nc*) and creation of the effective acceptors at late annealing stages ("reverse annealing", *Ny*):

$$\Delta Neff = N_{eff\,0} - N_{eff} = N_a(\Phi,t) + N_c(\Phi) + N_y(\Phi,t)$$

$$Na(\Phi,t) = g_a \cdot \Phi \cdot \exp(-t/\tau_{ra})$$

$$Nc(\Phi) = N_{C,0}\left(1-\exp(c\Phi)\right) + g_c\Phi$$

$$Ny(\Phi) = gy\Phi(1-\exp(-t/\tau_{ra})) + N_{Y,2}(\Phi,t)$$

where $N_{eff,0}$ denotes the initial dopant concentration, g_a and g_y introduction rate of defects assuming the 1st order dynamics and τ_{ra} and τ_a corresponding time constants. The removal of initial dopants is described by the first term in N_c ($N_{C,0}$ denotes the concentration of initial dopants being removed) and generation of stable defects by g_c. The long term annealing also obeys 1st order dynamics except in epitaxial silicon detector where the second order term also appears at much prolonged times [10].

5.2.1 Review of damage parameters

5.2.1.1 Beneficial annealing

The beneficial annealing seem to be the least significant part of the damage due to short (~14 days at RT, ~8 min at 80°C) time constant and introduction rate (g_a~0.01 cm^{-1} [9]) smaller than stable damage and long term annealing. Moreover it is difficult to measure the precise introduction rate and time constant especially at larger fluences due to so called "self annealing" during irradiations [11]. There are indications that at high fluences (>10^{15} cm^{-2}) the time needed for completion of beneficial annealing (time to reach minimum in V_{fd}) is prolonged up to few tens of minutes at 80°C [12].

5.2.1.2 Stable damage

The stable part in FZ silicon which was the only detector grade material up to recently was always of negative sign [13]. As the reverse annealing and stable damage represent the introduction of effective acceptors the increase of $|N_{eff}|$ and consequently V_{fd}, was kept as low as possible by keeping the detectors cold for most of the time. The RD48 collaboration has proven the positive role of oxygen for

detectors irradiated with fast charged hadrons [13]. The introduction rate of stable acceptors was reduced by around factor of 3 when compared to STFZ detectors. In addition it was shown that reverse annealing time constants are prolonged for high [O].

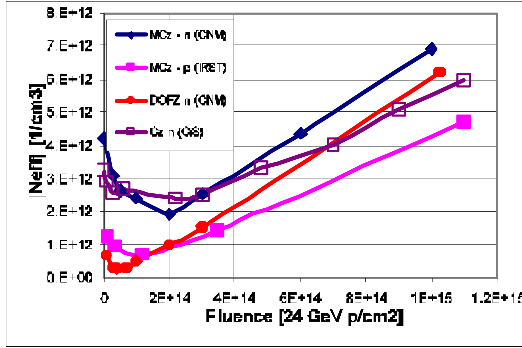

Fig. 5.4: The dependence of $|N_{eff}|$ on fluence for different oxygen rich materials [14-16] after completed beneficial annealing. The processing company is given in the brackets.

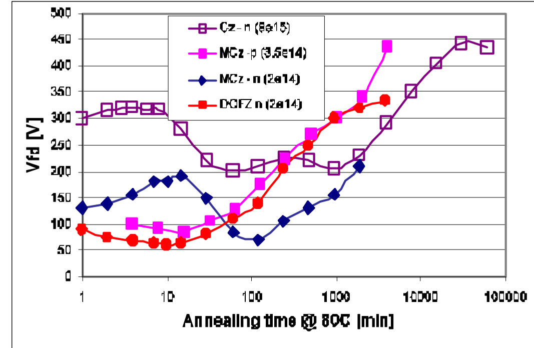

Fig. 5.5: The evolution of full depletion voltage with time for the same materials as in Fig. 5.4.

The oxygen concentration in DOFZ is around $2x10^{17}$ cm^{-3}, which is an order of magnitude lower than the [O] in MCz/Cz materials [14,15]. The latter materials seem not to undergo SCSI ("movement of the main junction") after irradiation with 24 GeV/c protons [14,15]. The N_{eff} of MCz-n or Cz-n type detectors first decreases, due to initial donor removal, and than starts to rise as the stable donors are introduced (see Fig. 5.4). A natural assumption would be that also MCz-p type detectors beyond certain fluence become n-type after the initial shallow acceptors are compensated by radiation induced stable donors. However, MCz-p type detectors after initial decrease remain p-type at all fluences [16,17] (see Figs. 5.4,5.5). As oxygen concentrations ($[O_{2i}]$ and $[O_i]$) are similar in MCz-n and p detectors there is no explanation so far how shallow acceptors could influence the formation of bistable donors, particularly as the concentration of bistable donors surpasses the concentration of initial dopants. The epitaxial silicon detectors exhibit also stable damage of positive sign after irradiation with high energy charged hadrons, but unlike MCz for both n and p type detectors (see Figs. 5.6,5.7).

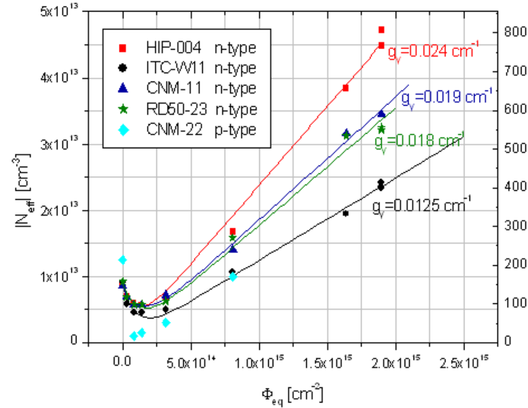

Fig. 5.6: Neff of different epitaxial detectors of 150 μm thickness irradiated with 24 GeV protons [39]. Please note that g_y in this case denotes introduction rate of stable donors. The epi-Si wafers were produced by ITME, Warsaw.

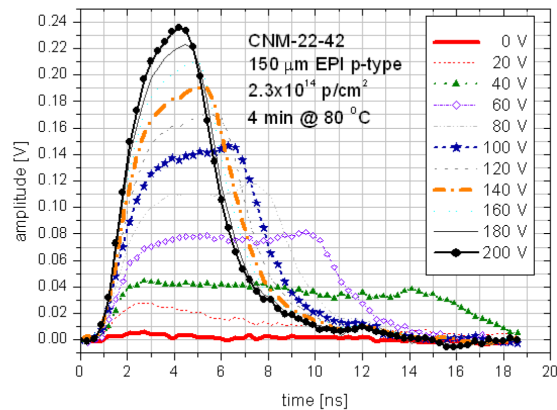

Fig. 5.7: Induced current pulses after hole injection in n-on-p type epitaxial pad detector (cyan diamonds in Fig. 6.) irradiated with 24 GeV protons. The current increasing with time is an indication of the increasing field and hence positive space charge.

The epitaxial silicon detectors have much lower [O] concentration of order 10^{17} cm^{-3} [10] than MCz/Cz, but the fraction $[O_{2i}]$/[O] in epi-Si detectors is much larger than in MCz [20]. The introduction of shallow donors is assumed to be related to the $[O_{2i}]$, which is assumed to be the precursor [18,19]. The most probable reason is out-diffusion of O_{2i} from Cz substrate to epitaxial Si during the thermal treatments involved in device processing. That also explains different introduction

rate of bistable donors for different detector thicknesses measured in [10, 20] and for the same thickness for different detector processes (see Fig. 5.6).
The stable damage seems to depend on detector thickness also for materials other than Epi-Si as shown in Fig. 8. [21]. The 50 μm FZ detector undergoes SCSI while 100 μm doesn't after 24 GeV/c proton irradiation indicating that in the thinner detector the diffusion of oxygen during processing can be more important. It should be noted that these detectors also have much lower resistivity (~100 Ωcm) than standard ones.

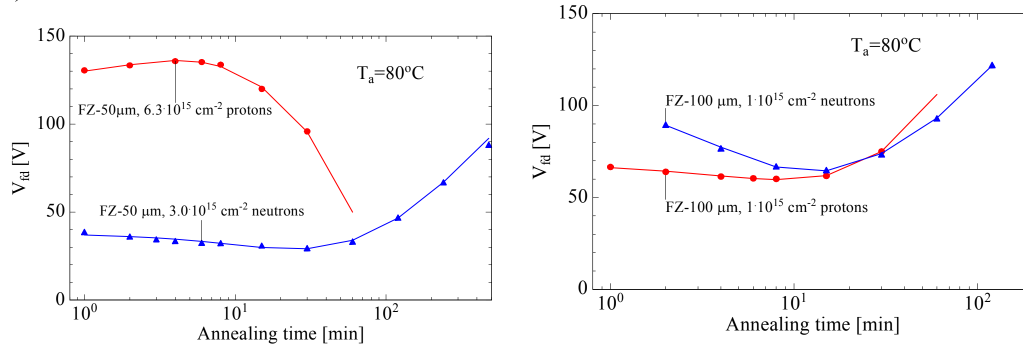

Fig. 5.8: Dependence of V_{fd} on annealing time for two FZ detectors of different thickness irradiated with 24 GeV/c protons and reactor neutrons. The neutron irradiated detectors show expected behavior: beneficial short term annealing followed by a harmfull reverse annealing while the 50 μm thick detectors show opposite behavior after 24 GeV/c proton irradiation.

Epitaxial n-type detectors don't undergo SCSI also with 26 MeV protons until the late stages of reverse annealing. On the other hand the MCz n-type detectors do undergo SCSI after few times $\Phi_{eq}=10^{14}$cm^{-2} of 26 MeV protons [22], which has been confirmed by annealing curves and TCT measurements. The 24 GeV/c protons are between the neutrons and 26 MeV protons in terms of ratio "cluster damage/point defects", which only adds to the controversy of no SCSI in MCz-n detectors after 24 GeV/c proton irradiations.

The annealing plots of 24 GeV/c irradiated MCz-n samples show a clear signature of material with positive space charge (see Fig. 5.5), confirmed also by TCT measurements up to fluences of $\Phi_p=5\cdot10^{14}$ cm^{-2} [23]. At very high fluences the interpretation of TCT data becomes questionable as the electric field and by that the side of the main junction is very sensitive to the value of effective trapping times. There is indication that these detectors may undergo SCSI [24]. The final answer will be given by irradiation of 24 GeV/c proton irradiated samples with neutrons. The irradiation by the latter introduces negative space charge and the subsequent change in V_{fd} will give the decisive answer.

The initial donor removal after 24 GeV/c p irradiations seem to be complete $N_{eff,0}=N_{C,0}$, while acceptor removal occurs only for MCz-p detectors [16,17,25]. In other p-type silicon detectors there seem to be no acceptor removal. The presence of acceptor removal in MCz-p only is not explained yet.

NEUTRON IRRADIATIONS

The stable damage in neutron irradiated detectors seems to be always of negative sign regardless of the silicon type. The only exception observed so far were thin n-type epitaxial detectors (50,75 μm) of low resistivity (50 Ωcm) [26], where no SCSI was observed and effective donors were generated. The introduction rate of stable acceptors seems to be related to resistivity or thickness. Around 3 times smaller g_c~0.006 cm^{-1} [27,28] was measured in epitaxial detectors, but also in thin FZ and MCz detectors of resistivity lower (see Fig. 5.9)[27] than in materials of standard thickness with g_c~0.02 cm^{-2}.

Recently also 300 μm thick MCz detectors processed by Micron show a smaller stable damage (g_c ~ *0.08* cm^{-1} [29]) for n and p type silicon as can be seen in Fig. 5.10. The detectors were processed on the wafers for which previous measurements g_c~0.02 cm^{-1} ([30] CNM, [31] CiS, [32] IRST) show no

difference to FZ or DOFZ materials [9]. This implies that the difference can be due to the process, which will be further investigated.

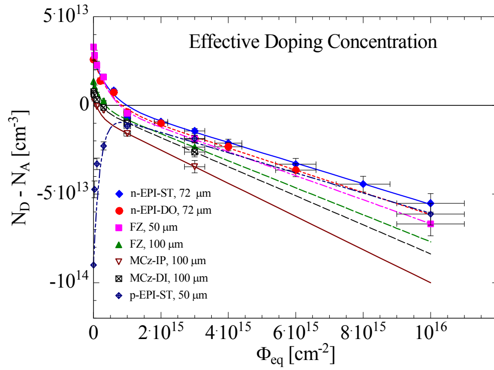

Fig. 5.9: Dependence of effective space charge (ND-NA) on neutron fluence for different materials after completed beneficial annealing.

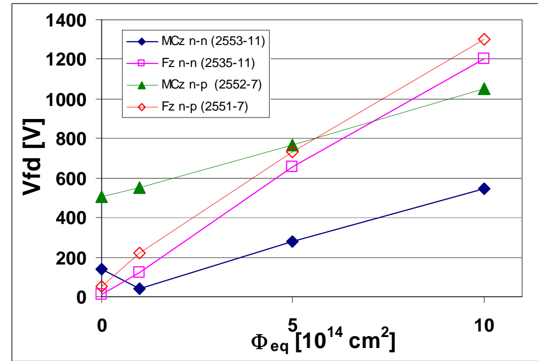

Fig. 5.10: Dependence of V_{fd} on fluence for different detectors (see legend) processed by Micron. The MCz-p,n detectors exhibit much smaller increase of V_{fd} with neutron fluence than seen before.

No acceptor removal was observed after neutron irradiations [30, 32] in all materials, while donors are partially removed [9].

5.2.1.3 *Reverse annealing*

In the first approximation the long term annealing on the time scales of interest for SLHC is independent on the material [10,13,16,17,33,34] or irradiation particle. The acceptor activation is governed by the first order process with the introduction rate g_Y varying between 2.6 and 4.8 cm^{-1} and the time constant of around 100 min at 80°C, depending on [O]. Significantly lower $g_Y = 1.6{\cdot}10^{-2}$ cm^{-1} was observed only in neutron irradiated epi-Si detectors [20]. In epi-Si detectors at much longer times of few 1000 min at 80±C (not so relevant for SLHC) more acceptors are created with a second order process [10]. The reverse annealing amplitude was observed to exhibit saturation at fluences >few 10^{15} cm^{-2} [27] in thin detectors (epi-Si, FZ and MCz). A similar observation at lower fluences was reported by RD48[10] for DOFZ detectors.

5.2.1.4 *Summary of results*

The key parameters of the model for 24 GeV/c proton irradiated detectors are shown in Table 5.1.

	g_{eff}, g_c, β_{eq} [10^{-3} cm^{-1}]	g_Y [10^{-3} cm^{-1}]	τ_{ra} [min at 80°C]
DOFZ-n,p [13,17]	~6-10	50 (a)	~200
STFZ-n,p [13,17,34]	~10-20 (b)	45 to 65	>80
MCz-n [22,34-36]	-4 to -6.5	28 to 45	80 to 200
MCz-p [16,17,36]	~7-10	~28	100 to 500 (d)
Cz-n [33]	~-5	~30	~80
Epi-n [17,32,38,39]	-3 to -20 (c)	~30	~130
Epi-p [38,39]	-12 to -24 (c)	-	-

Table 5.1: Survey of damage parameters in different silicon materials after irradiation with 24 GeV protons.(a) g_Y tends to saturate for DOFZ-n material at high fluences and may do so also in MCz. (b) The β_{eq} for STFZ-p type measured by [34] was found around 5 times lower than expected. Large variations between different STFZ materials were observed in the past also for STFZ-n type. (c) The introduction rate depends on thickness of the detector and on the process. (d) The huge difference in time constant reported in [16] is assumed to be related to thermal donors. Blue denotes introduction of negative space charge while red of the positive.

5.2.2 Bias-dependent damage

The damage in silicon detectors depends on the applied bias during the irradiation[40-42]. It anneals out after the bias is switched off for few days at 20°C [41,42]. After the bias is switched on again, part of the damage reappears. This is called the bistable damage and was observed in STFZ,MCz and Epitaxial detectors [43]. The V_{fd} and by that $|N_{eff}|$ always increase after applying the bias regardless of the space charge sign. An additional increase of $|N_{eff}|$ can be calculated as $|\Delta N_{eff}|=g\ \Phi$ with g~0.004 cm^{-1} and seem to be independent on irradiation particle type and material [43]. The change in V_{fd} was also verified in TCT [42] and signal measurements with electons from ^{90}Sr [43].

An example of V_{fd} evolution in time at T=-8°C (approximately operational temperature of LHC) is shown in in Fig. 11 [44]. At around 160 h the bias was switched on and consequently the V_{fd} started to increase with time constant of 10h for the short (~30% of the g) and 250h for the long component (~70% of the g). At t~1700 h the bias was switched off and the V_{fd} decreased to the level before the bias was switched on (due to low T no reverse annealing could be seen) with time constant of around 4h (single exponetial fits the data well). The leakage current on the other hand is not affected by applied bias.

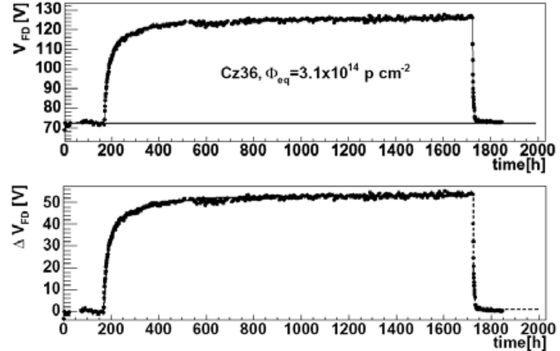

Fig. 5.11: The evolution of V_{fd} with time before the bias was applied, during the applied bias of 300 V and after it was switched off for an MCz-n type detector irradiated with protons to $\Phi_p=5\cdot10^{14}$ cm^{-2}. In the bottom plot the V_{fd} before switching on the bias was substracted.

5.3 Effective trapping times

Trapping of the drifting charge in the irradiated silicon detectors represents the limiting factor for their efficient use at highest SLHC fluences. The effective trapping probabilities are calculated as $1/\tau_{effe,h} = \beta_{e,h}(t,\ T)\cdot\Phi_{eq}$, where $\beta_{e,h}$ depends on time after irradiation and measurement temperature.

Particularly important in the last year were measurements of β in p-type silicon after proton (β_h= $4.1\cdot10^{-16}$ $\mathrm{cm^2/ns}$, β_e=$4\cdot10^{-16}$ $\mathrm{cm^2/ns}$) and neutron irradiations (β_h= $3.1\cdot10^{-16}$ $\mathrm{cm^2/ns}$, β_e=$3.8\cdot10^{-16}$ $\mathrm{cm^2/ns}$)[17] and measurement of t at very high fluences performend on thin epitaxial detectors [45]. Both were found to agree within the errors with previous measurements, however at the lower limit. Moreover, $\beta_{e,h}$ seems to decrease with fluence.

The values of effective trapping times damage constant from different groups [6,17,30,33,45-47] are gathered in the Table 2. The effective trapping times, within the error margins, don't depend on resistivity, [O], [C], wafer production (Cz, FZ, epi-Si) and type of silicon (p or n).

t_{min} , T = -10°C	β_h [$10^{-16}\mathrm{cm}^{-2}/\mathrm{ns}$]	β_e [$10^{-16}\mathrm{cm}^{-2}/\mathrm{ns}$]
Reactor neutrons	4.7± 1	3.5 ± 0.6
fast charged hadrons	6.6 ±1	5.3 ± 0.5

Table 5.2: Trapping time damage constants for neutron and fast charged hadron irradiated silicon detectors.

5.3.1 Modified CCM for thin pad detectors

The measurements using CCM/ECC method are limited to fluences below few 10^{14} cm^{-2} where sensors can be significantly overdepleted. At larger fluences one can use thinner detectors, but the shape of the TCT signal becomes so short that it is completely dominated by circuit properties (large diode capacitance) rather than current pulse. The integral of the pulse – charge can be nevertheless correctly measured. It was proposed in [45] to fit the simulated charge to the measured one at voltages above V_{fd}. Instead of correcting the measured current pulses and looking for τ_{eff} that gives no increase of charge for operation bias>V_{fd} (CCM method) the τ_{eff} is varied in simulation looking for the slope

that matches the measured one. The simulation is based on deep-level-model presented in [45] and used to describe the electric field within the detector.

The method was validated by the measuered trapping time constant with thick test structures which are irradiated with to fluences [41]. A comparision of the measured trapping times and the ones which are obtained by the new method leads to values which agree within 10% [45].

The procedure explained above was used on neutron irradiated thin epitaxial detectors (n-type, 75 µm, 150 Ωcm, CiS process) irradiated to $3{\cdot}10^{15}$ n/cm^2 and annealed to the minimun in V_{fd} *(see Fig. 12)*. Only determination of β_e was possible, due to back substrate preventing the hole injection. The combined fit with results obtained from CCM/ECC gives β_e=(3±0.1)·10^{-16} cm^2/ns. This points to around ~20% smaller electron trapping probabilities than the average value in Table 2.

The estimation of β from charge collection measurements with ^{90}Sr electrons will be discussed in the next chapter.

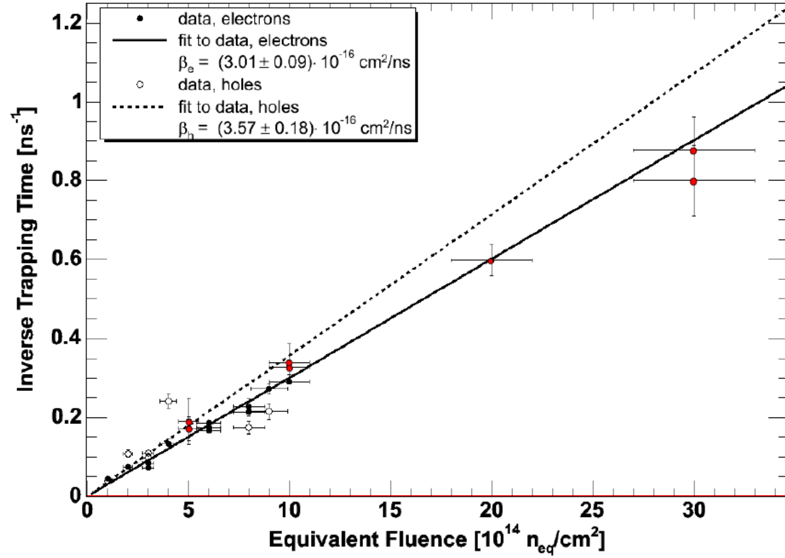

Fig. 12: Measurement of electron trapping times in n-type epi-Si detectors of 75 mm thickness.

5.3.2 Annealing of trapping times

The evolution of trapping probabilities with time after irradiation is described in the simplest model by the decay of the dominant trap to another dominant trap which is described by the following equation [4]:

$$\beta = \beta_0 \exp(-\frac{t}{\tau_{ta}}) + \beta_\infty \left[1 - \exp(-\frac{t}{\tau_{ta}})\right] = (\beta_0 - \beta_\infty)\exp(-\frac{t}{\tau_{ta}}) + \beta_\infty$$

, with β_0 and β_∞ measured immediately after irradiation and at very long times respectively. For the annealing temperatures of interest the β_0 is very close to β measured at the end of beneficial annealing. The same equation is also valid for two traps model where one is constant in time and the other decays. The same behavior was found also for other materials and irradiation particles [4,6,30,42,48,49]. The parameters describing annealing of effective trapping probabilities are gathered in the Table 3. The amplitude (β_0-β_∞)/ β_0 is an average from different groups [4,6,30,42,48,49]. Here it was assumed that the amplitude doesn't depend on the material, which is not clear yet.

Scaling of time constants to other annealing temperatures can be done by using the using Arrhenius relation ($\tau_{ta}=\tau0{\cdot}\exp(E_{ta}/k_BT)$). Although the time constant for reverse annealing of N_{eff} and τ_{ta} are comparable at T=60°C the difference in activation energy points to different underlying defects.

	τ_{ta} [min at 60°C]	(β_0-β_∞)/ β_0	E_{ta} [eV]
Electrons	650±250	0.35±0.15	1.06±0.1
Holes	530±250	-0.4±0.2	0.98±0.1

Table 5.3: Parameters used to model annealing of effective trapping times.

The annealing of $\beta_{e,h}$ is important for choosing optimum operation scenario for segmented detector operation. The charge collection of detectors with n$^+$ readout can in fact improve with time after

irradiation. This has been confirmed for irradiated ATLAS pixel detectors in test beam – see section on FDC.

The dependence of $\beta_{e,h}$ on temperature can be found in [4,6]. The trapping probabilities for both holes and electrons decrease with temperature. The differnce in $\beta_{e,h}$ between 20°C and -10°C is around ~15%.

5.3.3 Charge collection measurements

The collected charge depends on both electric field (hence N_{eff}) and on trapping probabilibties and is the most important parameter in charachterizaiton of any silicon detector. The measurement of charge collection were performed by different groups (CERN, IJS, SCIPP, Florence) using electrons from the ^{90}Sr source.

In the last report the charge collection measurments of MCz-p detectors with 24GeV protons and 26 MeV protons were presented up to the fluences of Φ_p=9·10^{15} p cm^{-2}. It was observed that that for not fully depleted diodes of standard thickness the collected charge decreases dramatically. Around 16000 electrons were collected at 500 V at 1.1·10^{15} p cm^{-2}, and only around 1000e at of Φ_p=9·10^{15} p cm^{-2} [16]. A full SLHC fluence range was covered also for n type epitaxial detectors of 50 and 75 micron thickness [50].

The studies of CCE on epitaxial detectors were extended this year to p-type devices of 150 µm thickness both with protons and neutrons [39,51]. In the region where strip detectors will be applied at SLHC the dominant damage comes from neutrons. Therefore more mesaurements were perfromed on neutron irradiated pad detectors. For the first time the charge collection meausurements were perfomed on strips detectors (with analog and binary electronics) and pad detectors processed on the same wafer and irradiated together.

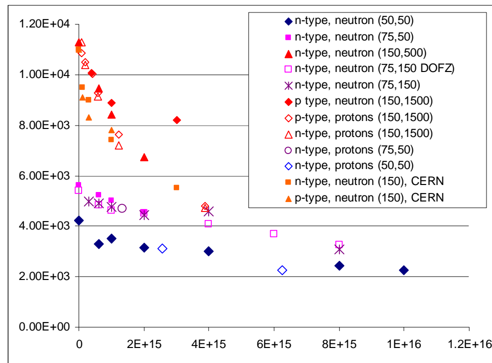

Fig. 5.13: Most probable charge dependence on fluence for overdepleted epi-Si detectors of different types; at each sample type, irradiation particles and in the brackets thickness and resistivity are given.

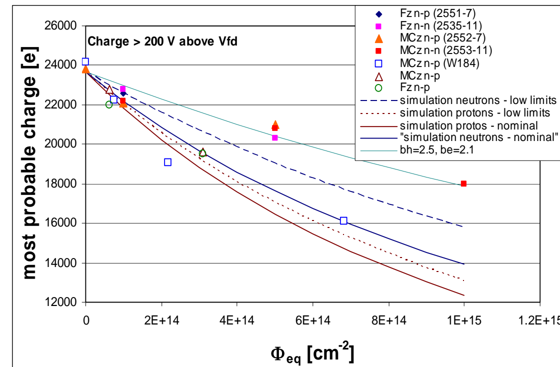

Fig. 5.14: Most probable energy loss in 300 µm diodes processed by Micron irradiatiated with neutrons (solid markers) and the ones produced by HIP and IRST irradited by 24 GeV protons

The collected charge for overdepleted epitaxial devices of different thicknesses, types, and resistivities is shown in Fig. 13 after completed “beneficial annealing”. The only exception is p-type 150 µm device at Φ_p=6.25·10^{15} cm^{-2} which could be operated at around V_{fd} (~500V, the highest bias applied to any of the detectors listed). For all proton irradiated devices (as for neutron 50 µm, 50 Ωcm) this is the worst point of operation in terms of V_{fd}. The positive space charge will be compensated by acceptors during reverse annealing leading to lower V_{fd}. Moreover the segmentation would result in increase of the collected charge which is for pad detectors around 5000 e at Φ_p=6.25·10^{15} cm^{-2}. It has been demonstrated in [51] that the V_{fd} coincides with the onset of saturation in charge collection efficiency ($V_{fd,CCE}$) also at SLHC fluences for thin epitaxial detectors. The correlation between V_{fd} and $V_{fd,CCE}$ will be further discussed in the next section for devices of standard thickness.

The V_{fd} of 300 μm thick detectors irradiated with neutrons to Φ_{eq}~10^{15} cm^{-2} often exceeds the breakdown voltage or maximum possible applied bias. However, the pad detectors produced by Micron on MCz exhibit smaller g_c (see Fig. 10) and can thus be depleted even at Φ_{eq}~10^{15} cm^{-2}. The collected charge for overdepleted detectors is shown in Fig. 14. Around 18000 electrons can be collected at Φ_{eq}=10^{15} cm^{-2} and almost 21000 at Φ_{eq}~$5\cdot10^{14}$ cm^{-2}. The maximum collected charge in neutron irradiated detectors decreases at the rate of ~700 e/10^{14} cm^{-2}. It can be also seen that at the same equivalent fluence fast charge hadrons are more damaging than neutrons (40-50%), thus confirming the measurements of effective trapping time measurements (see Table 2).

The measured values in Fig. 14 are larger than predicted by the simulations [48,51]. The reason is most likely in smaller trapping probabilities than extrapolated from measurements at lower fluences. Charge collection efficiency for a highly overdepleted detector is not very sensitive on electric field profile. In ideal case the electric field would be uniform ($N_{eff}=0$), which would yield highest CCE at given voltage. Assuming $N_{eff}=0$ the trapping probabilites were varied to obtain a good agreement with measurements and thus set upper limit for effective trapping probabilities. The ratio $\beta_e/\beta_h=0.8$ was fixed and taken from Table 2. While for the 24 GeV protons the CCE masurements can be fairly reproduced (brown lines in Fig. 14) this isn't true for the neutrons for Φ_{eq}>=$5\cdot10^{14}$ cm^{-2}. Even using the values of β_e ,β_h at the lower limits in Table 2 (see Fig. 12) the calculation significantly underestimates the collected charge for neutrons (blue lines in Fig 14). A good agreement is achieved for β_e=$2.1\cdot10^{-16}$ cm^2/ns , for β_h=$2.5\cdot10^{-16}$ cm^2/ns as depicted in the Fig. 14 by the green solid line.

5.3.4 Comparison with strip detectors

The difference in charge collection between pad and strip detectors comes due to different weighting fields which favors strip detectors providing that area around read-out electrodes is depleted and that the electrons drift to the readout electrodes (n^+-p detectors). In order to determine the difference strip and pad detectors (RD50 Micron wafers) were irradiated together with neutrons. Charge collection measurements were performed on: strip detectors in Liverpool (analog) and SCIPP (binary) and pad detetors at JSI. The dependence of charge collection efficiency on voltage was then compared. In the Fig. 15 collected charge is shown for Fz and MCz detectors irradiated with neutrons to 10^{15} cm^{-2}. Although the beneficial annealing was completed only for pad detectors, the strip detectors show, as expected, better CCE particularly at low voltages. At 500 V (ATLAS limit for strip detectors) the difference in collected charge is around 20%, but would be significantly larger ~40-50% if strip detectors were annealed to minimum in V_{fd} [53]. As the detectors become almost fully depleted (V_{fd}~1200 V, see Fig. 12) the difference becomes smaller. Nevertheless, the shape of Q/V curve is the same regardless of the measurement. In this way predictions on collected charge in strip detectors based on pad detector measurements are possible.

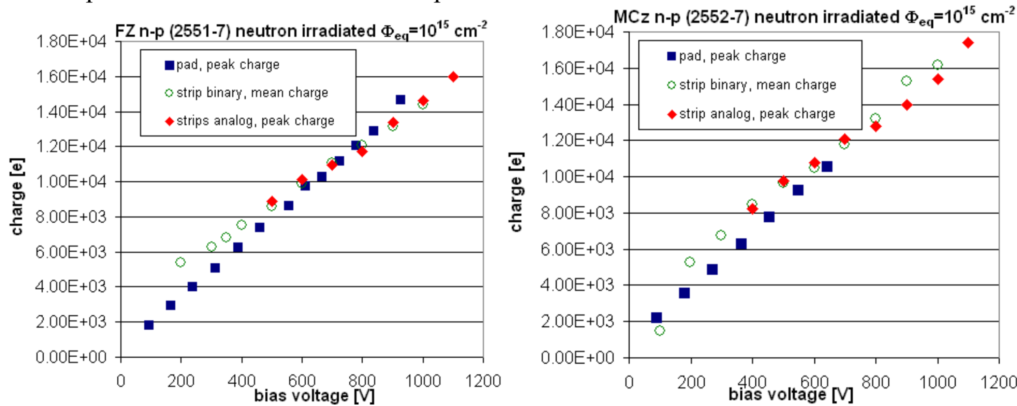

Figure 5.15: Collected charge as a function of bias voltage for Fz n-p and MCz n-p detectors irradiated with neutrons. Beneficial annealing for strip detectors was not completed. The signal measured with binary electronics is lower, due to high tresholds applied on the neighboring strips (note: mean charge, not most probable is shown).

Unlike detectors shown in Fig. 15, MCz n-n detectors irradiated to Φ_{eq}~10^{15} cm^{-2} (see Fig. 12) could be fully depleted at ~600 V. Charge collection measurements reveal a good agreement between pad and strip detectors (see Fig. 16). Moreover the onset of CCE saturation can be clearly seen at voltages close to V_{fd}. This proves the beneficial effect of low V_{fd} also for strip detectors.

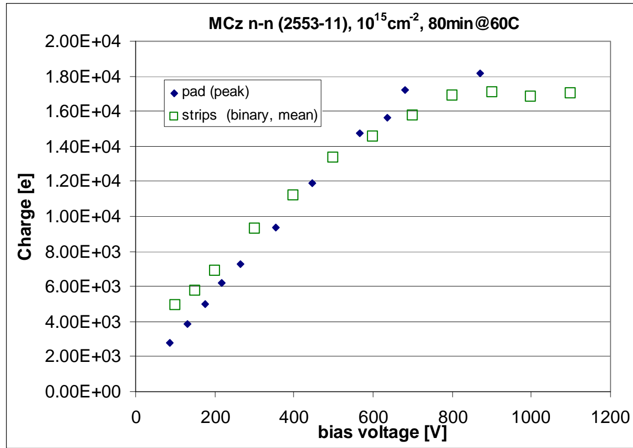

Fig. 5.16: Dependence of collected charge on applied bias voltage for MCz n-n strip and pad detector (V_{fd}=590 V).

The corelation between $V_{fd,CCE}$ and V_{fd} was checked on a set of MCz n-p, MCz n-n, Fz n-p and Fz n-n from RD50 Micron run irradiated to Φ_{eq}=1,5,10·10^{14} cm^{-2} neutrons. Obtained correlation plot is shown in Fig. 17. Taking into account the small offset the correlation is very good. The offset is also much smaller than in p-n strip detectors and it seems to become smaller with higher fluence and consequently higher full depletion voltage.

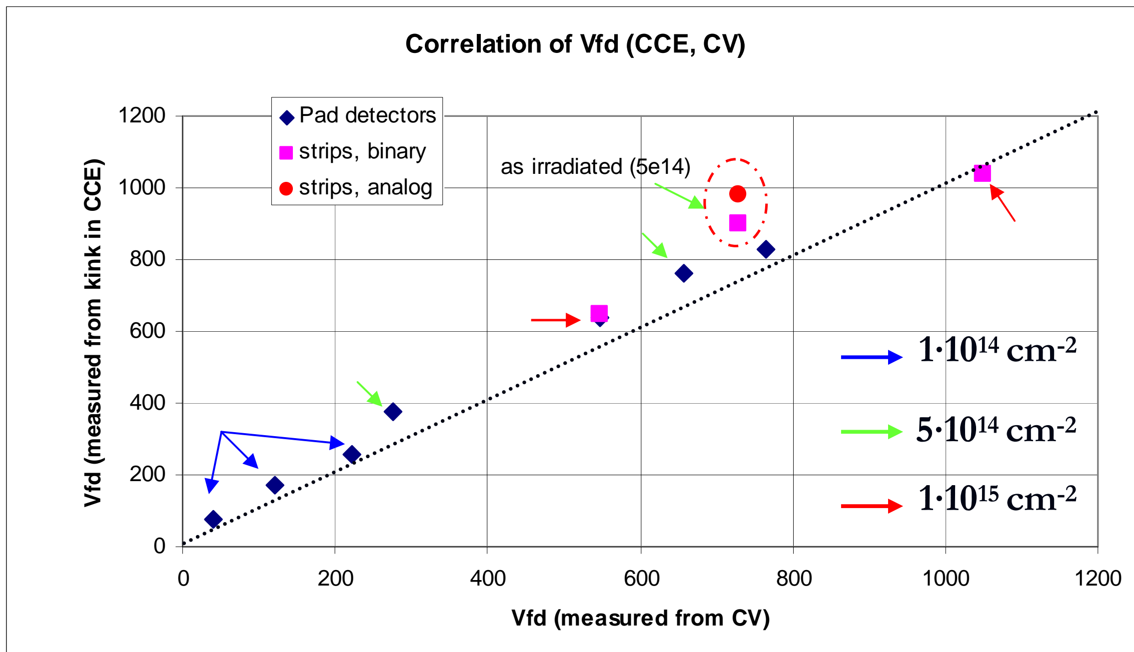

Fig. 5.17: Correlation of V_{fd} and $V_{fd,CCE}$ measured on as set of neutron irradiated MCz and Fz strip and pad detectors with n$^+$ readout. The samples have been annealed for 80min at 60°C, except detectors denoted in the figure.

5.4 Research Line New Materials

Charge collection efficiency improvement of SiC detectors under long term annealing

It was shown in the previous study [55, 56] that annealing of SiC detectors may improve their I-V characteristics and charge collection efficiency. Partial recovery of these parameters occurred at the annealing temperature T_{ann} of 400ºC. Since for SiC with a wide bandgap the temperature required for radiation damage annealing is higher than that for Si, the study performed in 2007 at the Ioffe Institute was concentrated at the increase of T_{ann} beyond 400ºC.

The study on annealing was carried out on SiC p^+–n–n^+ structures designed and processed by the INFN-Gruppo and University of Perugia [55]. The thickness of epi-layer was about 50 μm. The p^+ contact layer was made by Al implantation. SiC detectors were irradiated by 8 MeV protons with the equivalent fluence F_{eq} of $3{\cdot}10^{15}$ cm^{-2}. The samples were annealed in vacuum in two steps at 600ºC and 700ºC, successively, each step was 1 h. The reason for two steps arises from the fact that according to [57], the annealing of vacancy-bound defects occurs in two temperature stages whose onset depends on the politype modification of SiC and the type of radiation. Before and after annealing the samples were studied by nuclear spectroscopy technique using α–particles with the energy of 5.4 MeV and the range of 20 μm. The data on these measurements allow definition of CCE [58]. The measurements were carried out at 20 ºC at forward and reverse bias voltage. The carriers that drift through the total detector are respectively holes at forward bias, and electrons at reverse bias. Earlier results on the study showed that the electric field distribution is more stable in time in forward bias mode [59].

In Fig. 5.18 the CCE dependences on the bias voltage are demonstrated before annealing and at each annealing step. The CCE improvement occurs at each step, and approximately twofold total improvement of the CCE is observed regardless to the bias polarity. The final values of the CCE are 0.45 and 0.7 at forward and reverse bias, respectively, which points to an increase of the drift length of nonequilibrium carriers. A fitting of the curves in terms of the model described in [5] made it possible to determine the mobility–lifetime products for electrons and holes. These values were increased after the second annealing at 700ºC by factors of 6.5 and 2.3, respectively.

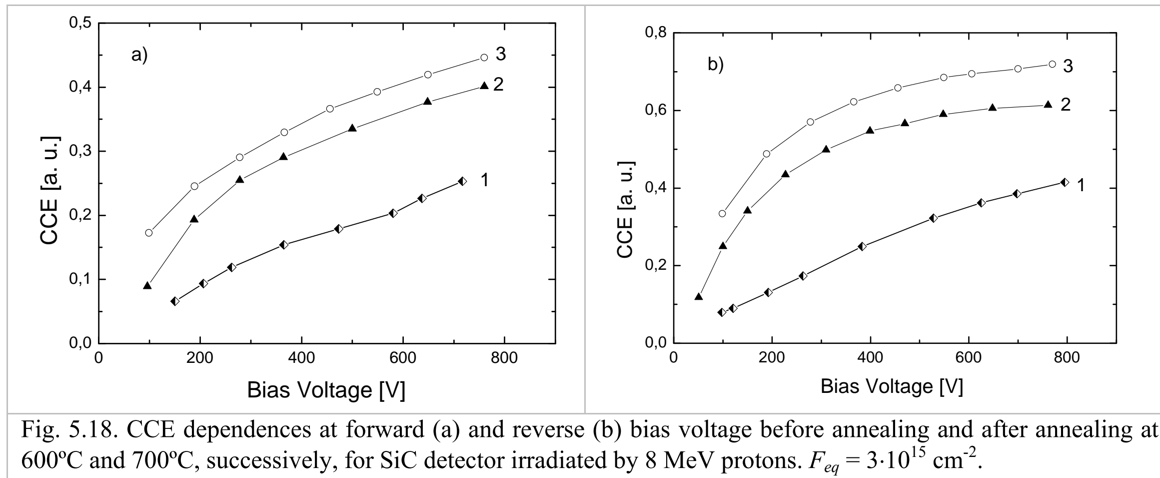

Fig. 5.18. CCE dependences at forward (a) and reverse (b) bias voltage before annealing and after annealing at 600ºC and 700ºC, successively, for SiC detector irradiated by 8 MeV protons. $F_{eq} = 3{\cdot}10^{15}$ cm^{-2}.

Still, along with a positive effect of the CCE recovery, the negative effect of detector polarization occurs. This polarization appears as the long term decay of the collected charge. This behavior implies that only partial annealing of radiation induced defects occurs and the trapping of nonequilibrium carriers to the non-annealed defects leads to the reduction of the collected charge in time. The residual defects are manifested also in the kinetics of the forward current I_f. An activation energy of the forward current defined from $I_f(1/T)$ dependence was equal to 1.06 eV and had the same value before and after detector annealing. Long term decay of the CCE may be eliminated by the

increase of the detector operational temperature up to 150 ºC that is above the operational temperatures of semiconductor detectors developed for SLHC.

5.5 REFERENCES FOR CHAPTER 5

[1] E. Verbitskaya, V. Eremin, A. Macchiolo, "First results on electric field distribution in irradiated epi-Si detectors", pres. 11th RD50 Workshop, Nov 12-14, 2007, CERN.
[2] E. Verbitskaya et al., Nucl. Instr. and Meth. A 557 (2006) 528-539.
[3] E. Verbitskaya, V. Eremin, Z. Li, J. Härkönen, M. Bruzzi, Nucl. Instr. and Meth. A 583 (2007) 77-86.
[4] G. Kramberger et al., Nucl. Instr. and Meth. A 481 (2002) 297-305.
[5] CERN-LHCC-2005-037 and LHCC-RD-009, RD50 Status Report 2005.
[6] A. Bates and M. Moll, Nucl. Instr. and Meth. A 555 (2005) 113-124.
[7] A. Macchiolo et al., "SMART detector project: recent results from the SMART experiment", pres. 9 RD50 Workshop, Oct 16-18, 2006, CERN.
[8] V. Eremin, "Recent results on electric field distribution in SMART irradiated detectors on MCZ and epitaxial silicon", pres. 9 RD50 Workshop, Oct 16-18, 2006, CERN.
[9] M. Moll, Ph.D. Thesis, Hamburg University, 1999, DESY THESIS 1999-040, ISSN-1435-8085.
[10] G. Lindstr¨om et al., Nucl. Instr. and Meth. A556 (2006) 451.
[11] G. Lindström, private communciations.
[12] E. Fretwurst et al., Nucl. Instr. and Meth. A552 (2005) 124.
[13] G. Lindström et al., Nucl. Instr. and Meth. A466 (2001) 308.
[14] CERN-LHCC-2004-031 and LHCC-RD-005, RD50 Status Report 2004.
[15] CERN-LHCC-2005-037 and LHCC-RD-009, RD50 Status Report 2005.
[16] H. Hödelmoser et al., "Charge collection efficiency of proton and neutron irradiated p-type MCz diodes", presented at the 6th RESMDD conference, Florence 2006.
[17] V. Cindro et al, "P-type Silicon irradiated with 24 GeV/c protons", presented at 10th RD50 Workshop, Vilnius, June, 2007.
[18] E. Fretwurst et al., Nucl. Instr. and Meth. A514 (2003) 1.
[19] Y.J. Lee et al., Phys. Rev. B 65 (2002) 085205-1-12.
[20] E. Fretwurst et al.,"Radiation tolerant epitaxial silicon detectors", presented at 6th RD50 Workshop, Helsinki, June, 2005.
[21] E. Fretwurst et al.,"First results on 24 GeV/c proton irradiated thin silicon detectors", presented at 11th RD50 Workshop, CERN, November, 2007.
[22] N.Manna et al., "SMART Detector Project: recent results from the SMART experiment", presented at the 6th RESMDD conference, Florence 2006.
[23] G. Kramberger and I. Mandić, " TCT measurements on CZ detectors", 4th RD50 Workshop, CERN, May, 2004.
[24] J. Härkönen et al.,"TCT and CCE measurements for 9 MeV and 24 GeV/c irradiated n-type MCz-Si pad detectors", presented at 11th RD50 Workshop, CERN, November, 2007.
[25] M. Bruzzi et al., Nucl. Instr. and Meth. A 552 (2005) 20.
[26] G. Lindström et al., Nucl. Instr. and Meth. A568 (2006) 66.
[27] E. Fretwurst et al.,"Comparison of neutron damage in thin FZ, MCz and epitaxial silicon detectors", presented at 10th RD50 Workshop, Vilnius, June, 2007.
[28] G. Kramberger et al.,"CCE measurements with Epi-Si detectors", presented at 8th RD50 Workshop, Prague, June, 2006.
[29] G. Kramberger et al.,"Charge collection measurements on MICRON RD50 detectors", ATLAS tacker upgrade workshop, Valencia, December, 2007.
[30] V. Cindro et al.,"Trapping of Electrons and Holes in p type Silicon Irradiated with Neutrons", presented at IEEE NSS-MIC Symposium, San Diego, October, 2006.
[31] E. Fretwurst et al.,"Radiation damage studies on MCz and standard and oxygen enriched epitaxial silicon devices", , presented at the 6th RESMDD conference, Florence 2006.
[32] N. Manna et al., "Study of radiation damage induced by protons and neutrons on heavily irradiated Magnetic Czochralski and Epitaxial silicon detectors", presented at 8th RD50 Workshop, Prague, June 2006.
[33] E. Fretwurst et al., "Survey of radiation damage studies at Hamburg ", presented at 3rd CERN-RD50 Workshop, CERN, November, 2003.
[34] G. Pellegrini et al., Meth. Instr. and Meth. A552 (2005) 27.
[35] J. Harkönen et al., Nucl. Instr. and Meth. A552 (2005) 43.

[36] G. Segneri, et al., Radiation hardness of high resistivity n- and p-type magnetic Czochralski silicon, Nucl. Instr. and Meth. A (2006), doi:10.1016/j.nima.2006.10.262
[37] V. Khomenkov et al., SOLID STATE PHENOMENA 108-109 (2005) 315
[38] V. Khomenkov et al., “”, presented at 11th RD50 Workshop, CERN, November, 2007.
[39] K. Kaska et al.,”Epitaxial silicon detectors irradiated with protons and neutrons ”, presented at 11th RD50 Workshop, CERN, November, 2007.
[40] V. Cindro et al., , Nucl. Instr. and Meth. A419 (1998) 132.
[41] V. Cindro et al., , Nucl. Instr. and Meth. A450 (2000) 288.
[42] V. Cindro et al., , Nucl. Instr. and Meth. A476 (2002) 565.
[43] G. Kramberger et al., “Effect of bias voltage on full depletion voltage measured for different materials ”, presented at 9th RD50 Workshop, CERN, October 2006.
[44] G. Kramberger et al., “Effect of bias voltage on full depletion voltage measured for different materials”, presented at 10th RD50 Workshop, Vilnius, June, 2007.
[45] J. Weber et al.,"Determinaton of Traping Time Constants in Neutron Irradiated Thin Epitaxial Pad Detectros”, presented at 11th RD50 Workshop, CERN, November, 2007.
[46] J. Weber et al., ““Measurement of the Trapping Time Constant in Neutron-Irradiated Silicon Pad Detectors”, presented at IEEE NSS-MIC Symposium, San Diego, October, 2006.
[47] O. Krasel et al., IEEE Trans. NS 51(1) (2004) 3055.
[48] T. Lari et al., Nucl. Instr. and Meth. A 518 (2004) 349.
[49] G. Kramberger et al., , Nucl. Instr. and Meth. A 571 (2007) 608.
[50] G. Kramberger et al., , Nucl. Instr. and Meth. A 554 (2005) 212.
[51] V. Khomenkov et al., recent measurements.
[52] H. Sadrozinski, “Charge Collection in Neutron Irradiated Micron SSD”, presented at 11th RD50 Workshop, CERN, November, 2007.
[54] T. Affolder et at., “CCE results with FZ and MCz p-type detectors after heavy neutron irradiation”, presented at 11th RD50 Workshop, CERN, November, 2007.
[55] CERN-LHCC-2007-005 and LHCC-RD-013, RD50 Status Report 2006.
[56] F. Moscatelli, Nucl. Instr. and Meth. A 583 (2007) 157-161.
[57] M. Huhtinen, Nucl. Instr. and Meth. A 491 (2002) 194-215.
[58] N.B. Strokan, et al., Semiconductors 39 (2005) 1394.
[59] N.B. Strokan, A.M. Ivanov, A.A. Lebedev, Nucl. Instrum. and Meth. A 569 (2006) 758.

6 New Structures

The past year has been a successful year for the new structures working group of RD50. The thin detectors sub-section progresses towards segmented detectors fabricated on epitaxial and SOI wafers. This work builds on the previously reported encouraging device fabrication and irradiation tests performed on 50 µm p-i-n diodes. The 3D detector section has seen the full characterization of the 3D devices fabricated by FBK/CNM in 2005; including characterization of short strip detectors with ATLAS readout electronics. Double sided 3D devices have now been fabricated by both FBK and CNM and initial encouraging electrical characterization is reported. The first full 3D devices from the commercial supplier IceMOS Technology has been delivered and are being characterised. The work on semi-3D detectors has progressed at BNL

6.1 Thin Detectors

This research line is investigating the properties of thin planar detectors for extremely high radiation fluences (> 10^{15} n/cm^2). The thickness of the detector should be matched to the effective drift length of the charge carries which will be reduced to the order of 100 µm and less due to radiation induced trapping. Though such detectors still suffer from a small signal size they offer operational advantages, such as low depletion voltages, low leakage currents and low detector power dissipation. There is also a reduced material budget. In addition to these benefits a better configuration of the electrical drift field might lead to an improved charge collection efficiency compared to conventional thick detectors operated partially depleted. The thin detectors will have n-type segmented implants so as to keep the highest electrical field under the readout implant throughout the lifetime of the device. The research is based on the success of fabricating pad diodes on thin epitaxial material that was reported in last year's status report [1] and in literature [2].

The R&D focuses on two technologies to built ultra-thin detectors:

a) Detectors using epi-layers as the sensitive volume.
b) Detectors based on SOI wafers where the high ohmic top wafer is thinned to the desired thickness.

Both options offer the advantage that the wafers can be processed on standard equipment in commercial detector facilities. The epitaxial devices for this research will be processed at CIS, Erfurt. The research is being pursued via the fabrication of test devices produced on the following substrate types and thicknesses:

a) Epitaxial: 50 µm, 75 µm, 150 µm (all n-in-p)
b) SOI: 75 µm (n-in-n), 75 µm and 150 µm (n-in-p)

The test structures include diodes; min-strip detectors (~ 7.6 mm strip length), small pixel arrays (wire-bondable) and pixel arrays (designed to be compatible with the ATLAS pixel detector) for bump bonding or solder connection.

Most of the design variations of the test devices address the isolation properties between the n-strips. P-spray isolation and modulated p-spray with different geometrical parameters will be implemented. Table 6-1 and Table 6-2 detail the different variations to be fabricated for the strip detectors.

Strip Pitch (µm)	N+ implantation width (µm)	p-spray moderation width (µm)
50	30	10
50	30	None
80	30	10
80	30	None

Table 6-1 SOI & Epi strip detector design variations

Strip Pitch (µm)	N+ implantation width (µm)	p-spray moderation width (µm)
50	24	10
50	30	6
50	36	6
80	20	None
80	20	24
80	30	24

Table 6-2 SOI only strip detector design variations

One R&D goal is to study charge sharing properties between neighbouring pixels for different detector thicknesses and bias voltages as a function of fluence. For operation in high radiation regions this effect may become critical due to trapping.

The epitaxial and SOI wafers have been produced. The layout of the test structures is ready and the processing of the wafers are about to begin (SOI wafers at the MPI semiconductor laboratory, epi-wafers at CIS, Erfurt). The test structures should be available in spring 2008. An extensive irradiation program is planned for summer 2008.

6.2 3D Detectors

The work on 3D detectors since the last status report has been split between the fabrication of new devices which are closer to the standard 3D detectors proposed by Parker et al. [3] and the completion of the characterization of the single sided 3D detectors, (3D-stc), produced by FBK/CNM in 2005. This status report reflects this effort and discusses the characterization of the 3D-stc devices first followed by the work on the new devices at the fabrication institutes and their characterization by RD50 collaborators.

6.2.1 Single-Type Column 3D Detectors

In 2005 FBK, (then know as ITC-irst), proposed the 3D-stc detector concept [4] as a simplified 3D detector design and as a first stage in the production of full 3D detectors. All the columnar electrodes are of the same type (n+) and are etched from the front side of the wafer; p-stops or p-spray are used for surface isolation. On the back side a blank p+ implant provides a uniform ohmic contact. The columns are empty and do not penetrate all through the substrate. Three batches of 3D-stc detectors with the same mask layout were fabricated at FBK-irst on high-resistivity p-type wafers [5] and [6].

Selected samples of pad and strip detectors from the three 3D-stc batches were delivered to some RD50 collaborators to perform functional tests, namely:

- The signal dynamics was investigated at JSI Ljubljana by means of position sensitive multi channel Transient Current Technique (TCT) on small strip detectors.
- Charge Collection Efficiency (CCE) tests were performed with IR laser sources. Position resolved CCE measurements were carried out at the University of Freiburg to study the dependence of the charge collection on the position of light incidence.
- CCE tests with β sources were performed on pad detectors at INFN Florence and Glasgow and on strip detectors at SCIPP and Freiburg.

Last year's status report details the results obtained from all of the above characterizations before irradiation expect for the β source tests performed at Freiburg. These results are updated and briefly summarised here followed by the β source tests performed at Freiburg.

Electrical simulations of the carrier dynamics show that the electrons generated by the incident radiation drift to the nearest column and are collected, while the holes have to drift across the full substrate thickness to the backplane. Thus, the read out signal shows a fast peak due to electrons and a long tail due to the slow drift of holes, and the complete charge collection is relatively slow. Another drawback of this structure is that when the volume between columns is fully depleted, the electric field in this region cannot be increased further. Fast charge collection is essential to counteract charge trapping, so 3D-stc detectors are not expected to be radiation hard. For a device fabricated on a

500 μm substrate and biased to 40 V, the peak of the simulated signal pulse will arrive at the read-out electrode in 2.5 ns, 92% of the charge will be collected in 15 ns and 97% in 36 ns [7].

The electrical characterization of the 3D pad diodes with 80 μm pitch shows that the volume between the columns is depleted at low bias (~10 V), and that the leakage current is low (<3 pA/column for the FZ detectors [7], [8]). After irradiation with neutrons to a fluence of 5×10^{14} n_{eq}/cm^2, the lateral depletion voltage is 40 V [9].

Charge collection efficiency tests have been performed with β particles on non-irradiated pad [7], [10], [11] and strip detectors [11]. In all cases the shaping time was long enough to avoid the ballistic deficit of the charge, even at low voltages when charge collection is slower. The results show the voltage dependence of the charge collection and confirm the two-stage depletion model predicted by simulations: first, the depleted region grows laterally from the n+ electrodes until the region between the columns is fully depleted, and then it progresses towards the back contact like in a planar device. Another interesting feature is that these devices have non-zero charge collection at 0 V, due to the depleted region already present around the columns in the unbiased device.

Position sensitive multi-channel TCT measurements have been carried out at the Jozef Stefan Institute on 3D-stc strip detectors, before and after irradiation with neutrons up to a fluence of 5×10^{14} n_{eq}/cm^2. A pulsed infrared laser, which simulates the interaction of minimum ionizing particles, was scanned over the detector surface. The position resolution of the laser was 0.5 μm with a FWHM ~7 μm. The devices tested were DC coupled 3D-stc strip detectors, with a strip pitch of 80 μm and p-spray insulation. Three neighboring strips were wirebonded to the readout electronics and the induced current pulse was measured for each position of the incident laser beam. The other strips were left floating. The experiments were carried out at a controlled temperature of 10ºC.

The TCT tests of non-irradiated detectors [12] confirm the pulse shape (fast rise and long tail) predicted by simulation of the carrier dynamics. The signal induced on the adjacent strips is much larger than in the planar strip detectors. This effect could be used to increase the position resolution of the device.

The charge collection efficiency (CCE) was estimated by integrating the transient current over 25 ns. As expected, the 3D-stc detectors are not well suited for applications that require high charge collection after irradiation. The results show a significant loss of efficiency for interaction points close to the strips: CCE is 60% for 10^{14} n_{eq}/cm^2 and 40% for 5×10^{14} n_{eq}/cm^2. This is due to the ballistic deficit and trapping caused by the slow drift of holes. The CCE is even lower in the mid-strip region where there is a saddle in the electric field [8] and [14]. Fig 6-1 shows the CCE as a function of the bias voltage for three fluences for a laser focused next to a strip and in the middle of the interstrip area.

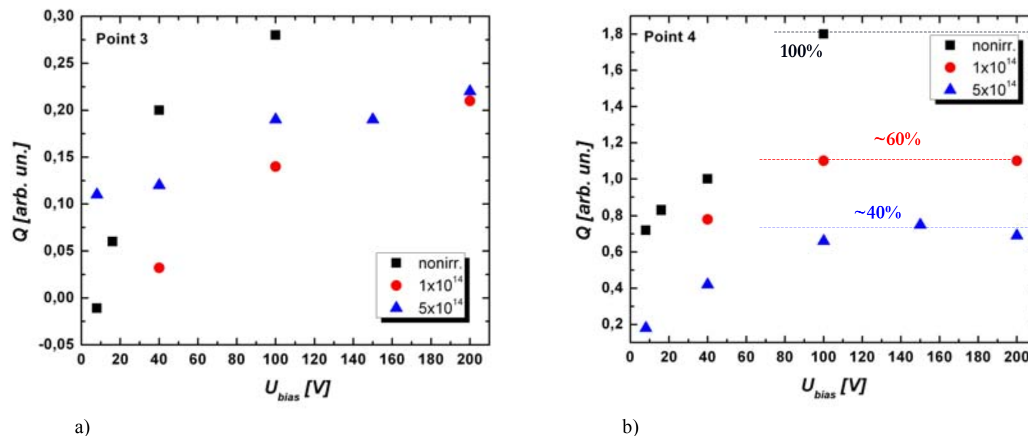

Fig 6-1 Charge collection efficiency of a 3D-stc strip device measured by integrating the transient current generated by an IR laser over 25 ns. The laser beam position is a) next to the strip; b) in the mid-strip area. The irradiation fluence, in 1 MeV neutrons, is shown in the legend.

At the University of Freiburg similar tests with infrared laser pulses on short 3D-stc strip detectors (64 strips, each 18mm long, formed from 230 individual n-doped columns) [13] have been performed

using the ATLAS SCT ABCD front-end chips and readout chain [15] and [16]. The shaping time of the ABCD is 20 ns. The 3D-stc sensors have n-type strips and therefore collect electrons and give negative signals. However, the ABCD3TA ASIC is not completely bipolar and was designed for positive signals. Adjusting the ASIC for negative signals is possible by employing the trimming circuit to shift the offset to its maximal value of around 4 fC [17].

Three different devices were tested: two sensors with FZ substrate material; one with a p-stop isolation structure and one with a p-spray isolation structure, both 525 μm thick. The third was 300 μm thick made of CZ substrate with a p-spray isolation structure.

The laser spot size was 2 μm which was scanned across the surface of the strip detector. At each point a full threshold scan was made of the electronics' discriminator threshold and the charge collected was calculated. The laser tests of detectors where the surface is insulated with a p-spray show a 25% drop in the collected charge in the region between the strips due to the "saddle" in the electric field. In addition, the detectors where the strips are isolated with p-stops have charge collection problems between the electrodes near the surface, in the vicinity of the p-stop surface isolation scheme. This can be attributed to a low field region created by the p-stop [13]. After an irradiation with 26 MeV protons up to an equivalent fluence of 10^{15} n_{eq}/cm^2 the detectors are still operational, with a lateral depletion voltage of 100 V. At this fluence the CCE, from laser illumination, shows a 15% reduction with respect to the non irradiated device in the vicinity of the strips and a 50% drop in the p-stop area between the strips [13].

Absolute charge collection efficiency measurements with a β source set-up have also been carried out at the University of Freiburg on the 3D-stc strip devices described above. The beta set-up used a 2.4 MBq Sr-90 source and was triggered to obtain MIP-like electrons by using two scintillators behind the module under test. Fake triggers are suppressed by using a coincidence of these two scintillators [18]. The whole system was set up in a freezer that allowed sensor operation at about -10°C. The measured quantities were noise, collected charge and detection efficiency at 1 fC threshold, a figure of merit for a binary readout system.

The noise of the module is dominated by the capacitance load on the front-end due to the detector. Before irradiation the 3D-stc devices show low noise levels which decreases rapidly with increasing bias voltage up to 25 V, as lateral depletion between the columns occurs. For bias voltages above 30 V the noise decreases more slowly, as the bulk of the device under the columns is depleted, and is around 1200 electrons, which is comparable to ATLAS SCT Endcap inner modules.

In Fig 6-2 the collected charge of three modules measured with 20 ns shaping time is shown. Most charge is collected by the FZ p-stop detector at a bias voltage of 80 V (red full circles). It collects 2.31 fC ± 0.04 fC, which corresponds to approximately 15000 electrons. The other two devices, (FZ p-spray and CZ p-spray) collect less charge (FZ p-spray 1.81 fC ± 0.03 fC, CZ p-spray 1.96 fC ± 0.04 fC), a difference which might be due to their different isolation structures. Values for higher bias voltages could not be measured due to the onset of microdischarge noise.

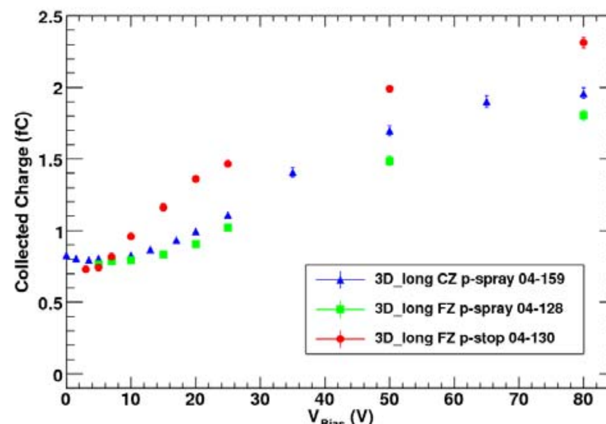

Fig 6-2 Collected charge of three unirradiated 3D-stc detectors measured for different bias voltages with a shaping time of 20 ns. Full blue triangles CZ p-spray detector, full green squares FZ p-spray detector, full red dots FZ p-stop detector

The devices were irradiated with 26 MeV protons to a 1 MeV equivalent fluence of 9.1 x 10^{14} n_{eq}/cm^2 and measured, prior to any annealing, at a temperature of -10 °C.

The FZ and CZ p-spray sensors had a constant noise of around 1300 electrons up to bias voltage of 50 V, followed by a fast decrease to 900 electrons, corresponding to the full lateral depletion between the columns. For higher voltages the noise rose slowly from 900 electrons to 1100 electrons. Up to a bias voltage of 250 V no microdischarge was observed. The noise performance of the FZ p-stop detector was flat up to bias voltages of 95 V and at a level of around 900 electrons, after which microdischarge occurred which lead to an abrupt increase in the noise. The noise was shown to still be dependent upon the capacitive load of the devices even though the leakage current had increased by approximately 50 times (post irradiation current, normalized to 20 °C, measured at 400 V was 17 mA/cm^3 compared to 0.3 mA/cm^3 measured before irradiation at 80 V).

Fig 6-3 and Fig 6-4 show the collected charge before (full symbols) and after (open symbols) irradiation for FZ p-spray (squares) and CZ p-spray (triangles) sensors, respectively. For the FZ device an increase in the collected charge begins at a bias voltage of 100 V, which implies that above this bias lateral depletion between the columns was achieved, which is in agreement with the expected bias voltage from the noise characteristics.

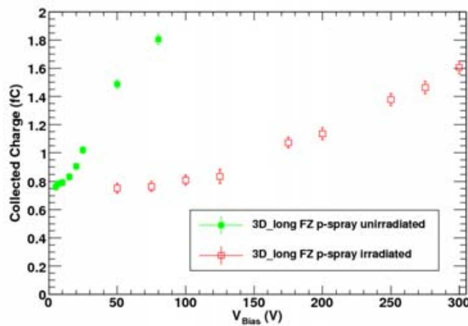

Fig 6-3 Collected charge of FZ p-spray module before (green full squares) and after (red open squares) irradiation with 26 MeV protons to a fluence of 9.1×10^{14} n_{eq}/cm^2.

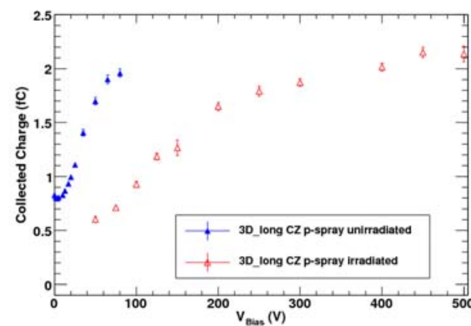

Fig 6-4 Collected charge of the CZ p-spray detector before (blue full triangles) and after (red open triangles) irradiation with 26 MeV protons to a fluence of 9.1×10^{14} n_{eq}/cm^2.

The maximal collected charge was 1.61 fC ± 0.04 fC. Full depletion was not measured as microdischarge started at voltages above 300 V. For the CZ device after irradiation the maximal collected charge was 2.14 fC ± 0.07 fC (which corresponds to ~ 14000 electrons) measured at a bias voltage of 500V. Furthermore saturation of collected charge for bias voltages above 450 V was observed, hence full depletion was achieved. Before irradiation the collected charge was ~ 2 fC at a bias voltage of 80 V.

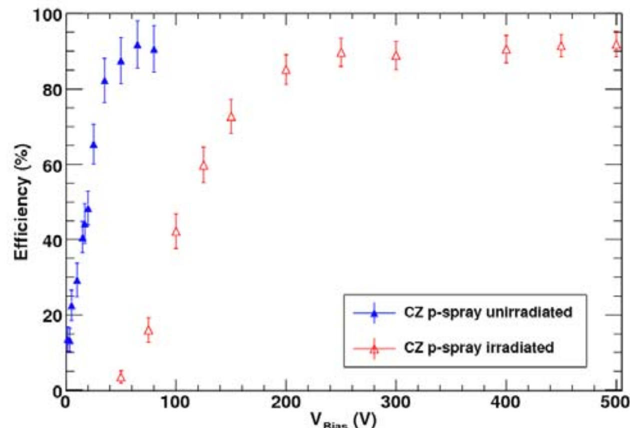

Fig 6-5 Efficiency at 1 fC threshold as a function of bias volatge for the CZ p-spray module before and after irradiation. Blue full triangles before irradiation, red open triangles after irradiation.

In addition to the charge collection measurements the efficiency for the device at a fixed threshold of 1 fC was measured. The efficiency is defined as number of hits over threshold divided by number of triggers in the beam area. The beam area was defined by the scintillator trigger detector which was smaller than the sensor area. In Fig. 5 the efficiencies at 1 fC for the CZ p-spray module before and after irradiation are shown. Before irradiation efficiencies around 90 % are reached for bias voltages above 75 V, after irradiation efficiencies above 90 % are obtained for bias voltages higher than 250 V.

In conclusion no radiation induced degradation of the maximum collected charge was observed for the CZ p-spray detector once the detector was fully depleted. That is after irradiation the collected charge is not reduced by trapping. The noise of the devices and the detection efficiency at 1 fC threshold were also only slightly affected by the irradiation. The signal-to-noise ratio (SNR) before irradiation at a bias voltage of 80 V for the FZ detectors were ~ 15 and for the CZ p-spray detector was ~ 11. After irradiation the FZ p-spray detector had a SNR of ~ 12 at a bias voltage of 300 V and the CZ p-spray detector had a SNR of ~ 13 for at a bias voltage of 500 V. The comparison of these values demonstrates again, that the CZ p-spray detector shows no degradation in the maximum SNR caused by irradiation; however a higher bias voltage was required to obtain saturation in the collected charge. A full write up of the Freiburg results can be found in [19].

6.2.2 CNM

CNM have produced a “Double-Sided” 3D detector that has both n- and p-type columns, as in a full 3D detector [20]. However, the holes of one doping type are etched from the front side of the wafer, and the holes of the other type are etched from the back side. This avoids the difficulty of etching and doping the two different kinds of holes on the same side of the wafer. Furthermore, the columns do not pass through the full thickness of the substrate, which makes the devices more resistant to mechanical stress than full 3D detectors, and makes the use of a carrier wafer unnecessary, if active edges are not required.

The electrical performance of the proposed device has been simulated at the University of Glasgow with the finite-element simulation package ISE-TCAD [21]. The simulations show that the area between the columns in a double-sided 3D detector depletes very quickly, with the depletion region growing cylindrically outwards from the electrodes like in a standard 3D detector. However, there are low electric field regions around the front and back surfaces of the detector that deplete more slowly, but full depletion is reached at voltages lower than 10 V for typical doping concentrations.

Where the columns overlap, that is throughout most of the device, the electric field pattern matches that of a full 3D detector and charge collection is fast because the charge carriers drift horizontally. In the low electric field regions the charge carriers are collected more slowly increasing the full collection time. For instance, in a double-sided detector with 250 μm columns and 300 μm substrate it takes 0.75 ns to collect 90% of the charge but 2.5 ns to collect 99%. This is still much faster than a conventional planar detector which takes 10–20 ns. Increasing the length of the columns reduces the size of the low-field regions and for columns of length 290 μm the detector gives the same collection speed as a full 3D sensor.

The behavior of the double-sided 3D detector after irradiation to SLHC levels has been simulated in Glasgow [22], [23] using the 3-level trap model proposed by the University of Perugia [24]. Some of the carrier cross sections in the Perugia model have been modified to match experimental trapping times.

After heavy irradiation the back surface of the sensor will not be depleted for voltages as high as 100 V, which will result in a loss of collection efficiency.

Fig. 6 shows the simulated average charge collection, simulated by flooding the pixel with uniform charge, of a double sided and a standard 3D detector with Medipix2 geometry (pixel size 55 μm by 55 μm). Both detectors use 250 μm columns, the standard detector has a 250 μm thick substrate while that of the double-sided device is 300 μm. As a consequence the double-sided device has higher charge collection at low fluences due to the greater substrate thickness. However, at high fluences, the charge deposited underneath or above the not fully penetrating columns is lost due to the low electric field and the results match those of the standard 3D with columns of the same size.

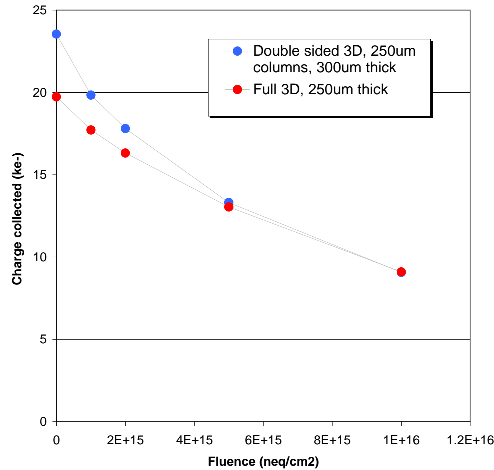

Fig 6-6 Average charge collection in a standard and a double-sided 3D detector. Both devices have 250 µm columns; the double-sided detector has a 300 µm thick substrate. The pixel is 55 µm by 55 µm, and the bias voltage is 100 V.

A first run of 3D pixel and strip detectors with double-sided geometry has been processed at CNM on n-type silicon. The wafer layout contains 3D detectors with Medipix2, ATLAS pixel and Pilatus geometry, simple pad and strip-like 3D detectors and test structures. The first fabrication run on n-type silicon with p-type readout electrodes implies that holes are collected which means that the ATLAS pixel detectors will not work. These will be tested on a second fabrication run using a p-type substrate. The fabrication of the n-type devices has just finished and been distributed to RD50 collaborators. The first electrical characterization has been performed while charge collection characterization before and after irradiation to SLHC levels will take place in 2008.

The preliminary results of the reverse and forward current are shown in Fig 6-7. The current voltage characteristics show that a rectifying p-n junction has been formed between the electrodes. The breakdown voltage is on the order of 60 V but it should be taken into account that the full depletion voltage foreseen for this devices is only 2 V, therefore the detectors can be operated in over depletion without any problem. Further electrical characterisation is to follow.

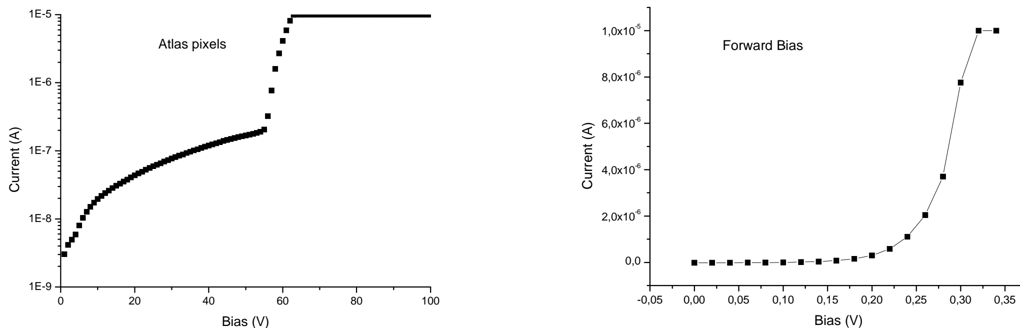

Reverse Bias Forward Bias

Fig 6-7 Reverse and forward current voltage characteristics of the CNM double sided 3D detectors.

6.2.3 Development at FBK

In order to overcome the limitations of 3D-stc detectors FBK has developed a new detector concept, namely the 3D Double-side Double Type Column (3D-DDTC) detector, which is expected to significantly enhance the performance with acceptable process complication. The schematic of the device is shown in Fig 6-8. This device is very similar to that proposed by CNM. The columns are etched by DRIE from both wafer sides (junction columns from the front side and ohmic columns from the back side), stopping at a distance *d* (ideally not exceeding a few tens of µm) from the opposite

surface. This results in easier masking of the DRIE etching. Moreover, since columns are not etched all the way through the substrate, a sacrificial wafer is not required: the process is indeed the same as in the 3D-stc technology for the front side, whereas on the back side lithography and DRIE has to be added.

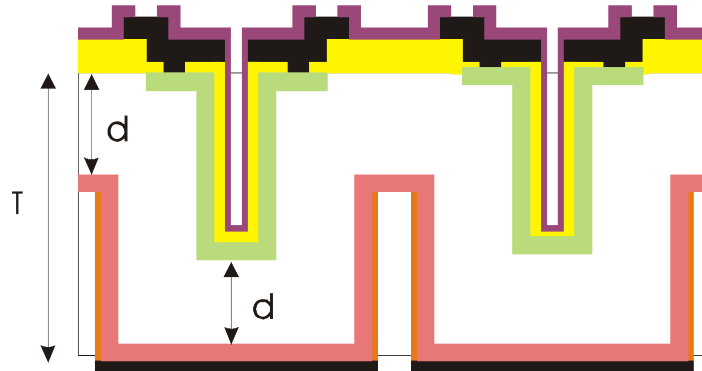

Fig 6-8 Schematic cross-section of the 3D-DDTC detector

Two wafer layouts have been designed to explore the 3D-DDTC technology, and two fabrication runs have been carried out. These include strip detectors, pixel detectors, pad detectors and test structures, among them planar and 3D diodes. Table 6-3 summarizes the main features of the two batches. The first batch features a bulk thickness of 300 µm with columns penetrating at most 200 µm into the substrate. The latter value is dictated by the DRIE etching constraints and is not optimal for detector performance. Nevertheless it allows a first evaluation of the 3D-DTTC technological approach. The second batch features wafers thinned down to 205 µm, with 180 − 200 µm column depth (see Table 6-3), so as to optimize the detector performance. The fabrication of the first batch has just been completed, whereas the second one will be completed by the end of the 2007.

Batch	DDTC 1	DDTC 2
Substrate type	n-type	p-type
Substrate Thickness	300 µm	205 – 250 µm
Column depth	180 – 200 µm	180 – 200 µm
Strip Design	AC/DC coupled, pitch 80/100 µm	AC/DC coupled, pitch 80/100 µm
Pixel Design	ALICE, MEDIPIX1	ATLAS, CMS

Table 6-3 The main features of the two FBK 3D-DDTC detector batches

The electrical characterization of the devices belonging to the 3D-DDTC1 batch has just started, and only preliminary results relevant to test structures are currently available. Measurements were performed at room temperature in the dark. Measurements performed on 4 mm^2 planar test diodes equipped with a large guard ring show good leakage current characteristics, evidence that the process quality is good and no degradation is induced from the DRIE steps. From the $1/C^2$-V curves measured on the planar device, a full depletion voltage of about 10V was extracted, corresponding to a very low substrate doping concentration of $1.5 \times 10^{11} cm^{-3}$.

Fig 6-9 shows the diode and guard-ring leakage current curves as a function of the reverse bias for the 3D diode test structures: devices with both junction and ohmic columns (dtc) and the earlier devices with junction columns only (stc) are shown, with 80 µm and 100 µm pitch between the columns of the same type. For both pitches the diode area is 2.56 mm^2, so that a different number of columns are involved; that is, 16 x 16 and 20 x 20 for the 100 µm and 80 µm pitch, respectively. In all cases, the diode current curves start to saturate at a very low voltage corresponding to the lateral depletion between columns. Moreover, the leakage current value is good, much lower than 1 pA/column, and no sign of early breakdown is observed in both diodes and guard rings for voltages as high as 100 V.

Fig 6-10 shows the capacitance of 3D diodes as a function of the reverse bias. In all cases, the capacitance abruptly decreases and tends to saturate at a very low voltage because of the lateral depletion between the columns. As expected, this happens at slightly lower voltages for the 80 µm pitch. The capacitance saturation values are the same for both the stc diodes regardless of the column pitch: this is in agreement with the fact that, when lateral depletion is achieved, the depletion proceeds towards the back side as in a planar diode, so that the capacitance depends only on the diode area [8]. On the contrary, in dtc diodes the main contribution to the capacitance comes from the junction-to-ohmic column capacitance. Therefore, the saturation values of dtc diodes are higher than those of the stc ones and, among dtc diodes, they are higher for the 80 µm pitch both because of the shorter distance between columns and of the larger number of columns. Finally, the capacitance-voltage curves of stc test diodes can be analyzed to yield the substrate doping concentration as a function of the depletion depth [8]. Results relevant to two diodes with 80 and 100 µm pitch are reported in Fig 6-11. As can be seen, the depletion under the columns reaches values of 110 - 120 µm, so that one can infer the column depth values to be 180 - 190 µm, in good agreement with measurements made with SEM on test wafers. A summary of the first results obtained on 3D-DDTC1 detectors has been published in [25].

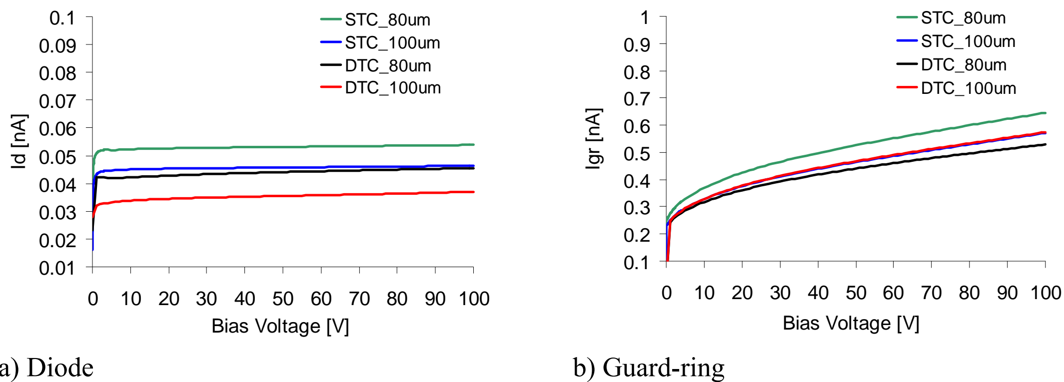

a) Diode b) Guard-ring

Fig 6-9 Leakage current vs. voltage curves in diode and guard ring of 3D test diodes from the 3D-DDTC1 batch

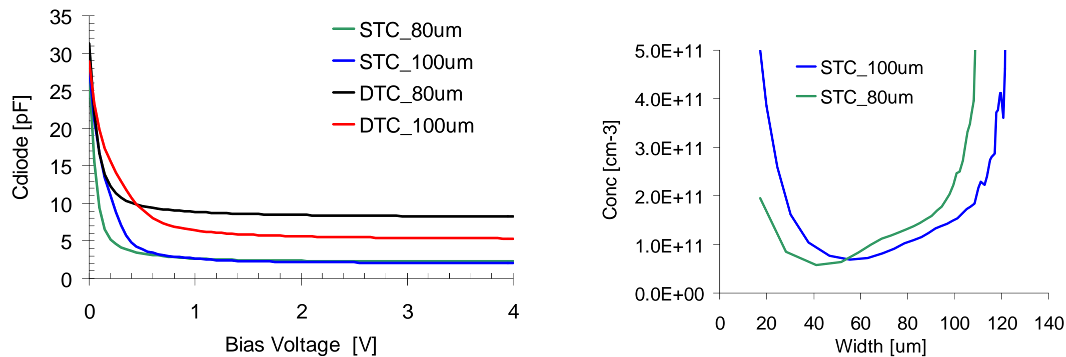

Fig 6-10 Capacitance vs. voltage curves in 3D test diode from 3D-DDTC1 batch

Fig 6-11 Graph of the substrate doping concentration as a function of depth as obtained from CV measurements of 3D test diodes having only the junction columns (stc).

6.2.4 IceMOS

The University of Glasgow has entered into a commercial development programme with IceMOS Technology Ltd. [26], a MEMS fabrication company based in Northern Ireland, to make full 3D detectors. This is a joint project between Glasgow and the Diamond Light Source Synchrotron [27] to produce 3D detectors for X-ray imaging applications. Some of the fabricated detectors will also be used for radiation hardness studies within the RD50 collaboration.

The full 3D devices fabricated in IceMOS are 250 μm thick and have p^+ and n^+ columns of 10 μm diameter fabricated on high resistivity n-type silicon. The key steps of the fabrication of these devices are outlined in Fig 6-12. No support wafer is required. Instead, a thick (500 μm) wafer is used for the fabrication. After a first oxidation, a set of electrodes is etched with an inductively coupled plasma, ICP, etching tool to a depth of 250 μm and filled with n^+-doped polysilicon (Fig 6-12a). The polysilicon is removed and the oxide etched, and the second set of electrodes, p^+, is processed in the same way, also from the front surface (Fig 6-12b). Next, the back side of the wafer is polished to expose the electrodes. The front surface is planarised leaving an unpatterned 250 μm wafer with p^+ and n^+ doped polysilicon columns going all the way through the substrate (Fig 6-12c). The field oxide is thermally grown, and the fabrication ends with the standard steps for contact opening, metallisation and passivation. The final device is shown in Fig 6-12d.

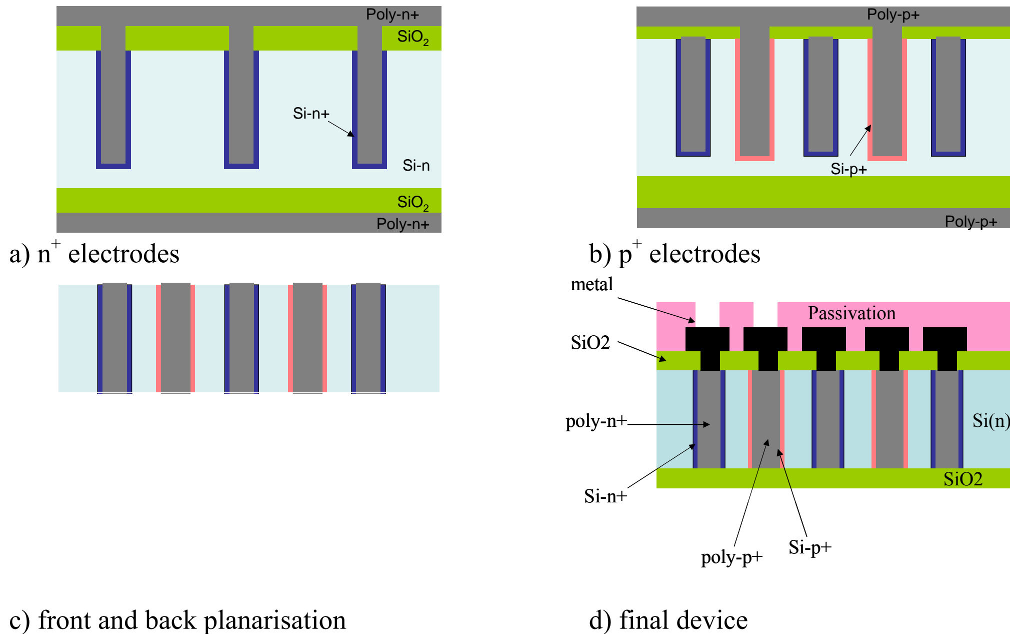

a) n^+ electrodes b) p^+ electrodes

c) front and back planarisation d) final device

Fig 6-12 Key steps of the fabrication of the IceMOS Glasgow/Diamond full 3D detector

To simplify the fabrication process for the first process run, the contacts to both the p+ and n+ electrodes are located on the front side of the wafer, so all the biasing (n+) electrodes are connected with routing metal lines on the front surface which is a significant draw back.

The mask has been designed at the University of Glasgow. The wafer includes pixel detectors (Medipix2 and Pilatus2), pads and microstrip detectors that will be coupled to LHC electronics for characterization. The first detectors are now ready, at Glasgow and testing is about to start.

A new process flow has been developed which will use 6inch wafers, a carrier wafer and which will allow back side metallisation to contact the bias electrodes. This will speed up the processing at IceMOS and remove the need to route the bias lines to all the n+ electrodes from the front surface.

6.3 Semi-3D devices

There is a new variation of the 3D-stc structure developed at BNL [28], where the ohmic contact is fabricated on the same side of the substrate as the column etching. This type of 3D-stc device is a true one-sided detector, since the back side is simply covered by silicon dioxide (without any processing) and is left floating during the device operation. The first prototype detectors, with stripixel configuration [29], have been fabricated on FZ p-type Si wafers with a 300 μm thickness and about a 10 kΩcm resistivity. The n^+ columns, about 240 μm deep, were etched by CNM using a deep reactive ion etcher. The planar processing steps, which include ion implantations and two-metal layers, were completed at BNL. CCE testing of the sensors is underway.

6.4 References for Chapter 6

[1] RD50 Status report 2006, CERN-LHCC-2007-005

[2] E. Fretwurst et al., Nucl. Instr. and Meth. A 552, Issues 1-2, 21 October 2005, Pages 7-19 "Proceedings of the 5th International Conference on Radiation Effects on Semiconductor Materials, Detectors and Devices"

[3] S. I. Parker, C. J. Kenney and J. Segal, "3D — A proposed new architecture for solid-state radiation detectors, "Nucl. Instrum. Methods A, vol. 395, pp. 328-343, 1997.

[4] C. Piemonte et. al., Development of 3D detectors featuring columnar electrodes of the same doping type, Nuclear Instrum. Methods. A 541 (441) 2005

[5] C. Piemonte et. al., Study of the signal formation in single-type-column 3D silicon detectors, Nuclear Instrum. Methods. A 579 (633) 2007

[6] S. Ronchin et. al., Fabrication of 3D detectors featuring columnar electrodes of the same doping type, Nuclear Instrum. Methods. A 573 (224) 2007

[7] C. Fleta, D. Pennicard, R. Bates, C. Parkes, G. Pellegrini, M. Lozano, V. Wright, M. Boscardin, G.-F. Dalla Betta, C. Piemonte, A. Pozza, S. Ronchin and N. Zorzi, "Simulation and test of 3D silicon radiation detectors", Nucl. Instr. and Meth. A, vol. 579, no. 2, pp. 642–647, Sep. 2007.

[8] A. Pozza et. al., First electrical characterisation of 3D detectors with electrodes of the same doping type, Nuclear Instrum. Methods. A 570 (317) 2007

[9] G. Kramberger, V. Cindro, J. Langus, I. Mandić, M. Mikuž, M. Zavrtanik, M. Boscardin, G.-F. Dalla Betta, C. Piemonte, A. Pozza, S. Ronchin and N. Zorzi, "Position sensitive TCT studies of irradiated 3D-sct sensors", 10th RD50 Workshop, Vilnius (Lithuania), 3–6 June 2007, available online at http://rd50.web.cern.ch/rd50/

[10] M. Boscardin, L. Bosisio, M. Bruzzi, G.-F. Dalla Betta, C. Piemonte, A. Pozza, S. Ronchin, C. Tosi, N. Zorzi, "Characterization of 3D-stc detectors fabricated at ITC-irst", Nucl. Instr. and Meth. A, vol. 572, no. 1, pp. 284–286, Mar. 2007.

[11] M. Scaringella, A. Polyakov, H.F.-W. Sadrozinski, M. Bruzzi, C. Tosi, M. Boscardin, C. Piemonte, A. Pozza, S. Ronchin, N. Zorzi and G.-F. Dalla Betta, "Charge collection measurements in single-type column 3D sensors", Nucl. Instr. and Meth. A, vol. 579, no. 2, pp. 638–641, Sep. 2007.

[12] V. Cindro, G. Kramberger, J. Langus, I. Mandić, M. Mikuž, M. Zavrtanik, M. Boscardin, G.-F. Dalla Betta, C. Piemonte, A. Pozza, S. Ronchin and N. Zorzi, "Position Sensitive TCT Measurements with 3D-stc detectors", 8th RD50 Workshop, Prague (Czech Republic), 25–28 June 2006, available online at http://rd50.web.cern.ch/rd50/

[13] T. Ehrich, S. Kuhn, M. Boscardin, G.-F. Dalla Betta, S. Eckert, K. Jakobs, M. Maaßen, U. Parzefall, C. Piemonte, A. Pozza, S. Ronchin and N. Zorzi, "Laser characterisation of a 3D single-type column p-type prototype module read out with ATLAS SCT electronics", to be published in Nucl. Instr. and Meth. A.

[14] M. Zavrtanik, V. Cindro, G. Kramberger, J. Langus, I. Mandi, M. Mikuz, C. Piamonte, M. Boscardin, G.-F. Dalla Betta, S. Ronchin, N. Zorzi and A. Pozza, "Position sensitive TCT evaluation of irradiated 3D-stc detectors", to be published.

[15] A. Abdessalam et al., "The ATLAS semiconductor tracker end-cap module," Nucl. Instrum. Methods A, vol. 575, pp. 353-389, 2007.

[16] F. Campabadal et al., "Design and performance of the ABCD3TA ASIC for readout of silicon strip detectors in the ATLAS semiconductor tracker," Nucl. Instrum. Methods A, vol. 552, pp. 292-328, 2005.

[17] K. Hara et al., "Performance of irradiated n^+-on-p silicon microstrip sensors," Nucl. Instrum. Methods A, vol. 565, pp. 538-542, 2006.

[18] S. Eckert, T. Ehrich, K. Jakobs, S. Kühn, U. Parzefall, M. Boscardin, C. Piemonte, S. Ronchin, "Comparison of irradiated stFZ silicon sensors using LHC speed front-end electronics," Nucl. Instrum. Methods A, to be published.

[19] S. Kuehn, G.-F. Dalla Betta, S. Eckert, K. Jakobs, U. Parzefall, A. Pozza, A. Zoboli and N. Zorzi, “Short strips for the sLHC: a p-type silicon microstrip detector in 3D-technology”, to be published

[20] G. Pellegrini, F. Campabadal, M. Lozano, J.M. Rafi, M. Ullan, R. Bates, C. Fleta and D. Pennicard, “Double sided 3D detector technologies at CNM-IMB”, Nuclear Science Symposium Conference Record, 2006. IEEE , vol. 2, pp. 1248–1252, Oct. 29 2006-Nov. 1 2006.

[21] D. Pennicard, G. Pellegrini, M. Lozano, R. Bates, C. Parkes, V. O'Shea and V. Wright, “Simulation results from double-sided 3-D detectors”, IEEE Trans. Nucl. Sci., vol. 54, no. 4, pp.1435-1443, Aug. 2007.

[22] D. Pennicard, “Simulation results from double-sided and standard 3D detectors”, 10th RD50 Workshop, Vilnius (Lithuania), 3–6 June 2007, available online at http://rd50.web.cern.ch/rd50/

[23] D. Pennicard, “Simulations of 3D detectors with radiation damage up to 10^{16} n_{eq}/cm^2”, ATLAS 3D Sensors R&D meeting, CERN, 2 July 2007, available online at http://indico.cern.ch/conferenceDisplay.py?confId=17797

[24] M. Petasecca, F. Moscatelli, D. Passeri and G.U. Pignatel, “Numerical simulation of radiation damage effects in p-type and n-type FZ silicon detectors”, IEEE Trans. Nucl. Sci., vol. 53, no. 5, pp. 2971–2976, Oct. 2006.

[25] G. F. Dalla Betta et al., New developments on 3D detectors at IRST, in 2007 IEEE Nuclear Science Symposium, Honolulu (USA), October 28 - November 3, 2007, Conference Record, Paper N18-3

[26] http://www.icemostech.com/

[27] http://www.diamond.ac.uk/

[28] Z. Li, W. Chen, Y.H. Guo, D. Lissauer, D. Lynn, V. Radeka, M. Lozano and G. Pellegrini, “Development, simulation and processing of new 3d Si detectors”, to be published in Nucl. Instr. and Meth. A.

[29] Z. Li, “Novel silicon stripixel detector: concept, simulation, design and fabrication”, Nucl. Instr. and Meth. A, vol. 518, no. 3, pp. 738–753, Feb. 2004.

7 Full detector systems

7.1 CCE measurements after severe neutron irradiation

The state of the art radiation hard silicon detectors use n-side read-out to improve the charge collection after severe radiation doses. The n^+ doped side (the ohmic contact) is segmented and connected to the read out electronics. The signal is provided by electrons moving towards the n^+ electrode in the high field side after irradiation. The three times higher mobility of the electrons compared to holes and the higher electric field on the n^+ side result in a much shorter collection time and therefore in less trapping of the charge carriers, yielding a higher signal pulse than the more standard p-in-n devices. The n-side read-out with p-type substrates (n-in-p) has been proven with miniature and large area detectors before and after irradiation with protons [1,2] to fluences in the range of the SLHC doses. In the SLHC, the radiation damage will be caused by charged particles emerging from the interactions and backscattered neutrons from the whole of the detector. The ratio between the flux of charged particles and neutrons varies with the radial distance to the beam axis, and it becomes equal for a radius between 20 to 30 cm. For larger radii the neutrons will contribute to most of the radiation damage [3]. The present tentative layout of one of the general purpose detectors anticipated for the SLHC (the upgraded ATLAS experiment) envisages installation of microstrip detectors in the tracking volume from 30 cm and 100 cm radius [4]. The sensors will be designed to operate at radii where the contribution of neutron radiation varies from 53% to 87% from inner to outer. It is therefore important to test the prototype silicon detectors after neutron irradiation in order to establish their radiation hardness properties. It is in fact well known that some parameters, like the full depletion voltage, have different degradation when irradiated with neutrons compared to fast charged particles [5]. No information on the degradation of the charge collection efficiency (CCE) after very high neutron doses was though available. The CCE of microstrip detectors after neutron irradiation has now been tested up to the extremely high dose of 1×10^{16} n cm^{-2}.

7.1.1 Irradiation of small p-type sensors

Small size (1×1 cm^2) 80µm pitch n-in-p silicon microstrip detectors have been designed by the University of Liverpool and produced by Micron Semiconductor. The small size of the devices allows easy handling and uniform irradiation and their properties can be extrapolated to full scale devices with the opportune corrections for the strip length (e.g. total interstrip capacitance, noise). P-type silicon with very high resistivity (30kΩ cm) with [100] crystal orientation has been used. The n-in-p geometry requires strip isolation to avoid the surface inversion due to electron accumulation at the Si-SiO_2 interface created by the positive charge trapped in the oxide. This positive charge is due to increase with radiation up to a saturation level of about $2\text{-}3 \times 10^{12}$ ions cm^{-2} for detector quality oxides. This would create a conductive channel at the interface that effectively shorts the segmented electrodes. To prevent this happening, two main techniques have been developed: individual p-stops (highly doped narrow p-implants surrounding the individual n-strips) or p-spray (lower implanted over the all wafer prior to further processing). Large area and miniature detectors with both types of insulation techniques have been successfully prototyped [1,2]. The p-spray offers the advantage of one less photolithography step, with some impact on the cost of the device and the possibility of tighter read-out pitch, not having to accommodate a p-stop implant between every strip. The detectors for the experiment here described use the p-spray strip isolation technology.

Few detectors have been irradiated in the Triga Research nuclear reactor in Ljubljana to 1.6 and 3×10^{15} n cm^{-2}. They have been shipped to Liverpool in a cold package and stored in the freezer at -20 ^oC. They have been bonded to a SCT128 40MHz clock analogue chip [6] and characterized in term of charge collection efficiency as a function of the bias voltage. The analogue data were digitised by a 40MHz Sirocco ADC. A reference non-irradiated 300µm thick detector with the known charge deposition of about 23000 electrons has been used to calibrate the read-out system. A detachable connection was used to bond the various irradiated detectors to the same electronics that was calibrated with the non-irradiated sensor.

The charge collection measurements [7] were performed at low temperature (-23°C) to control the reverse current and avoid thermal run-away. This allowed biasing the devices to very high voltages. The signal was induced by fast electrons from a ^{90}Sr source located above the detector and the trigger was provided by a scintillator below the detector and coupled to two photomultiplier in coincidence. The scintillator was covered by a 3mm thick plastic sheet to absorb the low energy part of the ^{90}Sr spectrum and provide a signal of the same intensity of a minimum ionising particle. Figure 7.1 shows the collected charge as a function of the bias voltage for a set of n-in-p detectors irradiated to 1.6, 3 and 10×10^{15} n cm^{-2}.

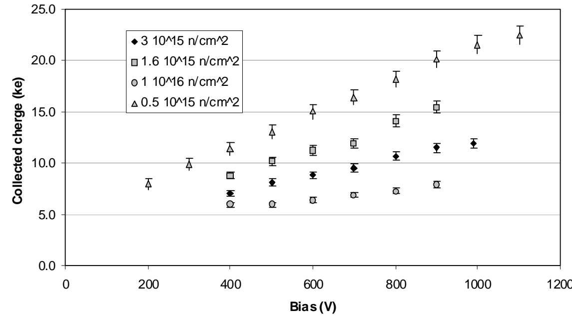

Figure 7.1. Collected charge as a function of bias with micro-strip sensors after several doses up to $1.\times10^{16}$ neutron cm^{-2}.

It has previously been reported that the changes of the charge collection efficiency as a function of the time after proton irradiation were negligible despite of a factor of four change of the anticipated full depletion voltage (V_{fd}) [2]. The increase of V_{fd} with time is strongly dependent on the temperature and it is known as reverse annealing [5]. The changing rate of V_{fd} can be reduced, and effectively eliminated, at low temperature (0°C or below). It is also well known that a *beneficial* annealing of the current takes place in the same time, with a similar dependence on the temperature. The reduction of the current would be a positive effect when operating the detector because it would decrease the contribution of shot noise and reduce the risk of thermal run-away of the current induced by local self-heating of the sensors.

The operation scenario of the silicon detectors in the present LHC has been optimised to the changes of V_{fd} with time by keeping the detectors cold also during shut-down periods, and accepting the higher currents that this choice implies. The previous results from [2] have changed the way the reverse annealing is regarded, having shown no correlation between the collected charge and the changes of V_{fd} taking place during the reverse annealing. The stability of CCE as

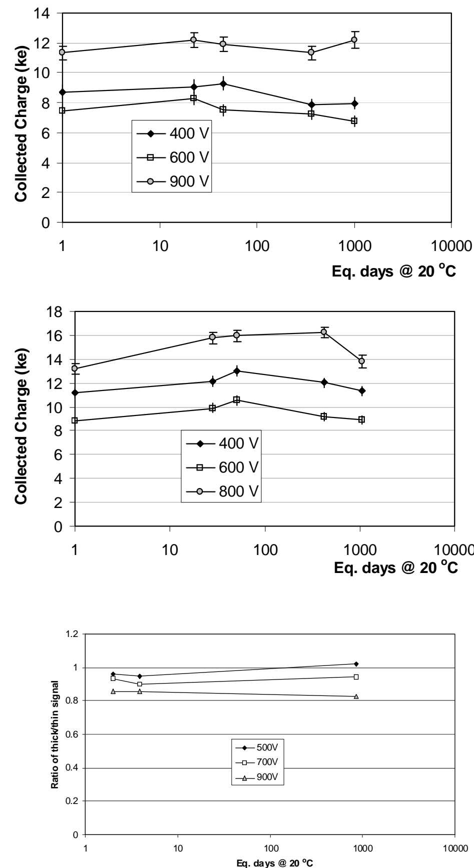

Figure 7.2. Collected charge as a function of the annealing time at different bias voltages with a detector irradiated with neutrons to 1.6×10^{15} cm^{-2} (above), 3×10^{15} cm^{-2} (middle) and $1x10^{16}$ cm^{-2} (below).

a function of time after irradiation allows reducing the reverse current of the detectors by keeping them at room temperature when not operated, without degrading the detector performance.

It was important to confirm these results also after neutron irradiation. Figure 7.2 shows the collected charge as a function of time after irradiation at different bias voltages with a detector irradiated with neutrons to 1.6 and 3×10^{15} cm^{-2} and $1x10^{16}$ cm^{-2}. The study was conducted by accelerating the annealing at $60^{o}C$ (the first two short steps) and $80^{o}C$ (the two longer annealing steps) and the results are plotted against the equivalent time at $20^{o}C$ (RT_{eq}).

While V_{fd} is expected to change from over 900V, 1800V and 3000V for the three doses to over 3900V, 7000V and 15000V respectively, the charge collected after three years RT_{eq} for these doses is similar at all the different voltages (Fig. 7.2). The collected charge seems to increase (10-15%) during the first 50 days for the two different fluences and the different bias voltages. This could be due to the annealing of the effective charge trapping time that has been measured after neutron irradiation [8].

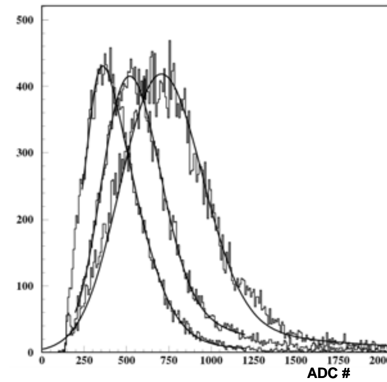

Figure 7.3. Energy distribution for three similar detectors, non-irradiated and irradiated to 1.6 and 3×10^{15} n cm^{-2} and (from right to left, respectively). The detectors have been measured with the same electronics chain.

7.1.2 Discussion

The charge collection properties of silicon micro-strip p-type detectors irradiated with neutrons to very high (SLHC levels) neutron fluences have been studied to confirm the excellent results already obtained after proton fluences. The results of the comparison are shown in Fig. 7.4, where the charge collected after neutron and proton irradiation is shown as a function of the neutron equivalent fluence. Two points (600V and 900V) are shown for the neutron irradiated devices, while the applied bias voltage for the proton irradiated ones are 500, 800 and 900 volts for the three increasing fluences. The comparison shows that after neutron irradiation the CCE is in line or above the charge collected after proton irradiation. A lower charge trapping constant is reported [8] in the case of neutron irradiation, that could explain the slightly higher efficiency exhibited by Fig. 7.4.

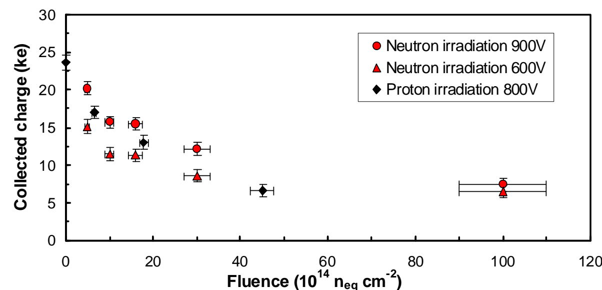

Figure 7.4. Collected charge with p-type detectors irradiated with 24GeV protons and reactor neutrons to SHLC doses (10^{16} cm^{-2}). Two points are shown for each neutron fluence corresponding to 900V and 600V bias voltage. The applied voltages are 500, 800 and 900 volts for the three different proton doses, respectively.

7.2 Results from the Micron 6" wafer program

An extensive campaign of irradiation and measurements has been carried out by RD50 institutes, using miniature silicon strip detectors (SSD) and pad diodes (PD) made with different silicon substrates (n and p-type FZ and MCz crystals). The devices were produced by Micron Semiconductor using a 6" mask designed by RD50. The strips have a 80µm pitch with a metal width over pitch ratio

of 1/3, while the PD have an area of 2.5x2.5 mm^2 with multiple (8) guard rings. The substrate materials studied are shown in Table 7.1 below.

Crystal type	MCz n	MCz p	FZ n	FZ p
Resistivity	2 kΩ	1.5 kΩ	20 kΩ	14 kΩ
Orientation	<100>	<100>	<100>	<100>

The devices have been irradiated with protons at CERN-PS, neutrons at the Ljubljana reactor and pions at Paul Scherrer Institue of Villigen (CH) and characterised with CCE and IV-CV measurements before and after irradiation. The following results [9] refer only to neutron irradiated devices. The investigation of the proton and pion irradiated detectors is ongoing. This study is a comparison of CV and CCE [10] measurements performed by the University of Liverpool (UL), the J. Stefan Institute of Ljubljana (JSI) and Santa Cruz (SCIPP) groups of RD50. The CCE measurements where performed by the three institutes using different set-up's and method, as shown in Fig.7.5.

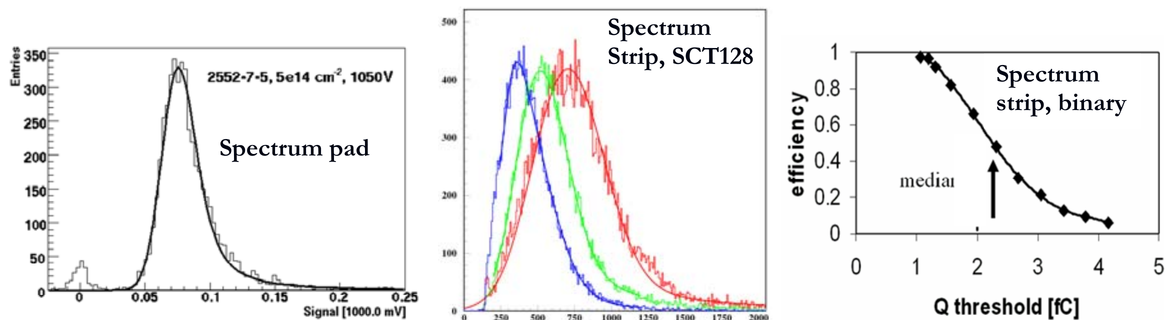

Figure 7.5. Different methods for CCE measurements. The energy spectrum measured with single channel electronics is used for evaluating the most probable (MP) value with PD (left); the energy spectrum measured with 128 channels analogue electronics is used to estimate the MP with SSD's (centre); the median value of the threshold scan with 128 channels binary electronics is used to evaluate the mean value of the energy distribution of SSD's (right).

The PD where characterised by JSI using a discrete component single channel electronics with 25ns shaping time; the SSD where measured by UL with 40MHz analogue electronics (SCT128 analogue chip, see before) and by SCIPP with a binary DAQ [11]. The full depletion voltage V_{fd} has been evaluated from the CV characteristic on PD.

Figure 7.6 shows the V_{fd} as a function of the neutron fluence for the four type of substrate as obtained with the CV method. It is apparent that MCz substrates show a slower degradation with fluence (V_{fd} increases about 55V every 10^{14} neutrons cm^{-2}) than FZ crystals (125V every 10^{14} neutrons cm^{-2}). The CCE measurements with diodes correlate with the CV results as shown in Fig. 7.7. In general, a clear advantage in term of deterioration of the performances is found with n-MCz substrate, that combines the lower degradation slope, similar to the p-MCz, with a much lower initial V_{fd} due to the higher resistivity, and with the further advantage of undergoing to donor removal until type inversion. As a consequence, the V_{fd} of the n-MCz after inversion is about 500V lower than p-MCz, although increasing with the same slope as a function of fluence. The measurements were performed with pad diodes. A different dependence of the CCE as a function of bias voltage is expected with SSD, due to the different geometry of the collecting

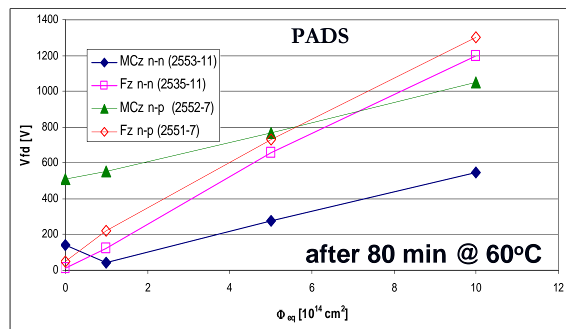

Figure 7.6. V_{fd} as a function of the neutron fluence for the 4 different crystal types.

electrodes. Figure 7.8 shows the comparison of the CCE with PD and SSD after $5x10^{14}$ n cm^{-2} and $1x10^{15}$ n cm^{-2}. The CCE increase with bias for the SSD is underestimated compared with PD due to the fact that PD were annealed to the minimum of the V_{fd} (beneficial annealing, about 10 days at room temperature), while the SSD where measured after irradiation. It is know that about 10% or more improvement of the CCE is expected for a similar annealing time with SSD.

This effect is described in Fig. 7.9, that shows the CCE as a function of the accelerated annealing at 60°C measured with binary electronics on SSD's irradiated to 5 and $10x10^{14}$ n cm^{-2}. An initial rise (beneficial annealing) of about ~10% (@500V) is followed by a decrease after long term annealing (1000 min. at 60 °C, equivalent to about 3 years at room temperature).

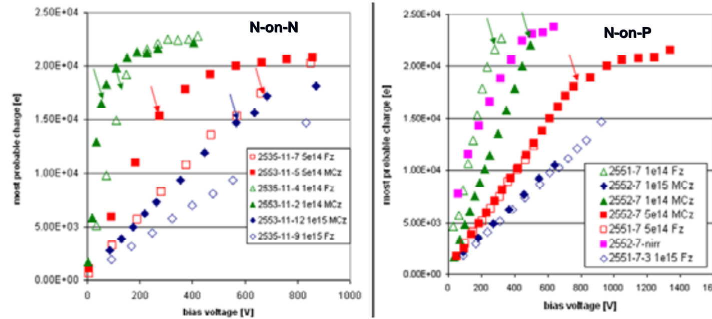

Figure 7.7. V_{fd} as a function of the neutron fluence for the 4 different crystal types.

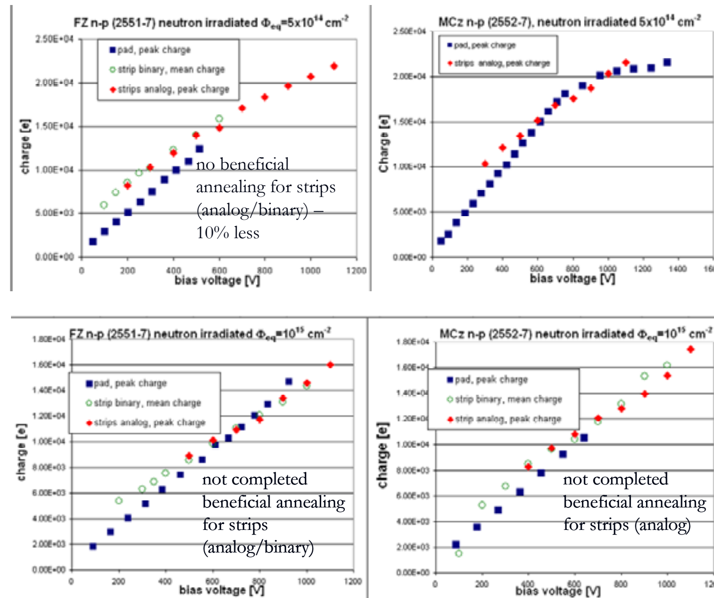

Figure 7.8.Comparison of CCE with PD and SSD's measured with the three different methods after 5 and $10x10^{14}$ n cm^{-2}.

7.2.1 Discussion

The study of PD and SSD detectors made with different crystals and performed with different methods and read-out electronics shows very good agreement. The CCE measurements show that the total collected charge, therefore the trapping, does not depend on the different crystal type. The same CCE is expected provided that sufficient bias can be applied to the detector. The measurements have

shown that with neutron irradiation the low resistivity, inverting MCz n-type substrate can offer significant advantages of CCE at low voltages due to the lower V_{fd} after irradiation. The studies of the annealing effects on the CCE of SSD's has confirmed that a limited variation of the CCE is observed over a period equivalent to 3 years at room temperature.

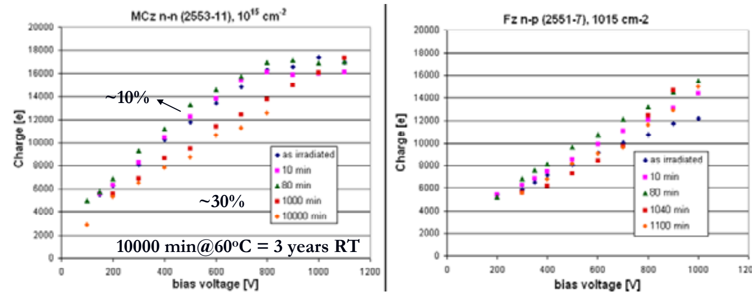

Figure 7.9. Annealing of the CCE, measured with binary electronics with FZ and MCz p-type SSD's.

7.3 Status of the evaluation of the SiGe technology for the ATLAS Upgrade Tracker and Liquid Argon Calorimeter ASICs.

Work continues at UC Santa Cruz and CNM Barcelona on the evaluation of the very fast SiGe technology. The total dose/fluence irradiations of the IBM 8HP technology parts are completed and the technology appears to be radiation hard enough for both the ATLAS upgrade tracker and the LAr. There is no hard spec for the level of radiation hardness required but the devices are still operating with reasonable current gain after 25 Mrad and a few 10^{15} neutrons cm^{-2}. More studies including the irradiation of a complete IC and low dose rate studies would be needed for full qualification.

We have been focusing our attention on the alternate SiGe technology, the IBM 8WL, because of its lower cost and greater compatibility with the standard 8RF CMOS process. We are now preparing samples to complete the gamma irradiation at BNL and the neutron irradiation at Ljubljana. Penn and Barcelona are on track to provide the pre and post testing of the gamma and neutron irradiated parts.

We are organizing our design efforts at UCSC, Penn and BNL for the submission of a prototype IC for fabrication, and will decide between 8WL and 8HP depending on radiation hardness.

7.4 SMART report

The research activity of the SMART project, collaboration funded by I.N.F.N. (Istituto Nazionale di Fisica Nucleare) of Italian research institutes members of RD50, has been focused during year 2007 on the study the performance of micro-strip detectors.

7.4.1 Sensors

The micro-strip sensors used in this work have been designed and processed in collaboration with ITC-IRST institution (Fondazione B. Kessler, TN).

The production has been made on 4" wafers, 300µm thick and growth with different techniques: MCz, FZ, Epitaxial (Epi). The wafers have n-type and p-type bulk doping and different crystal orientations (< 100 > or <111>). Micro-strip sensors have 50 µm and 100 µm pitches, and the strip length is 45 mm. Insulation of n+ strips on p-type sensors is guaranteed by p-spray technique with high ($5 \cdot 10^{12}cm^{-2}$) and low ($3 \cdot 10^{12}cm^{-2}$) dose. Wafers were processed in 2004, and results have been already published in [12][13][14].

The micro-strip sensors have been irradiated with protons and neutrons using different facilities:

- SPS (Super Proton Syncrotron) at CERN, with a 24 GeV/c proton beam at three values of fluence: 6×10^{13}, 3×10^{14}, and 3.4×10^{15} 1 MeV n cm^{-2} (n_{eq}).
- FZK (Forschungszentrum Karlsruhe Cyclotron) with a proton beam of 26 MeV at 11 different values of fluence in the range 1.4×10^{13}–2×10^{15} n_{eq}.
- Fast neutrons at Ljubljana nuclear reactor with 12 values of fluence ranging from 5.5×10^{13} to 8.5×10^{15} n_{eq}.

Measurements after irradiation and the radiation hardness of these wafers have been reported in references [14][15][16].

7.4.2 Experimental set-up

Micro-strip sensors are glued on a carbon fiber frames designed as support for the CMS tracker modules. A prototype assembly is shown in Figure 7.10.

The read-out is made with the front-end hybrid used in the CMS tracker, and the electronics is capable to measure electrons and holes signals. This assembly allows to perform tests on n-type and p-type bulk doped sensors, having almost the same integration dynamical range for both signal polarity.

Sensors are read-out with a CMS-like DAQ system, based on FEC, FED and optical links [17]. A 40 MHz clock and external trigger signals are generated and distributed to the module by the Trigger and Sequencer Card (TSC).

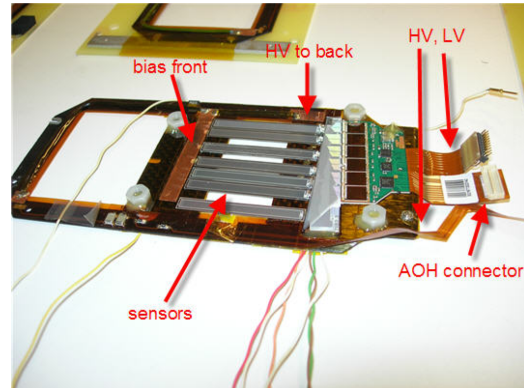

Fig 7.10. Picture of a module.

The trigger signal is provided by the coincidence of two small plastic scintillators and the ionization event is generated by a ^{106}Ru beta source.

The sensor is housed in a metal box to guarantee electrical and thermal insulation. The cooling system is made of a liquid nitrogen tank equipped with an electric pump. The nitrogen vapour is fluxed inside the metal box housing the sensor. Temperatures as low as −40 °C can be achieved with this system. This low temperature level is needed to have stable detector operation after irradiation.

We have assembled 8 of such frames; each one contains irradiated sensors together with non irradiated ones to be used for comparison.

7.4.3 Pre irradiation Measurements

A typical electronic noise figure of a prototype module is shown in Figure 7.11. Micro-strip sensors have 32 or 64 strips, and the wire bonding to the read-out electronics does not use all the available ROC connections. Channels bonded to ROC are clearly identified by the higher noise level. The spikes at the borders of the sensors are due to pick-up edge effects given by the non optimized set-up.

For both not irradiated and irradiated sensors we have measured the signal (S), the noise (N) and the Signal over noise ratio (S/N). These are the most relevant parameters to evaluate the radiation hardness.

Signal values are extracted by data using a Landau distribution convoluted with a Gaussian fit function. The Noise value is measured by a Gaussian fit to the noise

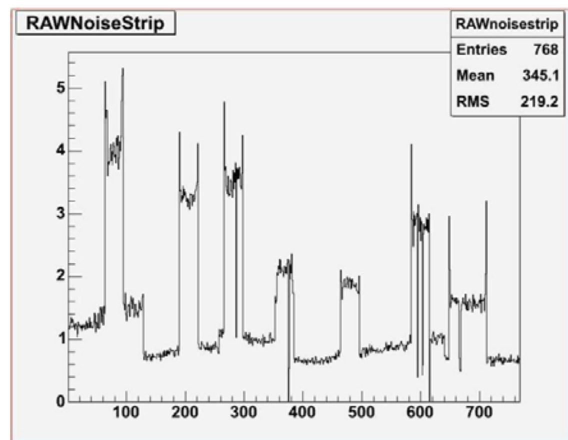

Fig. 7.11. Noise figure of micro-strip sensors with no bias voltage at −30 °C. A 6 chip hybrids is equipped with 7 devices (32 or 64 strip each). Non connected channel are those exhibiting a noise value smaller than 1 ADC channel

profile. The measurements errors on this scale are negligible. All data are analyzed with a dedicated C++ code based on ROOT [18].

The micro-strip depletion voltage has been evaluated measuring S, N and S/N as a function of the applied voltage. An example of such measurement is shown in Figure 7.12, where a clear saturation effect is observed for values of voltage above depletion. The depletion voltage (Vd) can be measured by fitting (red lines) the Signal data: the value is compatible with the one evaluated on diodes. The mean noise value of a depleted micro-strip sensor at −30 °C is about 1.2 ADC channels. All sensors tested in this work have shown a stable behaviour with a noise value below 1.5 ADC.

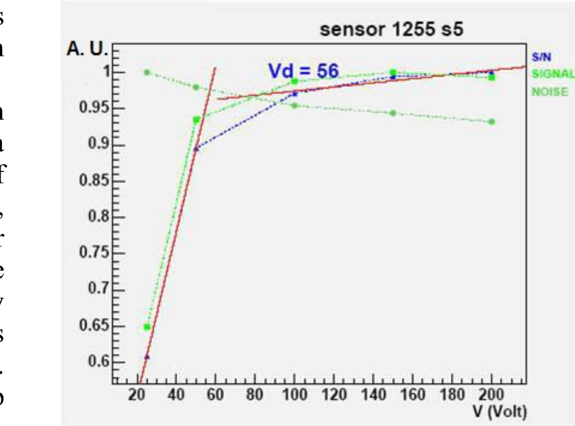

Fig.7.12. Signal, Noise and Signal/Noise (normalized to the relative highest value) measured for an Fz n-type micro-strip sensor as a function of the applied voltage.

A comparison of signal distributions for three different materials, MCz, Fz and Epi, is shown in figure 7.13. No differences have been observed before irradiation among different materials and bulk doping. The signal values scale with the wafer thickness as expected.

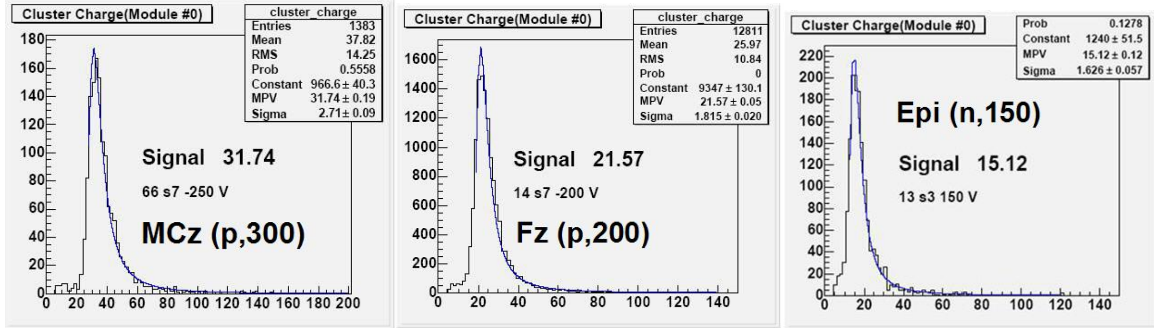

Fig. 7.13. Landau spectra of different micro-strip sensors: MCz p-type 300 μm thick (MCZ (p,300)), Fz p-type 200 μm thick (Fz (p,200)) and Epitaxial n-type 150 μm thick (Epi (n,150)).

7.4.4 Post irradiation Measurements

Radiation hardness of micro-strip sensors is evaluated by measuring the deficit in the collected charge. Measurements have been performed on 15 micro-strip sensors with n-type and p-type bulk doping: 12 sensors irradiated with low energy proton (Karlsruhe) and 3 with reactor neutron (Ljubljana). The investigated fluence range is from 1.2 10^{14} to 3.5 10^{15} n_{eq}.

A typical Landau spectrum recorded by a p-type MCz sensor is shown in figure 7.14. This sensor has been irradiated at 0.7 $10^{15} n_{eq}$ and biased with a voltage Vbias=600 V. The Landau is well defined and the noise is slightly affected by the irradiation: at that fluence a S/N of about 30 is achieved, with a reduction of 16% compared to a similar non irradiated detector.

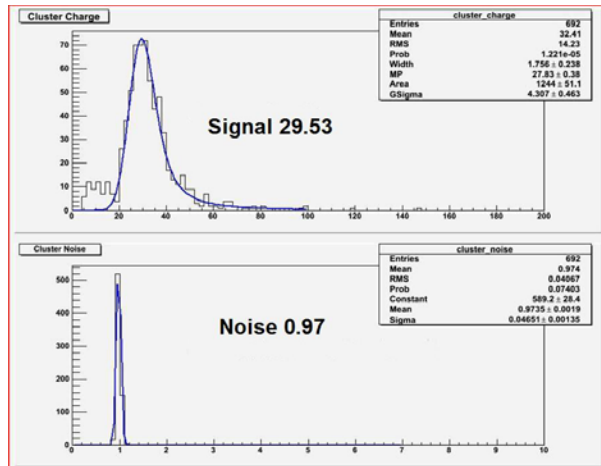

Fig 7.14. Landau spectrum and noise figure for a MCz p-type micro-strip sensor irradiated at 0,7 10^{15} n_{eq}

A summary of results for detectors processed on Epi and MCz materials is shown in figure 7.15, where S/N is plotted vs bias voltage at different fluences. Satisfactory results, with saturation at high voltage, are achieved up to 0,7 10^{15} n_{eq} for MCz and 2,55 10^{15} n_{eq} for the Epitaxial. S/N values scale with the wafer tickness as expected and saturation values for Epitaxial sensors is reached at lower voltages given the smaller thickness to be depleted.

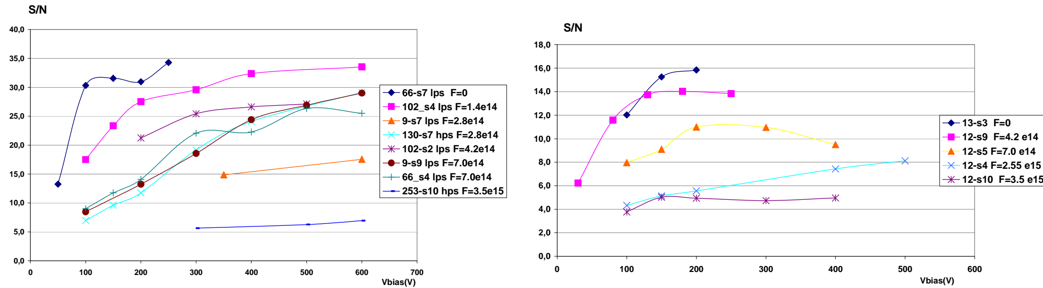

Fig. 7.15. S/N values measured on micro-strip detectors as a function of the bias voltage for different irradiation levels. Left: MCz p-type detectors. Label 'lps' identify low p-spray isolation dose while label 'hps' the high p-spray dose case. Right: Epitaxial n-type detectors. Fluences F are in n_{eq} .

The behavior of the S/N measured at the saturation as a function of the fluence is summarized in figure 7.16. A deficit in the charge collection of the prototypes can be seen at fluence around 10^{15} n_{eq} as consequence of the radiation damage. Nevertheless materials have different performance. Some preliminary conclusions on material radiation hardness can be drawn:

1) MCz n-type can be hardly used at high fluence: signal disappears and clustering efficiency strongly decreases. The S/N performance is better than foreseen, maybe enhanced in the medium fluence range by the double junction effect;
2) MCz p-type have acceptable performance up to a few 10^{15} n_{eq};
3) Epitaxial n-type show a moderate decrease with fluence;
4) Fz p-type seems competitive.

If we consider as a safe detector operation limit S/N=10 the most promising materials have the following radiation hardness level: MCz p-type up to 3 10^{15} n_{eq}, Epi n-type up to 2.55 10^{15} n_{eq}. In these operational conditions the charge collected by sensors processed with these materials is larger than 6000 e^- per m.i.p., enough to design pixel or micro-strip devices. As a comparison the fluence 3,1 10^{15} n_{eq} corresponds to the expected value for the tracker layer placed at 9 cm from the beam line at SLHC.

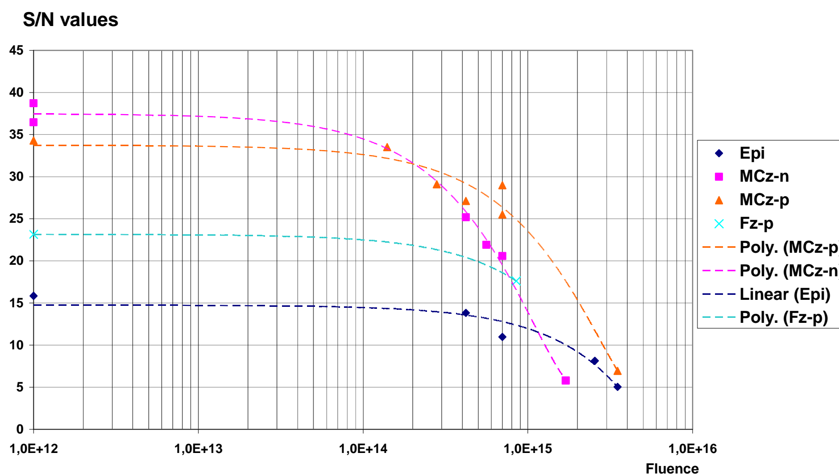

Fig.7.16: S/N vs irradiation fluences for micro-strip sensors processed on Fz, MCz and Epi materials. The Poly/Linear labels indicate the superimposed trend line. Fluences are measured in n_{eq} .

7.5 References for Chapter 7

[1] G. Casse et al., Nucl.Instrum.Meth.A487 (2002) 465-470.
[2] G. Casse et al., Nucl.Instrum.Meth.A535 (2004) 362-365.
[3] I. Dawson, "Radiation background ", talk at ATLAS Tracker upgrade workshop, Genova, Italy, 18-20 July 2005.
[4] P.P. Allport, "Sensor Considerations and a Possible Tracker Layout for sLHC", talk at ATLAS Tracker upgrade workshop, Genova, Italy, 18-20 July 2005.
[5] G. Lindström et al., (The RD48 Collaboration). Nucl. Instr. and Meth *A* 466 (2001), p. 308.
[6] J. Kaplon et al. IEEE Transact. On Nucl. Sci. 44 (1997)2 98.
[7] G. Casse et al., Nucl.Instr. Meth.A581(2007), Pages 318-321.
[8] G. Kramberger et al., Nucl.Instr. Meth.A481 (2002) 247-305.
[9] G. Kramberger, http://indico.cern.ch/conferenceTimeTable.py?confId=21398
[10] M. K. Petterson, R. F. Hurley, K. Arya, C. Betancourt, M. Bruzzi, B. Colby, M. Gerling, C. Meyer, J. Pixley, T. Rice, H. F.-W. Sadrozinski, IEEE, Senior Member, J. Bernardini, L. Borrello, F. Fiori, A. Messineo *"Determination of the Charge Collection Efficiency in Neutron Irradiated Silicon Detectors"*, Presented at the 2007 IEEE NSS/MIC, Honolulu, HI,October 27 - November 3, 2007.
[11] M.K. Petterson et al., Nucl.Instr. Meth.A583 (2007) 189-194.
[12] RD50 Status Report 2006-Radiation hard semiconductor devices for very high luminosity colliders -CERN-LHCC-2007-005 and LHCC-RD-013
[13] RD50 Status Report 2005 -Radiation hard semiconductor devices for very high luminosity colliders -CERN-LHCC-2005-037 and LHCC-RD-009
[14] BRUZZI M. et al., Processing and first characterization of detectors made with high resistivity n- and p-type Czochralski silicon. NUCLEAR INSTRUMENTS & METHODS IN PHYSICS RESEARCH. SECTION A, ACCELERATORS, SPECTROMETERS, DETECTORS AND ASSOCIATED EQUIPMENT. vol. 552, pp. 20-26 ISSN: 0168-9002.
[15] Radicci V. et al, Study of radiation damage induced by 24-GeVc and 26-MeV protons on heavily irradiated MCz and FZ silicon detectors. NUCLEAR INSTRUMENTS METHODS IN PHYSICS RESEARCH SECTION A-ACCELERATORS, vol. 570 pp 330
[16] Macchiolo A. et al, Characterization of micro-strip detectors made with high resistivity n- and p-type Czochralski silicon. NUCLEAR INSTRUMENTS METHODS IN PHYSICS RESEARCH SECTION A-ACCELERATORS, vol. 573 pp 216
[17] CMS tracker Technical design report: cmsdoc.cern.ch/cms/TDR/TRACKER/tracker.html
[18] The ROOT system Home Page, http://root.cern.ch

8 Resources

All participating institutes organize their own resources required for the research activities in their home laboratories. Integration in a CERN approved R&D project allows them to apply for national funding in terms of financial and manpower resources. The collaboration comprises several institutes, which have access to irradiation sources (reactors and accelerators, see [1]), as well as clean room and sensor processing facilities. A very wide range of highly specialized equipment for characterization of sensors and materials is also available (see [2]).

8.1 Common Fund

RD50 has a Common Fund to which each institute contributes every year a certain amount. The Common Fund is used for project related investments, like processing of common test structures or purchasing of special material and equipment. Furthermore it is used to cover the organization of collaboration workshops, common irradiation runs, or other specific activities of common interest.

8.2 Lab space at CERN

The RD50 collaboration was temporarily using existing infrastructure and equipment at CERN in 2007 and requests to continue to do so in 2008. As a member of the collaboration, the section PH-DT2/SD can provide access to available lab space in building 14 (characterization of irradiated detectors), in building 28 (lab space for general work) and in the PH Departmental Silicon Facility (hall 186, clean space). The collaboration would like to keep the RD50 visitor office in barrack 591 and use the CERN infrastructure to organize one workshop at CERN in 2008.

8.3 Technical support at CERN

A low level of support from PH-DT2/SD (wire bonding and sensor mounting) may be profitable. The expected work volume for 2008 is estimated to be very limited.

8.4 Support of the CERN RD50 members

It is requested that the RD50 members affiliated to CERN are further financially supported in their research activities through the CERN PH Department. The corresponding activities shall be coordinated by the PH-DT2 group assuring a balanced research program following on the one hand the RD50 research strategy and on the other hand the research interests of all LHC experiments towards radiation tolerant silicon detector upgrades for the SLHC.

In 2008 the RD50 collaboration looks forward to see the "CERN DG-Whitepaper project" coming into life which will financially support silicon detector research activities at CERN in the framework of the work package WP4 "Radiation Hard Semiconductor Detectors".

[1] An extensive list of irradiation facilities open to RD50 can be found on the RD50 web page: http://www.cern.ch/rd50/

[2] R&D Proposal - DEVELOPMENT OF RADIATION HARD SEMICONDUCTORDEVICES FOR VERY HIGH LUMINOSITY COLLIDERS, LHCC 2002-003 / P6, 15.2.2002.